Ph. D DISSERTATION

Experimental analysis on quasi-mode-locked regimes of fiber laser

광섬유 레이저의 준 모드 잠금 영역에 대한 실험 연구

By

SEUNGJONG LEE

FEBRUARY 2018

DEPARTMENT OF ELECTRICAL AND

COMPUTER ENGINEERING

COLLEGE OF ENGINEERING

SEOUL NATIONAL UNIVERSITY

Experimental analysis on quasi-mode-locked regimes of fiber laser

광섬유 레이저의 준 모드 잠금 영역에 대한 실험 연구

지도 교수 정 윤 찬

이 논문을 공학박사 학위논문으로 제출함
2018 년 2 월

서울대학교 대학원
전기컴퓨터 공학부
이 승 종

이승종의 공학박사 학위논문을 인준함
2018 년 2 월

위 원 장 _____ (인)

부위원장 _____ (인)

위 원 _____ (인)

위 원 _____ (인)

위 원 _____ (인)

Abstract

Experimental analysis on quasi-mode-locked regimes of fiber laser

SEUNGJONG LEE
DEPARTMENT OF ELECTRICAL AND
COMPUTER ENGINEERING
COLLEGE OF ENGINEERING
SEOUL NATIONAL UNIVERSITY

In this dissertation, quasi-mode-locked (QML) regimes of fiber laser are experimentally investigated. The study focuses on four subjects: (1)The shot-to-shot coherence, (2)the wave-packet formation, i.e., noise-like pulse (NLP) packet formation, (3)the cascaded pulse interaction and (4)the super rogue wave triggering via dispersive wave synchronization. It is important to note that the subject (1) and the subject (2) are strongly correlated by the nonlinear phase shift accumulated and the degree of soliton interaction. The subject (3) triggers the super rogue wave in the subject (4) by accumulation of extreme events through the cascaded pulse interaction explained in the subject. In the introduction, I explain the principles and brief history of fiber optics, fiber laser, mode-locking, passively mode-locked fiber laser and QML fiber laser as groundwork for research presented in later sections. I provide motivation and scope of the dissertation to emphasize the novelty and set boundaries of my research.

In the first part of the dissertation, I carry out extensive experimental analysis on the shot-to-shot coherence and the wave-packet formation in QML regimes, including NLP, symbiotic, and multi-soliton (MS) regimes in an anomalous-dispersion fiber ring cavity. In order to overcome the limitation of classical techniques in real-time measurement, I utilize the spatio-temporal analysis for shot-to-shot measurement of stochastically natured QML regimes. Each QML regime exhibits significantly distinct coherence characteristics, depending not only on the amount of nonlinear phase shift (NPS) accumulated per roundtrip but also on the degree of soliton interaction, the latter of which crucially governs the bunching (i.e., the wave-packet formation) or anti-bunching mechanisms in the corresponding QML regimes. It is clear that solitons with higher intensities tend to undergo higher NPS and stronger soliton interactions. Subsequently, the intensified soliton interactions among the individual solitons in the MS regime cavity trigger them to form a bunched soliton-group, i.e., a wave packet, thereby resulting in QML pulses in the noise-like pulse or symbiotic regime. The complicated nonlinear process, in turn, causes a severe degradation in the shot-to-shot coherence of the resultant QML pulses and shows clearly distinct characteristics among each regime. The shot-to-shot coherence trends observed in the experiment are in good agreement with numerical analysis verifying the strong correlation between the shot-to-shot coherence of QML pulses and the corresponding NPS accumulated per roundtrip. In addition, such trend and formation process suggests that cavity formation into NLP, symbiotic, MS or

other QML regimes are governed by the degree of soliton interaction among soliton pulses in case of anomalous dispersion regime.

In the second part of the dissertation, I report intermittent burst of a super rogue wave in the breathing multi-soliton regime of an anomalous fiber ring cavity. I utilize the spatio-temporal shot-to-shot measurement technique to capture the dynamics of extreme wave formation in the cavity and intensity probability density function of pulse events in the cavity for more than 800 roundtrips to assist my analysis of every pulse event. In MS regime, where hundreds of solitary waves and dispersive waves can exhibit nonlinear dynamics due to complex pulse-to-pulse interactions, dispersive waves can synchronize, constructively interfering, to trigger localized extreme waves nearly 10 times higher than the average solitons observed in the cavity. I trigger the process by increasing the soliton population inside of the cavity to stimulate the pulse interaction probability. The synchronization of dispersive waves intensifies and localizes extreme events until it reaches the maximum point and burst into super rogue wave, which quickly breaks and returns to the initial state with the least number of extreme events. Without any cavity modification or external control, the process naturally repeats in ten seconds order, roughly analogous to sub-hundred years in the open ocean considering the speed of tidal waves. The phenomenon demonstrates the optical analogy of the "hundred-year wave" observed in the ocean.

Experimental analysis presented here regarding the shot-to-shot coherence, wave-packet formation, and intermittent super

rogue wave triggering are pioneering work in the realm of the QML regimes of fiber laser. I believe the study carried out in this dissertation should function as a cornerstone for further study of pulse dynamics in QML fiber lasers and extreme wave generation not only in the optical domain but also in other disciplines such as oceanography.

Keywords : Nonlinear fiber optics, fiber lasers, ultrashort pulses, mode-locked lasers, rogue waves.
Student Number : 2012-30943

Contents

List of Figures

List of Tables

Chapter 1

Introduction

1.1 Overview of fiber optics

Fiber optics is optical discipline based on transparent, flexible and micro-sized cylindrical waveguide, capable of transmitting light [1-4]. With the groundbreaking theory and realization of low-loss light transmission through an optical fiber based on total internal reflection, fiber optics emerged to the center of research interest with enormous possibilities in the optical discipline. Beyond the passive nature as a waveguide, later, scientists and engineers pushed the fiber optics further and gave life to optical fibers by doping them with rare-earth ion, such as ytterbium, erbium, neodymium, thulium, bismuth, etc. The rare-earth-doped optical fibers functioned as gain media and introduced fiber laser and fiber amplifier to fiber optics [5-12].

Fiber lasers and amplifiers have been extensively studied and made indispensable in numerous areas owing to their reliable, compact, alignment-free, highly efficient and power scalable nature [13-34]. Research based on fiber lasers can generally fall into two groups of continuous wave (CW) operation, and pulsed-operation. In CW fiber lasers, power scaling and understanding and overcoming detrimental nonlinear effects, such as the stimulated Brillouin

scattering (SBS) arising from fiber nonlinearity and thermal effects have remained as significant issue [35-76]. Novel techniques and fibers were developed to push the output power limit of the fiber lasers. Double-cladding optical fiber was introduced to utilize high power semiconductor pump lasers to clad-pump and increase the output power [77-85]. Various schemes of monolithic and master oscillator and power amplifier (MOPA) with large mode-area (LMA) fiber pushed the power limit even further [86-99]. Beam combination techniques such as the coherent beam combing (CBC)and the spectral beam combining (SBC) have been utilized to combine output from tens and hundred of high power fiber lasers into a bundle for effective power scaling [100-102]. Ever since reaching the 1 kW in 2004 [83], 20 kW single-mode fiber laser and 500 kW multi-mode fiber laser are now available commercially [103].

With the pulsed-fiber lasers, research focus was to generate stable, ultrafast, high-energy and high-power optical pulses depending on the research and application requirements and understanding the pulse behavior of inside of the fiber lasers. In many application areas, pulsed-operation is essential. Different pulsation technique such as Q-switching, gain-switching and mode-locking have been introduced for pulsed fiber laser operations. Although, the fiber lasers cannot generate as high-energy pulse as the solid-state counterparts, advantages of high beam-quality, efficiency and reliability provided by fiber lasers are still promising and widely used in various areas [104-156].

Technologies developed in the research area have matured and

are increasingly applied to numerous applications. The market demand for fiber lasers in defense, medicine, and industry is still growing with no signs of slowing down and fiber optics research is expected to strive for many years to come.

1.1.1 Principles of optical fiber

An optical fiber is a dielectric cylindrical waveguide capable of transmitting light and is corner stone for fiber technologies [1−5]. Normally they are fabricated with fused silica and consists of core, cladding and polymer jacket for protection, as shown in Fig. 1.1.1. Optical fibers come in different structures and sizes depending on their applications. Single−mode fibers are the most common fibers transmitting a single propagation mode, Double−cladding fibers enables high power fiber lasers with cladding pumping, and specialty fibers such as the photonic crystal fibers, polarization−maintaining fibers, dispersion−managed fibers different options for fiber applications[157−197].

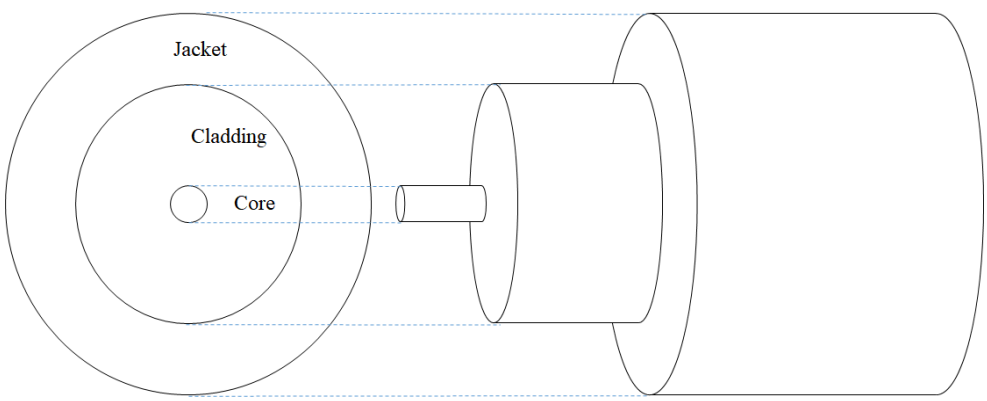

Fig. 1.1.1. Optical fiber structure.

Optical fibers guide optical waves with extremely low loss based on total internal reflection, as shown in Fig. 1.1.2.

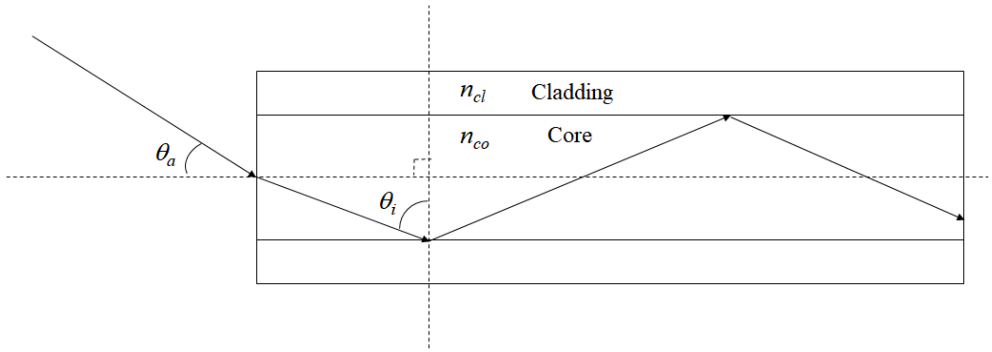

Fig. 1.1.2. Total internal reflection.

Total internal reflection condition is that the angle of incidence has to be greater than the critical angle and the refractive index of the core must be higher than the refractive index of the cladding in order to follow the Snell's law, expressed as follows:

$$\theta_i > \theta_c = sin^{-1}\left(\frac{n_{clad}}{n_{core}}\right), if \;\; n_{core} > n_{clad}, \qquad (1.1.1)$$

Therefore, each fiber will have range of angle that can be guided according to their reflective indices of its core and cladding. The angle of acceptance is normally expressed as Numerical aperture (NA), as follows:

$$\mathrm{NA} = \sqrt{{n_{core}}^2 - {n_{clad}}^2}, \qquad (1.1.2)$$

Optical fibers have optical paths called fiber modes where each mode has different propagation characteristics such as field distribution, polarization, propagation constant, etc. Number of modes in an optical fiber depends on the size of the core, NA, and wavelength of propagating optical field. V-parameter describes the number of

existing modes inside of a conventional step−index optical fibers, as follows:

$$\mathrm{V} = \frac{2\pi a}{\lambda}\mathrm{NA}, \qquad (1.1.2)$$

Where a corresponds to core radius, λ is the wavelength of the light, and NA is the numerical aperture. A single mode fiber will have V−parameter less than 2.405 guiding just the fundamental mode. The V−parameter cutoff values are zeros of the Bessel function used to express field behavior in optical fibers

1.1.2 Principles of fiber laser

Laser is a light amplification process based on famous theory of stimulated emission [198] as shown in Fig.1.1.3. During stimulated emission, an excited electron or ion moves to the excited state from the ground state, absorbing the pump energy. The excited electron or ion will move the meta-stable state, dependent on the structure of the gain material, and upon the incoming photon which associated frequency of the energy level, electrons or ions fall down to a lower energy level while inducing the electron to emit a clone photon exhibiting same optical characteristics. Therefore, the photons of generated from the stimulated emission is highly coherent showing same frequency and phase, where photons emitted with spontaneous emission are incoherent.

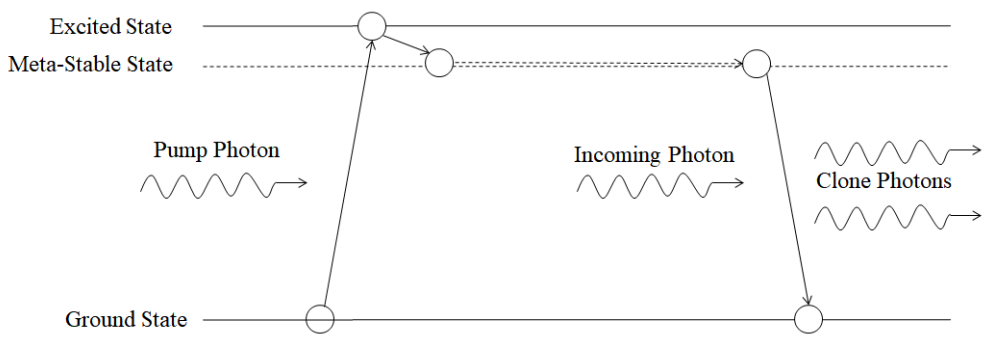

Fig. 1.1.3. Stimulated emission.

Fiber lasers utilizes rare-earth-doped optical fiber as active medium, in which the stimulated emission amplifies light coherently. Optical fibers are dopes with rare earth ions such as, ytterbium, erbium, neodymium, thulium, bismuth, etc. These rare-earth ions

each has distinct energy levels and accordingly absorption and emission cross-sections. Therefore, by selecting the ions and doping concentration along with the core and size and structure of an optical fiber, variety of active fibers can be fabricated for different application. The active fibers are excited with pump source such as the semiconductor laser through core pumping or cladding pumping depending on the laser application and fiber structure and achieve population inversion in the ion energy level to maintain gain level.

In order to achieve light amplification, feedback is essential to maintain stimulated emission process. Most of a feedback system will be achieved by two reflecting materials i.e., mirrors, where one of them is ~ 99% reflection and the other is a partially reflecting mirror to let the amplified laser out to pass the mirror, as shown in Fig. 1.1.4.

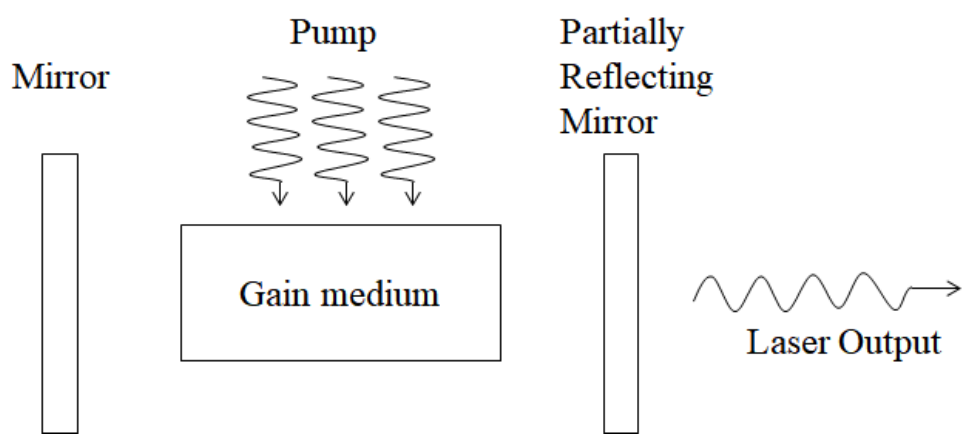

Fig. 1.1.4. Laser cavity with mirrors.

Pumped gain medium emits photons and the feedback enables photons emitted from stimulated emission to amplify themselves continuously to generate laser output. Mirrors can be used in fiber

lasers by placing two mirror on both ends of the active fiber either butt-coupled or with collimated through lenses. However, different approach such as the fiber Bragg gratings or ring cavity can be used to achieve feedback in fiber lasers. Fiber Bragg gratings is a periodic perturbation of refractive index on the core of optical fiber usually fabricated by inducing UV light periodically. The periodic perturbation of refractive index, depending on the grating period and refractive index, causes fiber to reflect narrow band of wavelength. Placing fiber Bragg grating in both ends of active fiber function as narrowband mirror for amplifying wavelengths and achieve feedback in the system, as shown in Fig. 1.1.5.

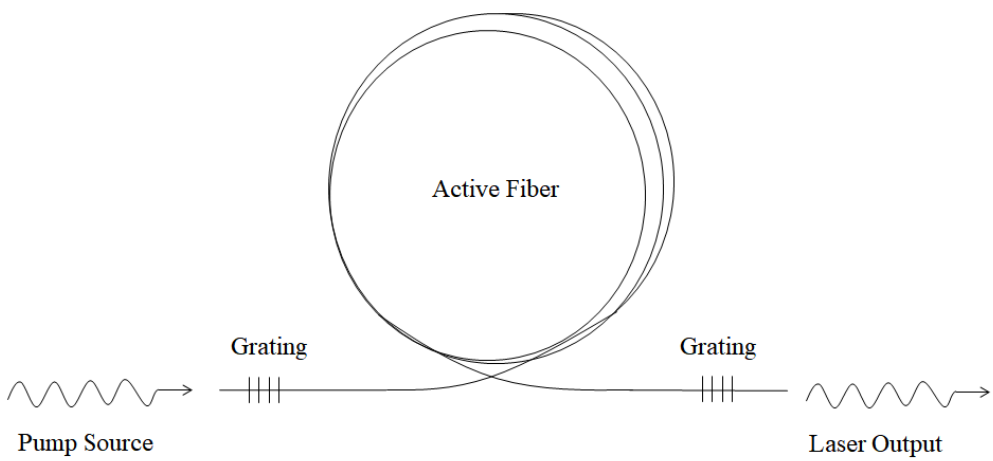

Fig. 1.1.5. Fiber laser based on gratings.

Feedback is also possible without mirrors or gratings by configuring a fiber laser in a ring shaped cavity, as shown in Fig. 1.1.6.

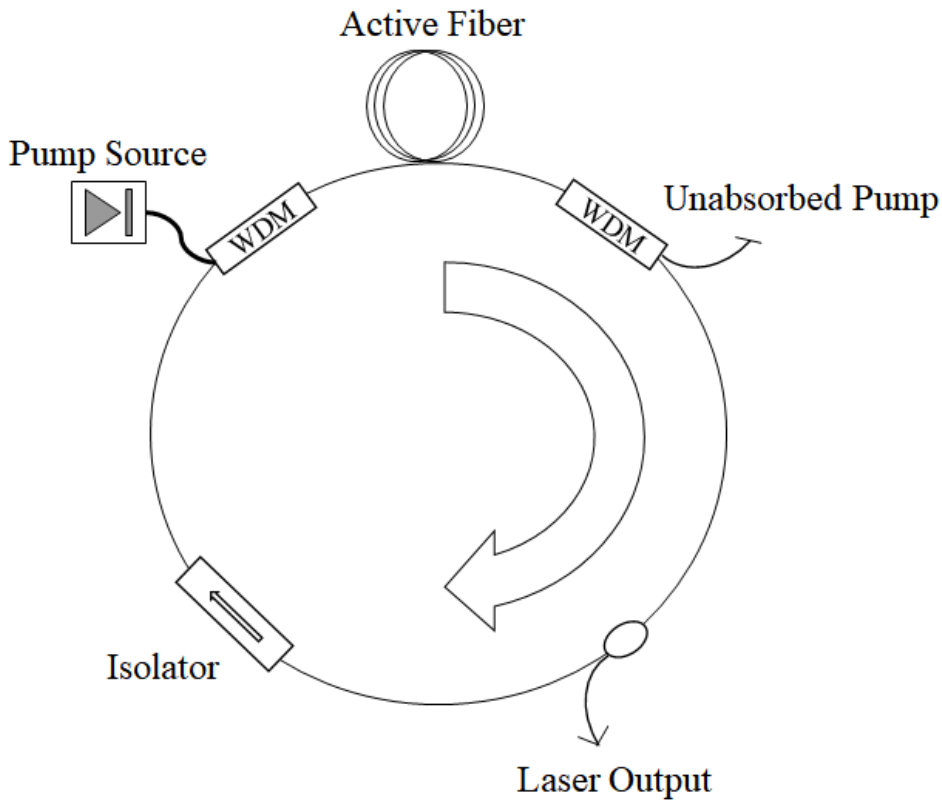

Fig. 1.1.6. Fiber laser based on ring configuration.

Rather than having reflective components on both ends to achieve feedback, the ends are connected and an optical coupler and isolators are spliced in a ring shaped cavity. The coupler operates as a partially reflecting mirror to provide loss to the cavity, and the isolator is placed to maintain unidirectional propagation of optical waves inside of the cavity. Ring configuration is convenient to setup and free from spatial hole burning effect occurring in linear cavity where the standing wave generated between the reflective components spatially depletes the gain medium[199,200].

In addition to fiber laser, an optical amplifier can be realized using

based on the stimulated emission. Optical signal can be amplified passing through an active fiber pumped. Incoming optical signal will generate clone photons with the electrons or ions in the excited state of the active fiber. Therefore, all fiberized high power fiber laser can be setup by a fiber laser followed by active fibers spliced after the laser in multiple stages to step up the power level in a MOPA system.

1.1.3 Principles of mode-locking

Fiber lasers can operate in different operational regimes depending on the cavity configuration and cavity parameters. CW operation and pulsed-operations are two main operation form of fiber lasers. For pulsed-operation of fiber lasers, various techniques have been developed to achieve different types of optical pulses depending on the research interest and application requirements. Demand for ultrafast optical pulse has always been high in scientific and industrial fields because fiber lasers can offer many advantages such as compactness, flexibility, large bandwidth, high beam quality and power scalability. Fiber lasers can operate in pulse-mode with techniques such as Q-switching, gain-switching, mode-locking, etc. Normally, fiber based source can generate a broad range of pulse width (ns to fs) and pulse repetition rate (kHz to GHz). For example, Q-switched laser can emit relatively high-energy pulse in many laser configurations [104-109]. The gain switching technique provides, electrically modulated ~ps pulse with ease of controlling the repetition rate of output pulse [110].

Mode-locking is one of the most frequently used pulsation technique in many types of lasers to generate ultrafast optical pulse. Normally, mode-locked fiber lasers are capable of generating fs to ps pulses at high repetition rate ranging from kHz to GHz. Mode locking is a technique to phase lock longitudinal modes of a cavity. Laser cavity has discrete modes known as the longitudinal modes as a result of constructive interference of specific wavelengths

depending on the cavity length, as shown in Fig.1.1.7. If the longitudinal modes are phase locked, meaning they have constant phase values, the laser output will generate a pulse train with pulse separation equal to the fundamental repetition rate decided by the cavity length.

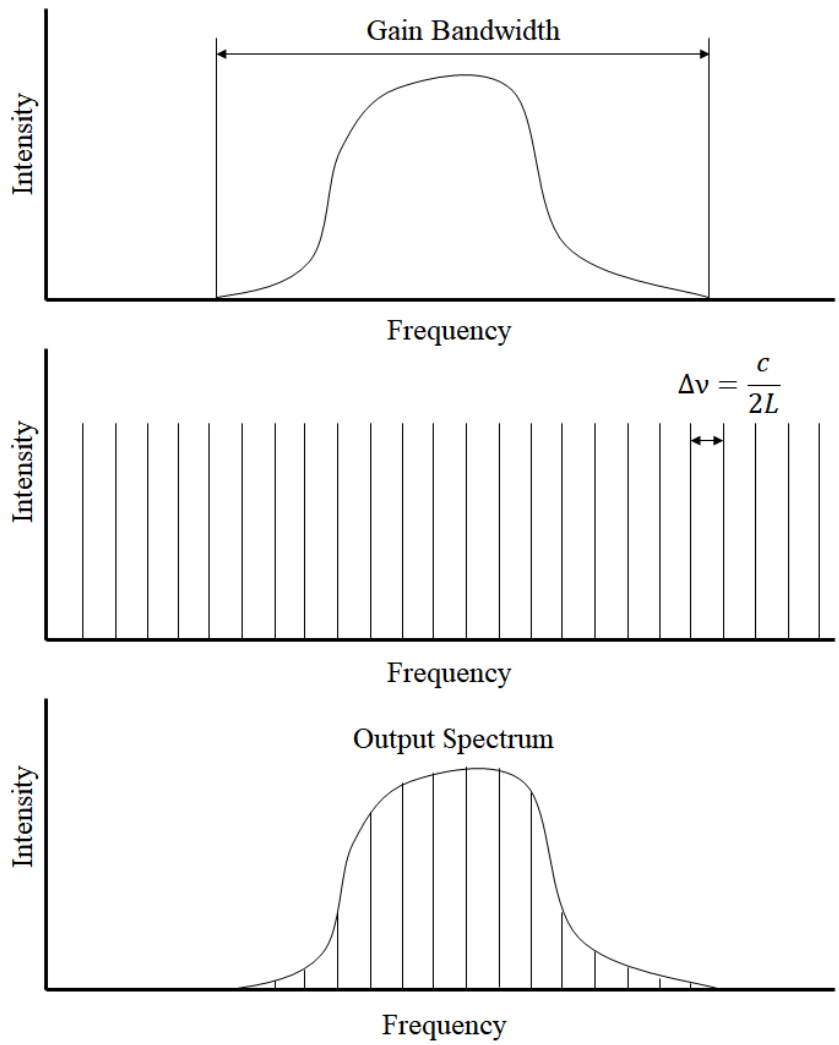

Fig. 1.1.7. Longitudinal mode of laser.

Mode-locking can be catergorized into active and passive mode-locking. In active mode-locking, intracavity losses are actively modulated with an electro-optic devices, synchronized to the cavity roundtrip. In passive mode-locking, cavity loss is modulated with interplay between the fiber nonlinearity and intensity fluctuation inside of the cavity without external modulation. Passive mode-locking uses different approach such as the frequency-shifted feedback lasers[201], slow saturable absorbers based on semiconductor devices , graphene or carbon nanotubes [202-222], nonlinear amplifying loop mirror [223-232], and nonlinear polarization rotation (NPR) [232-236]. Among these methods, NPR generates artificial saturable absorption effect relying on the interaction of Kerr effect and a polarizer inside of an optical fiber. Artificial saturable absorbers have much faster recovery time than the slow saturable absorbers and the much faster pulses and because it is polarization dependent, cavity parameter can be manipulated easily just with help of polarization controller.

NPR is driven by the intensity dependent change of elliptically polarized pulse inside of an optical fiber. Figure 1.1.8 shows the nonlinear polarization evolution inside of an optical fiber, where optical waves are filtered based on the intensity dependent polarization state of optical wave.

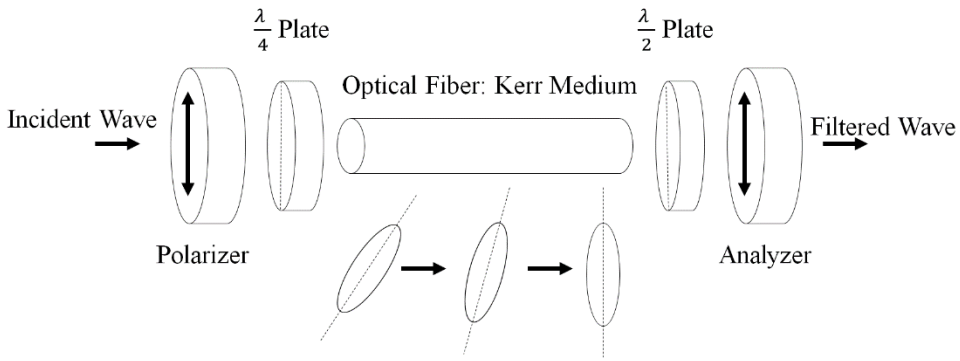

Fig. 1.1.8. Nonlinear polarization evolution.

Incident wave is linearly polarized after the first polarizer. The linearly polarized wave becomes elliptically polarized after the quarter-wave plate. The elliptically polarized wave undergoes nonlinear polarization evolution within the optical fiber resulting from phase shifts induced by self-phase modulation and cross-phase modulation. The wave exiting the fiber has different polarization state depending on the intensity profile of the wave due to the intensity dependent nonlinear phase shift (NPS) induced inside of the Kerr medium. The half-wave plate locates the polarization state of the peak intensity of the wave to pass through the analyzer. As a result, the low intensity wings are cutoff and the pulse is shortened. An example of passively mode-locked fiber laser (PMLFL) based on NPR is shown in Fig. 1.1.9.

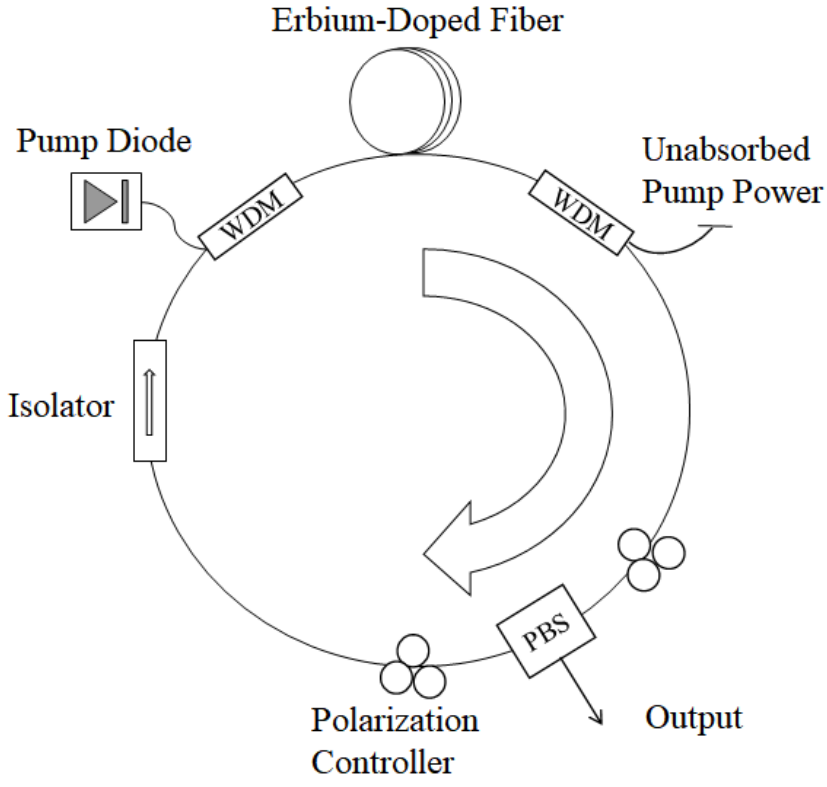

Fig. 1.1.9. Passively mode-locked fiber laser based on NPR.

1.2 Overview of quasi-mode-locked fiber laser

QML fiber lasers generate non-stationary optical pulses where ultrashort pulses are randomly spaced in a cavity round trip or bunched in a wave packet propagating at the fundamental repetition rate. It can also operate in a state where main wave packet and satellite pulses propagate together. The complex dynamics of the QML regime has been extensively studied over the past decade ever since interesting reports of QML regimes. These non-stationary optical pulse-based sources made themselves useful in the application fields of low spectral coherence interferometry, micromachining , supercontinuum generation, and etc. However, the true significance of studying the QSML comes in understanding the fundamental physics of chaotic pulse generation and its evolution in nonlinear fiber-optic media such as the Raman rogue waves or dissipative solitons in fiber laser cavities. In this section, I provide an overview of PMLFLs and QML fiber lasers focusing on NLP regime.

1.2.1 Passively mode-locked fiber lasers

PMLFL technology has made remarkable advances with high demand in scientific and industrial applications, offering attractive and reliable solutions to a wide range of, which include micromachining [237], optical metrology [238], and various biomedical applications such as multi-photon microscopy [239], optical-coherence tomography [240], and ophthalmology [241]. In fact, their numerous advantageous features inherited from fiber laser technology allow them to compete in terms of performance and practicality with other ultrafast laser technologies, including various bulk-type counterparts [242]. In particular, the waveguide architecture in a form of fiber allows for scalable high gain in single pass configurations, easy thermal management, and excellent spatial mode quality [243], notwithstanding its thin and long geometry in turn may give rise to undesirable nonlinear effects, such as self-phase modulation (SPM), stimulated Raman scattering (SRS), etc. The broad emission spectra readily achievable from rare-earth-doped fibers (~20 THz) are another merit to note for generating ultrashort pulses [244]. Furthermore, the alignment-free, all-fiberized compact configurations implemented to most PMLFLs eventually bring in unheard of practicality and reliability on top of their outstanding performance.

Up to date, a variety of operating regimes of PMLFLs have been demonstrated and investigated to generate stable, coherent ultrashort pulses, including the net anomalous dispersion regime that

generates conventional soliton pulses [245], the dispersion-managed soliton regime [246], the self-similar pulse regime [247], the all-normal dispersion (ANDi) regime [248], and most recently the dissipative soliton resonance regime [249,250]. In general, the pulse energy routinely achievable from such sources ranges from sub-nJ to tens of nJ, depending on the operating regime [245-248].

1.2.2 Quasi-mode-locked fiber lasers

As described in the previous section, conventional PMLFLs generate stable, coherent ultrashort pulses in ordinary mode-locking conditions, however they can switch and operate in extraordinary regimes known as the Quasi-mode-locked (QML) regimes. Categorizing and defining an operation state generated from a PMLFL may differ from a study to a study. However, the general definition of QML regimes include PMLFL operations states with multi-pulse and stochastic behavior. Scientists have reported and studied various regimes of QML fiber lasers including, the soliton molecules, soliton rain , harmonic mode-locking, multi-soliton (MS), symbiotic, noise-like pulse (NLP), etc. Figure 1.2.1 shows examples of QML regimes. All of these regimes operate in the very similar cavity configurations with multiple ultrashort pulses independently, in the form of quasi-stable wave packets, or in the form of both. This happens when some of the cavity parameters are tweaked from the ordinary operating conditions, e.g., when the cavity is highly pumped or the cavity loss or transmission is significantly altered [251, 252].

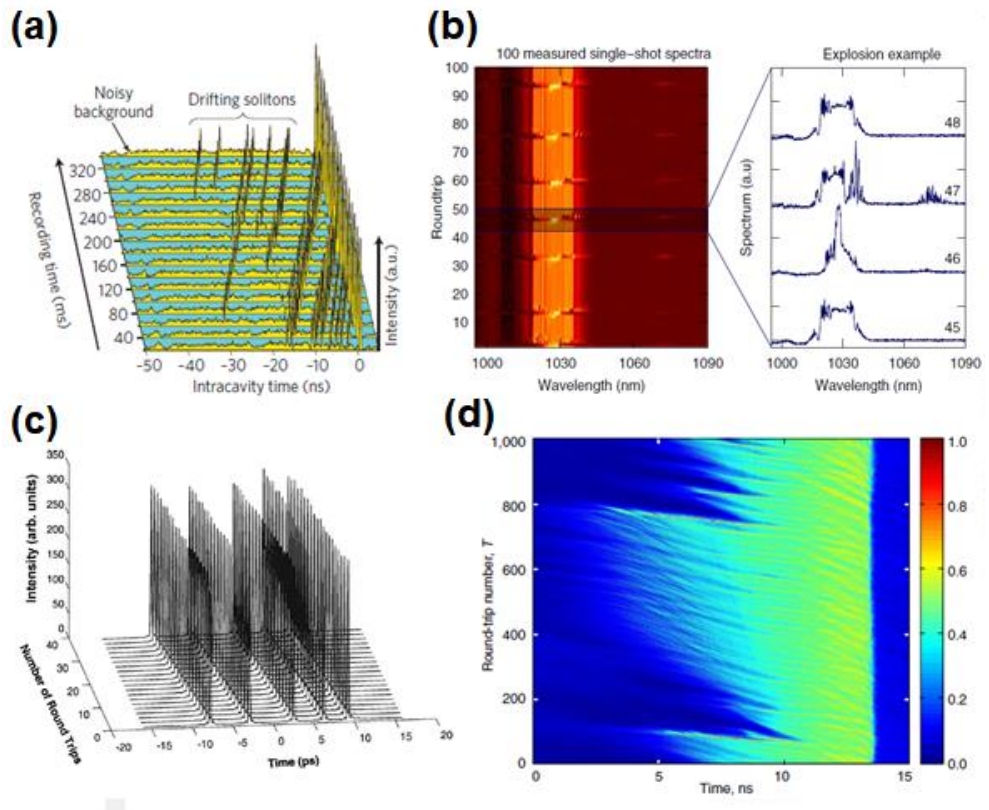

Fig. 1.2.1. QML regimes in fiber lasers: (a) Soliton rain [279], (b) Soliton explosion [280], (c) MS [281], and (d) NLP [282].

Over the past decade, a number of research groups have reported and investigated such extraordinary features accompanied by a variety of types of PMLFLs [251–257]. Among them, study on the formation and operation characteristics of NLP regime was dominant because it was observed regardless of cavity configurations or cavity dispersion regimes [251, 254, 255], and the bunched state of multi-pulse without satellite pulses appeared to be clearly distinct among QML regimes. In general, although the NLPs are randomly generated and distributed, they can eventually form quasi-stable, bunched-pulses traveling at the fundamental repetition rate of the laser cavity

[251]. The autocorrelation trace of NLPs typically shows a coherence spike in the femtosecond time scale located on top of a broad pedestal usually in the picosecond time range. In fact, the latter indicates the actual duration of a whole NLP packet. In addition, NLPs can form very broad output spectra, which are sometimes even broader than the gain bandwidth of the active fiber [256–258] if the intracavity nonlinear effects are significantly involved.

In recent years, a series of research reports presented highlight that the study on the detailed nature of QML regimes can provide a better understanding of the fundamental physics for pulse evolution in nonlinear fiber–optic media, including Raman rogue waves or dissipative solitons in fiber laser cavities [259, 260]. In addition, fiber–based NLP sources make themselves useful in applications of low spectral coherence interferometry [261–263], micromachining [264], supercontinuum generation [265, 266], etc., as shown in Fig. 1.2.2. Thus, the impact of the decade–long research efforts on the fiber–based QML sources cannot be underestimated.

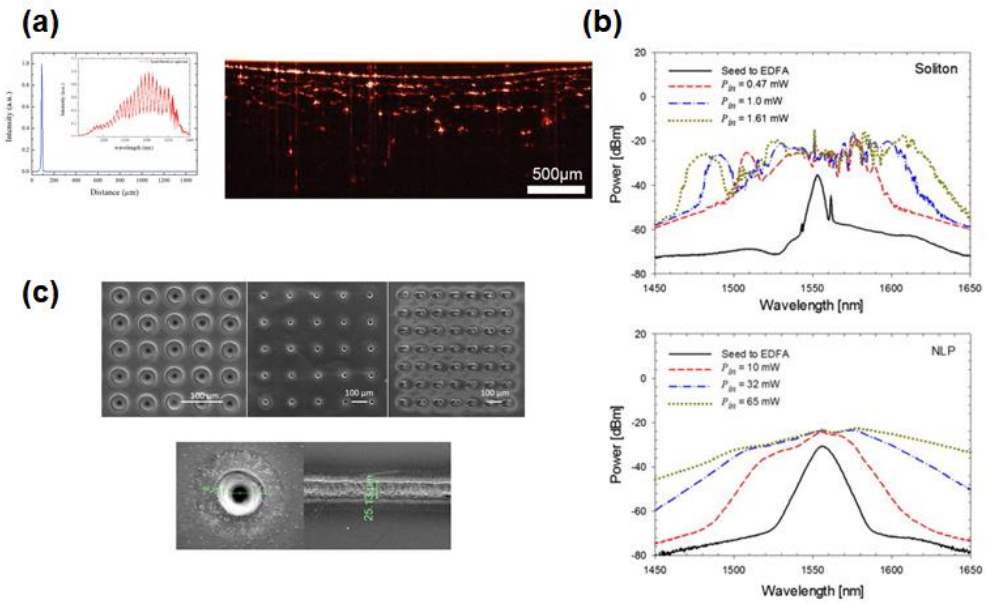

Fig. 1.2.2. Applications of NLP regime: (a) optical coherence tomography [283], (b) suppercontinum generation [284], (c) micro machining [285].

While a description of NLPs in a PMLFL started to appear in the literature in the early 1990s [268], a detailed investigation of their characteristics was first carried out by Horowitz et al. in 1997 [252]. Around that time, fiber-based NLPs started to receive a considerable amount of research attention because of their distinctive, extraordinary features contrasted with ordinarily mode-locked laser pulses [245]. The early results reported mainly on the various typical characteristics of NLPs for different cavity configurations, including anomalous and normal dispersion regimes [253], and also focused on describing the interrelationship between the specific NLP characteristics and the corresponding cavity configurations: Horowitz et al. firstly attributed the formation of the NLPs to the

combination of the cavity birefringence (walk-off effect), the cavity gain, and the nonlinear transmission element [252]. Later on, they also investigated the effects of the cavity dispersion and cavity length in Ref. [269], showing that short cavities with low dispersion tended to generate NLPs with a pulse width of a few ps, whereas longer cavities tended to generate high-energy pulses whose temporal widths increased with pump power. It is worth noting that this regime should not mistakenly be regarded as the so called dissipative soliton resonance regime [248], in which the pulses must encompass a linear frequency chirp, thereby having temporal compressibility. In general, such characteristics do not appear to NLPs because of the absence or near absence of the temporal coherence across the NLP packet. Kang et al. investigated in Ref. [253] the behavior of NLPs as a function of the cavity dispersion in more detail, showing that NLPs could be generated in dispersion-mapped cavities with either anomalous dispersion or normal dispersion. However, in their experiments, broader spectral widths were only obtained from cavities with large normal dispersion [253]. In addition, Lei et al. discussed in Ref. [270] the effect of birefringence of the cavity fiber on the spectral width of NLPs formed in cavities with anomalous dispersion, showing that spectral width broadening was mainly related to the bend-induced birefringence of the cavity fiber. This was further corroborated with numerical simulations using the beat length of the cavity as a variable parameter.

Following the early experimental research on the characteristic features of fiber-based NLPs, a significant amount of attention has

also been paid to analyzing their formation mechanisms. For example, in Ref. [251] Tang et al. suggested that the NLP formation was a consequence of the combined effect of soliton collapse [271] and positive cavity feedback. In Ref. [258], Zhao et al. investigated the dependence of the spectral width of NLPs on the length of the active fiber, reporting that the longer active fibers were used, the broader spectral widths were obtained. For example, they could obtain NLPs with a spectral width of 93 nm in terms of the full width at the half maximum for a 17.6-m length of EDF with anomalous dispersion [258]. In addition, their numerical simulations included the Raman soliton self-frequency shift effect, which could qualitatively explain the increase of the spectral width of the generated NLPs for the long cavity length [258]. In Ref. [254], Zhao et al. reported gain guided solitons and NLPs in an all-normal configuration where they attributed the formation of square-shaped NLPs to the power clamping effect in the cavity. That is, the excessively high pump power could result in increasing the dispersive waves and background noises, thereby initiating the formation of bunch of NLPs.

In addition, there have been a handful of investigations on the formation of NLPs with extraordinarily broad spectral emissions, which could sometimes extend beyond the gain bandwidth of the active fiber included in the cavity [256, 257, 272]. For example, Zhao et al. reported that they could generate NLPs of 120-nm spectral width in an EDF ring cavity configuration when a segment of a fiber of slightly normal dispersion was included in the cavity [257]. They attributed the extra spectral broadening of the NLPs to four-wave

mixing and Raman soliton self-frequency shift effects. North et al. reported on a dual-wavelength NLPs generated in an EDF ring cavity with a ~ 1-km length highly nonlinear fiber. In this experiment, they reported NLPs at 1550 nm could also lead to a second series of Stokes pulses at 1650 nm by means of a Raman conversion process [272]. Spectral width of 135 nm was reported from an NLP oscillator based on a polarization-maintaining EDF ring cavity incorporating a 12-m length highly nonlinear fiber, showing that noise characteristics of the super-broadband NLPs were comparable with those of a typical supercontinunm source based on a conventional fiber-based mode-locked source [256].

In more recent years, there have been a few attempts to analyze the phase fluctuations and noise characteristics of NLPs more precisely [267, 273, 274]. In Ref. [274], Smirnov et al. discussed how the high-frequency phase fluctuations in NLPs impeded the pulse compression, investigating the transition of the operating regime between a single-pulse regime and an NLP regime in the same all-normal cavity configuration. In Ref. [274], Kobstev et al. also highlighted the smooth spectra seen with typical NLPs was a result of averaging over a large number of pulses containing irregular noisy peaks, investigating the NLPs obtained in an all-normal configuration incorporating an ytterbium-doped fiber (YDF). In Ref. [267], Runge et al. could obtain single-shot spectral measurements of a trail of NLPs obtained from a long ring cavity configuration (180 m), quantifying the pulse-to-pulse spectral fluctuations, which showed the lack of phase coherence between consecutive NLP

packets. Figure 1.2.3 shows the spectral fluctuation of NLP regime.

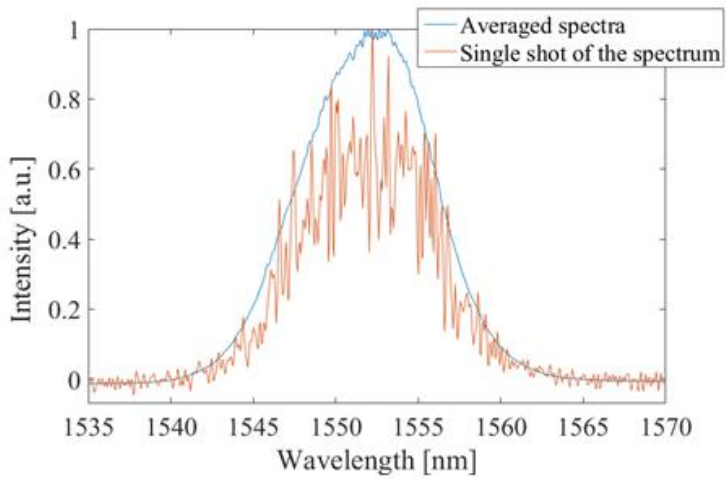

Fig. 1.2.3. Spectral fluctuation and time averaged spectra of NLP.

One may notice that most experimental investigations on fiber-based NLPs have been carried out in ring [251-254, 256-258, 267] or figure-of-eight [255, 266, 275] cavity configurations, exploiting additive-pulse mode-locking techniques to create artificial saturable absorber function [276]. This is due to the fact that artificial saturable absorbers offer a large degree of flexibility in adjusting its effective functional response, compared to novel material-based saturable absorbers, such as semiconductor, carbon-nanotube, and graphene saturable absorbers [277]. In ring cavity configurations, an artificial saturable absorber can be obtained NPR technique, described in the previous section.

Tang et al. have numerically shown that in the case of a laser cavity with anomalous dispersion, the formation of NLPs is caused by the combined effect of soliton collapse and positive cavity

feedback [251, 271]. A cavity operating in soliton regimes, the strength of the critical saturation power limits the range of the peak power of the soliton that can be amplified in the cavity, and eventually determines the stability of the roundtrip oscillation [251]. If the critical saturation power is substantially high, the soliton' s peak power can undergo a rapid growth accompanied by an abrupt narrowing of its pulse width and a consequent broadening of its spectrum. Then, the pulse collapse may occur due to excessive SPM, gain dispersion [251, 271], or higher-order nonlinear effects of the saturable absorber [255]. Once initial solitons are collapsed, new solitons with longer pulse width and shorter spectral width will build up randomly from the residual energy of the collapsed solitons [251]. It is worth noting that in this situation, the cavity is assumed to have a high linear loss. Therefore, new solitons can only be formed at locations where previous solitons have collapsed [251]. If the cavity operates with enough gain to amplify the newly formed solitons, then they will follow the same cycle of amplification and destruction, and will eventually form a trail of random ultrashort pulses. It should be pointed out that as increasing the unsaturated gain in the cavity, i.e., the pump power, dispersive continuum waves may reach the lasing threshold and further be amplified, thereby also contributing to the formation of new pulses [278].

In contrast, in cavities with normal dispersion where the formation of coherent soliton is inherently not allowed, the NLP formation is attributed to the modulation of the pulse wave by strongly amplified dispersive waves and background noises [254]. In

other words, a substantial increment in the cavity gain can make the pulse peak power see higher losses than dispersive waves or background noises do, due to the oversaturation of the saturable absorber, i.e., the pulse peak power passes over the critical saturation power. In this regard, over consecutive roundtrips, the dispersive waves and background noises will be amplified to a significant level. In fact, they can give rise to high modal fluctuations and instabilities, thereby leading to the formation of NLPs.

1.3 Motivation

Fiber lasers are reliable, versatile, and compact source capable of generating high power and ultrafast optical pulses. Not only the conventional means of research approach in achieving high power and desirable pulse operation, fiber lasers can serve as a platform to observe and simulate unique nonlinear phenomena and even phenomena analogous to that of other disciplines. An optical fiber inherits strong nonlinearity due to its tight mode area and long interaction length. Nonlinear effects such as self-phase modulation, stimulated Raman scattering, stimulated Brillouin scattering, etc. are detrimental in some of the applications based on optical fibers but they also offer incredibly rich pulse dynamics.

QML regime is a broad definition and the exact boundary of the QML regime still remains ambiguous up to date due to its broad operation window and unpredictable pulse dynamics. Based on previous research, QML regime normally describes unconventional operation state of mode-locked regime where a cavity holds more than a single pulse in a fundamental roundtrip and shows stochastic behavior where the roundtrip to roundtrip may change periodic or completely chaotic way.

Research based on QML regime is increasingly becoming popular for many reasons. First of all, understanding pulse dynamics in the QML regime is much more difficult than comprehending the pulse dynamics of conventional single pulse regime and there are still many gaps to fill in order to complete QML theory. A cavity with more than

a pulse inside of the cavity can lead to intriguing behavior where pulse-to-pulse interaction starts to play as significant factor in overall pulse dynamics. With the increasing pulse population inside of a cavity, the pulse behavior is even harder to predict and analyze. Second, experimental analysis of such complicated systems was limited due to lack of novel technique or high-speed equipment. Stochastic nature of the QML regime requires a real-time measurement in order to understand their pulse dynamics. Recently, real-time measurement techniques such as the dispersive Fourier transform [286], and the spatio-temporal analysis [282] have been rigorously applied in studying QML regimes enabling extensive investigation in QML regimes beyond the classical means of optical characterization.

Scientists have come up with interesting research results regarding QML regimes and among many intriguing behaviors of QML regimes, I focus on the shot-to-shot coherence characteristics, wave-packet formation and extreme events in QML regimes. The shot-to-shot coherence of QML regime was first studied by Runge et, al. where NLP regime did not exhibit any noticeable shot-to-shot coherence due to the spectral fluctuation. However, my experiment results showed that partial coherence can be observed in QML regimes and the shot-to-shot coherence characteristic of QML regimes cannot be ruled out. Figure 1.3.1 shows experimental evidence of shot-to-shot coherence of NLP regime.

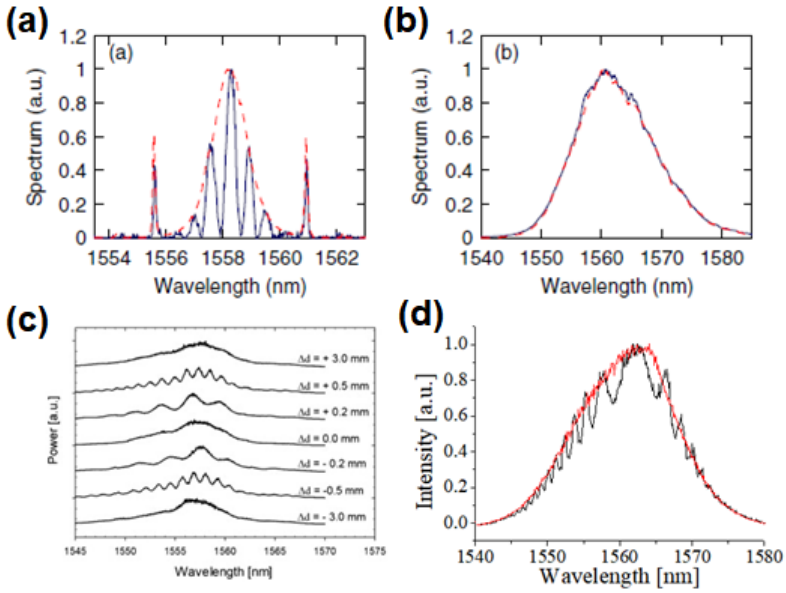

Fig. 1.3.1. Experimental evidence of shot-to-shot coherence of QML regimes in fiber lasers: (a) coherent soliton [267], (b) NLP [267], (c) partially-coherent NLP [284], and (d) symbiotic.

Therefore, in my dissertation, the shot-to-shot coherence of QML regimes is systematically investigated and operational regimes in the QML regimes are categorized more specifically according to their coherence characteristics. I utilized the real-time measurement technique to analyze the pulse dynamics in these regimes to show the strong correlation between NPS induced due to increased pulse intensity and degree of pulse-to-pulse interaction and the shot-to-shot coherence.

In addition to the shot-to-shot coherence property, there have been various attempts to investigate the formation mechanism of NLP wave packet. However, there has not been a study linking MS regime to NLP regime or intermediate state. In this dissertation, I show the

wave-packet formation mechanism is strongly related to the soliton interaction utilizing the spatio-temporal analysis and QML regimes can be regarded single regime with different degree of soliton interaction.

Another interesting and intensively researched area of QML regimes is extreme event generation such as the rogue waves. Due to the chaotic and highly nonlinear nature of QML regimes, they have been a promising platform to observe and study extreme event studies. Rogue waves randomly appear and disappear out of nowhere. Therefore, probability density function of every pulse events for certain amount of time is first measured and normalized to the average intensity of the pulse events. QML regimes with extreme events tend to have histogram with longer tail to the right side representing high intensity pulse events, as shown in Fig. 1.3.2.

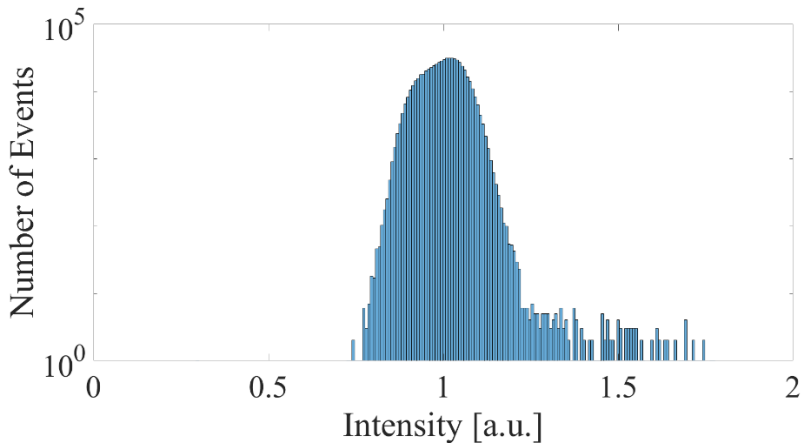

Fig. 1.3.2. Histogram of pulse events normalized to the average intensity of a QML regime.

Extremes events have been studied in various QML regimes.

Different observations were made regarding extreme events and attempt to control these events numerically and experimentally. However, there have not been enough research on extreme event generation in MS regime. MS regime exhibits discrete pulse separation that can be resolved with high-resolution photodiode and high-speed oscilloscope. MS regime can be considered as an adequate platform to investigate extreme event generation without being resolution-limited compared to other QML regimes where single pulse is likely to be veiled in a wave packet and a typical oscilloscope and a photodiode are not fast enough to resolve each pulse to investigate the pulse-to-pulse interactions. In the dissertation, I show that not only rogue waves can be generated from MS regime, they can accumulate to eventually trigger massive wave by increasing soliton population inside of the cavity.

I believe that the experimental results provided in this dissertation provide significant knowledge in the research area of QML regimes observed in fiber lasers. The findings should be beneficial to not only in the area of optics but disciplines working with nonlinear wave dynamics

1.4 Scope and organization

In this dissertation, I analyze different operation regimes of QML regimes in fiber lasers and their characteristics. Mainly, I focus on three regimes of NLP, symbiotic, and MS regimes. Four important topics in QML regimes of fiber laser are discussed in the dissertation: Shot-to-shot coherence, wave-packet formation mechanism, extreme events generation, and super rogue wave triggering. I use spatio-temporal shot-to-shot analysis for real time capturing of pulse evolution in QML regimes. Spatio-temporal analysis is done by using a high-speed oscilloscope and a photodiode to take single shot of huge span, dividing it into the roundtrip time and stacking in an order of roundtrip to obtain a 2D image of roundtrip-to-roundtrip pulse evolution, as shown in Fig. 1.4.1.

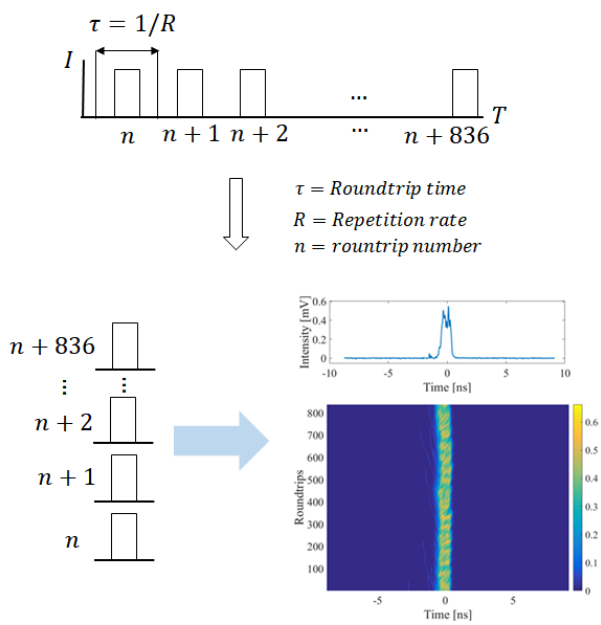

Fig. 1.4.1. Spatio-temporal shot-to-shot analysis.

In Chapter 2, I investigate various operation regimes of QML fiber laser. Focusing on the three regimes of NLP, symbiotic and MS, I explain pulse dynamics in each regime and linking mechanism among these regimes discussing different QML regimes of fiber lasers . Chapter 2.1. shows the experiment setup of the QML fiber lasers. An erbium-doped fiber ring cavity mode-locked by NPR is introduced. Also the measurement technique and equipment for the shot-to-shot coherence and the spatio-temporal measurement are provided in this section. In Chapter 2.2, I discuss the experimental results of QML regimes in fiber laser. In this section, I introduce three main QML regimes of NLP, symbiotic, and NLP and characterize their optical parameters, optical spectrum, autocorrelation, and spatio-temporal measurement. I also show six interesting regimes worth future study. In Chapter 2.3, dedicated discussion on the NLP, symbiotic and MS regime is conducted analyzing the shot-to-shot coherence and wave-packet formation mechanism. Utilizing the real-time shot-to-shot measurement techniques, the source of coherence degradation and wave-packet formation mechanism are revealed with extensive analysis of pulse dynamics of the QML regimes.

Chapter 3 provides analysis of extreme events observed in QML regime of fiber laser, especially in MS regime. In Chapter 3.1, I provide experiment setup of the QML fiber laser mode-locked by NPR and measurement equipment used in the experiment. In Chapter 3. 2, I discuss the experiment results focusing on the extreme events occurring in the MS regime and consequent change in the histogram

and optical spectrum. In this section, increasing number of extreme events without any kind of external cavity modification is reported and discussed. I explain the origin of the cascaded pulse events triggered by probabilistic occurrence of extreme events seeded from soliton collisions. In Chapter 3.3, I provide experimental evidence and discuss super rogue wave triggering from the cascaded pulse interaction observed in Chapter 3.2. In this section, I explain that the cascaded pulse interaction inside of the cavity can occur from probabilistic pulse interaction and dispersive wave synchronization. With enough accumulation of such synchronization, extreme events can occur in a heavily localized manner and eventually trigger super rogue wave.

Finally, I summarize my research and conclude my dissertation in Chapter 4.

Chapter 2

The shot-to-shot coherence and wave-packet formation in quasi-mode-locked regimes

Whilst passively mode-locked fiber lasers (PMLFLs) have extensively been studied as a compact, flexible, and efficient platform for generating coherent and stable ultrashort pulses, such as soliton, Gaussian, dispersion-managed solitons, and dissipative soliton pulses [1-14], they are, in fact, a complex nonlinear dissipative system of a multitude of cavity parameters, including dispersion, nonlinearity, spectral selectivity, amplification, and saturable absorption [15], thereby tending to exhibit a chaotic or stochastic nature of photon dynamics if forced to operate in an extraordinary condition [16-38]. Quasi-mode-locked (QML) regimes that distinctively generate partially coherent or incoherent multiple optical pulses are among such stochastic regimes of PMLFLs [39]. In general, QML regimes emerge when a laser cavity is excessively pumped or amplitude-modulated, regardless of its configuration or dispersion regime, which can be classified into incoherent/partially-coherent noise-like pulse (NLP), symbiotic, and coherent/partially-coherent multiple-soliton (MS) regimes from the perspective of their coherence and packet-forming natures [38-40]. In recent

years a number of investigations on QML regimes have been carried out, aiming to clarify their formation mechanisms and coherence characteristics by means of controlling various cavity parameters, including the degree of nonlinear polarization rotation (NPR) [16–28], the level of pumping [27,38], and the amount of cavity dispersion [16,20,23,38]: Horowitz et al., for the first time, reported the formation of the NLP and described it in terms of the cavity nonlinear transmission and the birefringence of the propagation medium [16]. Tang et al. explained the NLP formation process as a combined effect of the soliton collapse and positive feedback, reporting the MS formation mechanism resulting from the peak–power–limiting effect of the given laser cavity [20,21]. Yet, the detailed chaotic or stochastic nature of QML regimes could not be fully unveiled by means of conventional measurement techniques, such as simple spectral– or temporal–domain measurement techniques [16–24]. Thus, novel techniques, such as the dispersive Fourier transform and spatio–temporal measurement methods have recently been implemented, providing real–time shot–to–shot information of pulse dynamics in QML regimes [34–37]. In fact, with the aid of the real–time measurement techniques, Runge et al. analyzed the coherence property of a QML regime, reporting the lack of coherence in an NLP regime as a result of substantial roundtrip–to–roundtrip spectral fluctuation [36]. Gao et al. attributed the QML formation process to the vector parametric frequency conversion and coherence loss by the intra–cavity polarization rotation [37]. Some of the authors have shown experimental evidences of the existence

of partial coherence in QML pulses, while investigating the characteristic origin of the NLP formation in a fiber ring cavity [38,40].

Notwithstanding, QML regimes have remained obscured in many aspects, including their shot-to-shot coherence properties and wave-packet formation mechanisms, in particular. More recently, the authors have conducted a phenomenological numerical study on the shot-to-shot coherence characteristics of QML regimes in terms of the NPS accumulated per roundtrip [39]. In addition to the numerical analysis, the authors have also presented a preliminary experimental observation that the wave-packet formation in QML regimes could also be initiated by various dynamic interactions among the MS pulses generated in the cavity [40].

In this chapter, I present detailed experimental evidences to expand the frontier of comprehension further to the previous numerical result [39] on the shot-to-shot coherence and wave-packet formation in QML regimes in a fiber ring cavity of anomalous dispersion mode-locked by NPR. With fine adjustment of the cavity saturation power, I make the laser cavity operate in three distinct constitutional regimes of NLP, symbiotic, and MS regimes. I investigate the individual regimes through experimentally analyzing their optical spectra, autocorrelation traces, and the shot-to-shot spatio-temporal evolutions for every roundtrip up to 800-roundtrip times. Based on the experimental results, I discuss the transitional processes among different QML regimes and explain the role of the peak powers of the solitonic pulses in their pulse-to-pulse (i.e., MS)

interactions, which subsequently determines their coherence characteristics and bunching dynamics. In order to elucidate the consequences by MS interactions, I conduct a very dedicated experiment, closely analyzing intermediate states across two adjacent QML regimes in relation with their modulus of the complex first-order degree of coherence (MDOC) characteristics, in which MS pulses are about to cluster or break up right before forming a wave packet or losing it, respectively. I verify that the shot-to-shot coherence trends observed in the experiment are in good agreement with the previous numerical result [39]. I highlight that my experimental results will justify how critically the formation of QML pulses of the three distinct constitutional regimes depends on the degree of interactions among the MS pulses within the cavity, which is, in fact, closely correlated with the peak-power levels of the MS pulses and the NPS accumulated within the cavity.

2.1 Experiment Setup

Figure 2.1.1 depicts the schematic of the fiber laser utilized in my investigation. It was a passively mode-locked fiber ring laser based on NPR. The active medium was an erbium-doped fiber (EDF) with an absorption coefficient of 6 dB/m at 1530 nm. It was core-pumped at 980 nm with a single-mode diode laser through a wavelength division multiplexer (WDM). An additional WDM placed after the EDF removed unabsorbed pump power. The combination of a fiberized polarizing beam splitter (PBS) and two in-line polarization controllers (PCs: λ/4-λ/2-λ/4) spliced before and after the PBS, offered the functionality of fast-response saturable absorption.

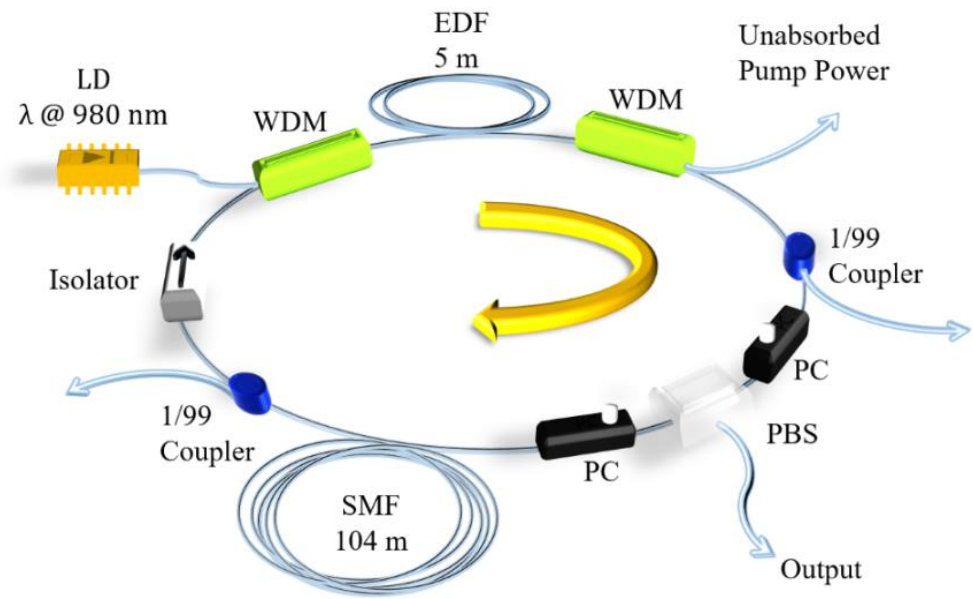

Fig. 2.1.1. Experimental setup for a passively mode-locked EDF ring laser cavity based on NPR.

The two 1/99 tap couplers were placed before and after the PBS in

the cavity to monitor pulse evolution inside the cavity. The polarization insensitive isolator on the left side was incorporated to maintain unidirectional operation of the cavity. The total length of the cavity was ~ 120 m and had a net anomalous dispersion of β_2 ~ –2.95 ps^2. At low pump power (< ~ 65 mW) the cavity operated in the single-soliton regime, generating a single soliton per cavity roundtrip having pulse width of ~ 3 ps and bandwidth of ~ 4 nm, which varied slightly, depending on the specific conditions of the PCs. In fact, the single-soliton regime tended to be obtained by first increasing the pump power up to ~ 65 mW and carefully decreasing it down to ~ 40 mW owing to the pump hysteresis effect [21]. In contrast, at high pump power (> ~ 151 mW) the cavity operated in QML regimes, including NLP, symbiotic, and MS regimes. It is worth noting that there existed various intermediate or transitional states that did not clearly fall into the categories of the aforementioned regimes for very specific conditions of the PCs even without changing the pump power level. I are not going to discuss all of them in this paper, but believe that some of them may be worth to report elsewhere with a more thorough examination and further discussion.

Figure 2.1.2 depicts the fiberized Michelson interferometer utilized to measure the shot-to-shot coherence of the QML pulses generated from the laser cavity shown in Fig. 2.1.1.

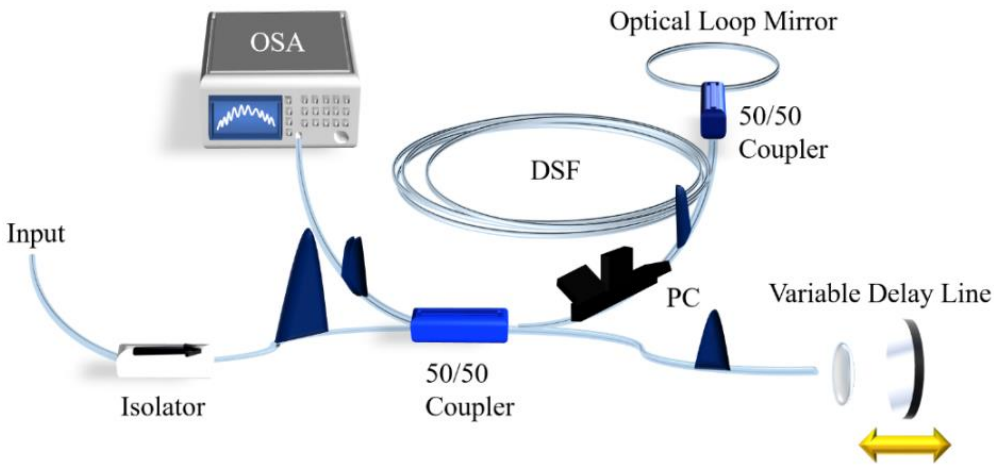

Fig. 2.1.2. Fiberized Michelson interferometer utilized for pulse characterization.

The 50/50 tap coupler equally split the input signal (i.e., the output QML pulses from the laser cavity) into two arms: A half of the input signal into one end of the coupler was reflected by an optical loop mirror through a dispersion-shifted fiber (DSF). The use of the DSF was mainly to avoid unnecessary pulse broadening due to dispersion of the standard single-mode fiber (SMF) at ~ 1550 nm. The other half of the input signal into the other end of the coupler was reflected by a high-reflecting broadband dichroic mirror through a free-space variable delay line. It is worth noting that the length of the DSF was roughly determined to provide a single-roundtrip path difference between the optical pulses returning through both ends of the coupler, and that the free-space delay line was fine-adjusted to maximize the overlap between the two returning optical pulses once they had been combined together through the third end of the coupler

connected to the optical spectrum analyzer (OSA). In fact, the combined optical pulses with a single-roundtrip path difference produced an interference fringe pattern, the fringe visibility (FV) of which corresponded to the MDOC of the output signal of the laser cavity.

I also measured its autocorrelation trace using an autocorrelator (FR-103XL, Femtochrome), which gave us the information on the spike-to-pedestal ratio (SPR) and the average pulse-width when it formed a wave packet. An autocorrelation trace of a typical NLP normally consisted of a sub-ps coherent spike on top of a broad shoulder from a hundreds of picosecond (ps) to nanosecond (ns) pulse-width [38]. This characteristic trace represented a group of sub-ps pulses irregularly distributed and bunched in an even wider temporal window. In contrast, the trace of the signal optical pulse in an MS regime only exhibited a single peak without forming a broad shoulder. Besides recording the spectral interference pattern and autocorrelation trace, I also carried out spatio-temporal measurements on the output QML pulses for up to 800 consecutive roundtrip times, using a photodetector having a 45-GHz bandwidth and a high-speed oscilloscope having an ~ 80-ps-time-scale resolution (DSO91204A, Agilent: 12-GHz bandwidth and 40-GS/s sampling rate).

2.2 Experiment result

I pumped the EDF of the cavity at ~ 220 mW to make it operate in QML regimes. A specific QML regime could be picked up by adjusting the PCs. Most of them resembled the regimes already observed in previous studies [16–38], whereas some others appeared to be exclusively different from any previously reported regimes in very particular conditions. Notwithstanding, relying on the MDOC and SPR measures, I could identify and classify them into the most dominant, three constitutional regimes, i.e., the NLP, symbiotic, and MS regimes [39,40]. In fact, the specific regimes discussed in the previous numerical study [39] could readily be reproduced within the operation windows of the three constitutional regimes. They exhibited clear distinctions in terms of the spectrum, interference fringe pattern, and autocorrelation trace for the output signal, as shown in Fig. 2.2.1. It should be noted that the maximal scan range of the autocorrelator used in my experiment was set to ~ 200 ps.

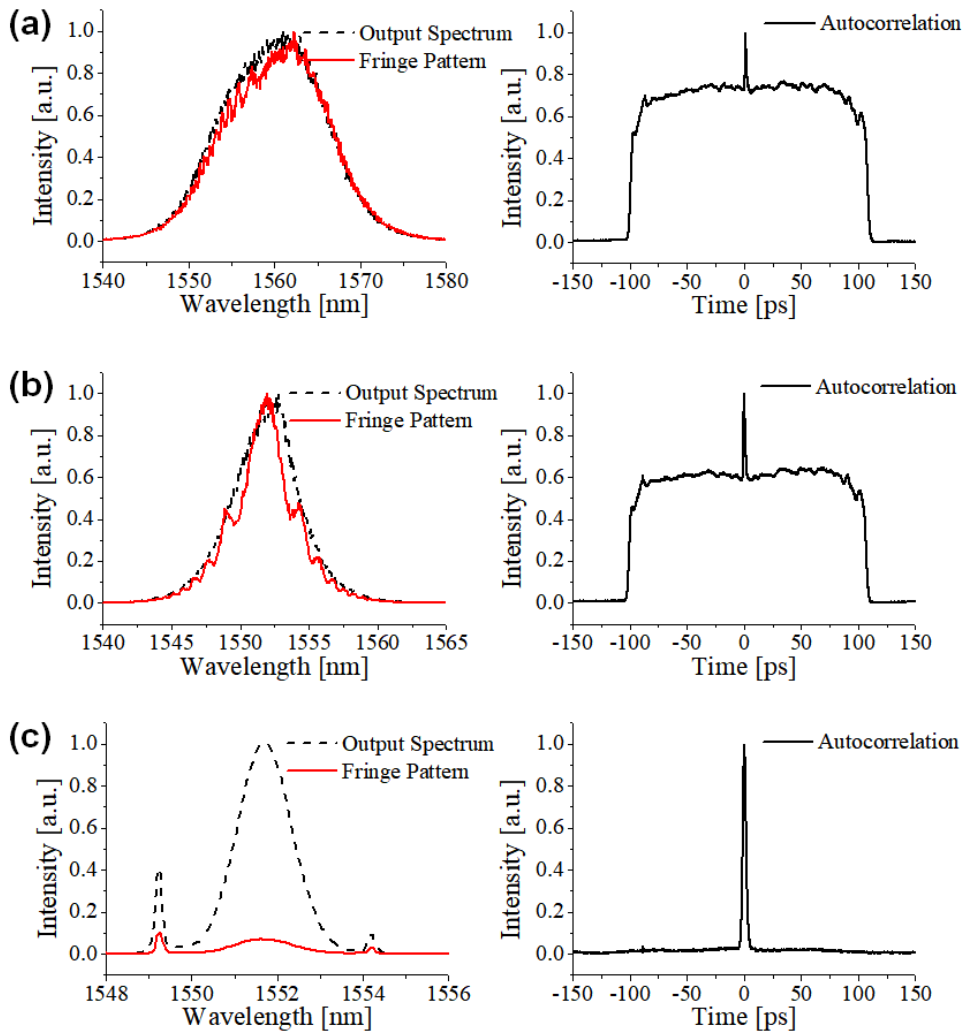

Fig. 2.2.1. Spectra, interference fringe patterns, and autocorrelation traces of typical QML pulses: (a) the NLP regime, (b) the symbiotic regime, and (c) the MS regime.

In addition, I conducted the real-time spatio-temporal measurement, tracing the shot-to-shot pulse evolutions up to 837-roundtrip times, as shown in Fig. 2.2.2. It is worth noting that all the intensities are normalized relative to the maximum value obtained from the NLP

regime, which will hereafter hold in this chapter unless stated otherwise.

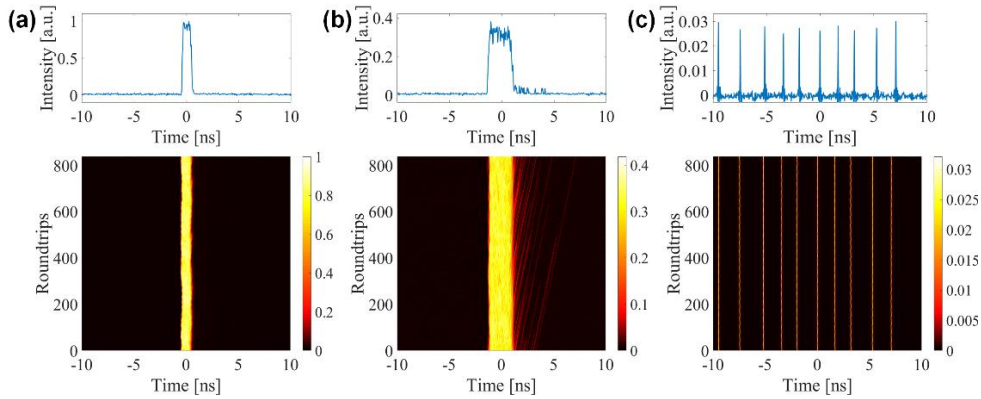

Fig. 2.2.2. Spatio-temporal shot-to-shot measurement results: (a) the NLP regime, (b) the symbiotic regime, and (c) the MS regime. Note that the color bars represent the matched normalized intensities.

NLPs are normally characterized by their broad spectrums, wave-packet containing sub-pulses, and an autocorrelation trace of a coherent spike on top of a broad shoulder, which may vary slightly depending on the precise cavity conditions [16-20]. From the viewpoint of specific experimental observation on my laser system, I specifically defined the NLP regime as the case in which the output signal had a broad spectrum of > 10-nm bandwidth, a moderate pulse width of < 1 ns, and an autocorrelation trace with SPR of < 0.293. In the NLP regime, the output signal was comprised of a group of optical pulses tightly confined within a wave packet, which had substantially higher intensities in comparison with those operating in the other two regimes. Satellite pulses outside the main wave packet were hardly present as clearly shown in Fig. 2.2.2(a). In addition, it is worth

noting that this regime resulted in the lowest MDOC, i.e., the shot-to-shot coherence measure, as reported in the previous numerical study [39].

By slowly tweaking the PCs further, I could make the cavity operate in the symbiotic regime [39,40], observing that the bandwidth of the output spectrum was reduced to as low as ~ 5 nm. The tightly bunched optical pulses within a wave packet (previously in the case of the NLP regime) started to be released a bit, thereby holding a loosely confined wave packet approximately 4 to 5 times as broad as that of the NLP regime. In the autocorrelation trace, I could observe that the relative height of the coherent spike on top of the pedestal became taller than that of the NLP regime. The distinct, characteristic feature of the symbiotic regime was the fact that a main wave packet and satellite solitons could coexist in the cavity. They could interact or propagate independently, depending on the precise cavity conditions. For example, satellite solitons could remain separate from the main wave-packet, being stationary or running away from it; in some cases they could rejoin the main wave packet after moving around and interacting with others; etc. Thus, in Fig. 2.2.3, I illustrate in more detail various characteristic features of the symbiotic regime obtained from the cavity with fine adjustments of the PCs.

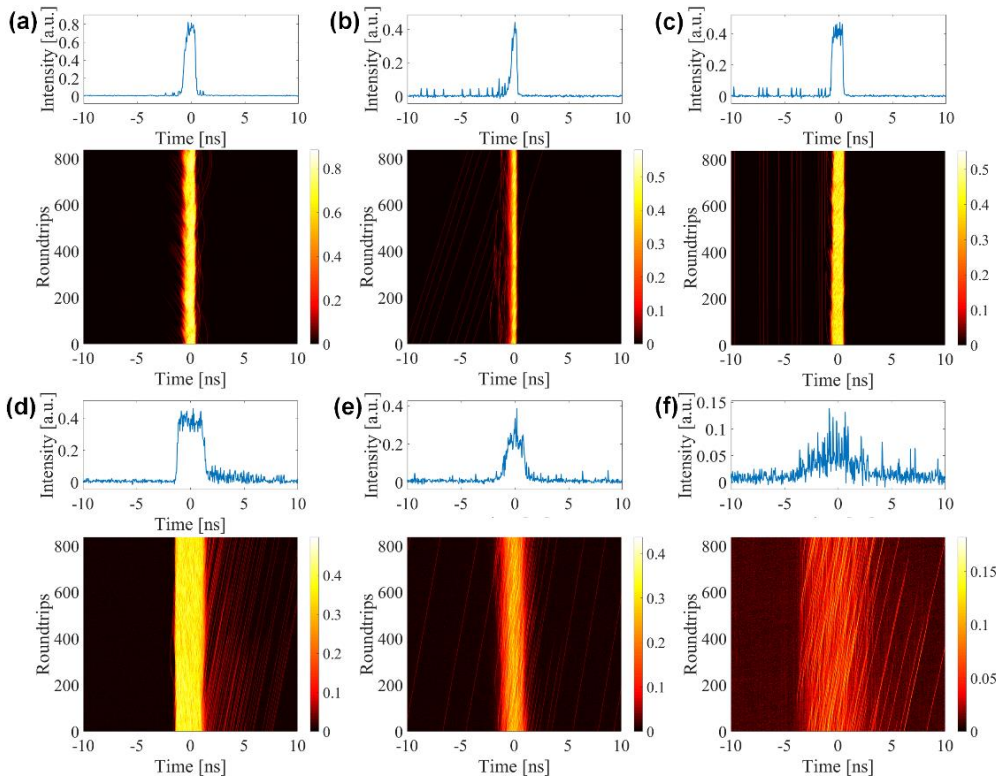

Fig. 2.2.3. Spatio-temporal shot-to-shot measurement results for various states of the symbiotic regime: (a) the tear-drop state, (b) the inclined rain state, (c) the straight rain state, (d) the radiating state, (e) the tornado state, and (f) the hurricane state. Note that the color bars represent the matched normalized intensities.

In general, the symbiotic regime had a wide operational range in between the NLP and MS regimes, so that it tended to exhibit various characteristic features in terms of wave-packet-to-soliton interactions. I classified them into six sub-groups in terms of phenotypic behaviors of the regime, which included the tear-drop, inclined rain, straight rain, radiating, tornado, and hurricane states (see Fig. 2.2.3). It is worth noting that some of them seemed to resemble what had been reported [25], but others did not. I noticed

that the cavity conditions for triggering the symbiotic regime was quite close to that for the NLP regime. As a result, the overall shape of the main wave packet was quite similar to that of the NLP regime. It is, however, worth noting that the intensity of the main wave packet in the presence of satellite solitons, i.e., in the symbiotic regime, became significantly lower than that in the NLP regime [see the relative intensity levels in Figs. 2.2.2(b) and 5 in comparison with that in Fig. 2.2.2(a)].

By tweaking the PCs even further, I observed the main wave packet eventually collapse into MS pulses [21], so that the symbiotic regime turned into the MS regime. The collapse of the wave packet can be explained as a result of the decrease in binding forces among solitons that will be discussed in detail in chapter 2.3. During this process, the shot-to-shot coherence gradually increased as the cavity condition turned away from the NLP regime. In the MS regime, well-separated solitons were the only optical pulses that could exist in the cavity, which were, however, capable of forming neither bunched pulses nor a wave packet. These solitons travelled at the same group velocity. The spectrum of the output signal in the MS regime was nearly identical to that of a conventional single-soliton pulse with Kelly sidebands. In the MS regime, the autocorrelation trace was comprised of a single coherent spike without having any broad pedestal, indicating the complete temporal separation between adjacent solitons in the span of at least 200 ps (i.e., the maximal scan range of the autocorrelator used in my experiment). The shot-to-shot coherence reached close to unity in this regime

On the whole, I could clearly notice that the MDOC tended to increase as I altered the cavity condition from the NLP regime to the symbiotic regime, and subsequently to the MS regime [see Fig. 2.2.1]. In particular, the NLP regime exhibited the lowest MDOC, ranging from 0.0204 to 0.125. I also noticed that the evolution of the SPR with respect to the PC adjustment showed the very similar trend as the MDOC did. In fact, the NLP regime had the lowest SPR, decreasing down to 0.293 [see Fig. 2.2.1(a)]. The MDOC of the symbiotic regime ranged from 0.1 to 0.562. The corresponding SPR could increase significantly up to 0.412 [see Fig. 2.2.1(b)]. The measured MDOC and SPR values indicate that QML pulses in the symbiotic regime exhibited significantly increased partial coherence and decreased pulse complexity in comparison with those in the NLP regime. The MDOC kept on increasing in the symbiotic regime as the cavity condition turned further away from the NLP regime. However, once the MDOC had reached beyond 0.869, the main wave packet eventually collapsed, and the operating regime of the cavity was switched to the MS regime. In the MS regime, the MDOC was greater than 0.869, and the SPR was as close as unity. That is, QML pulses operating in the MS regime exhibited nearly complete coherence as well as clear separation between consecutive pulses. The general trends of these experimental observations were in accord with the previous numerical work [39]. Table 1 summarizes the operation parameters of the QML regimes.

TABLE 2.2.1. OPERATION PARAMETERS OF THE QML REGIMES.

Operation parameters	Noise−like pulse	Symbiotic	Multi−soliton
Pump power	~ 151 mW	~ 151 mW	~ 151 mW
Bandwidth	> ~ 10 nm	~ 10 to ~ 4 nm	~ 4 nm
Wave packet/Pulse width	~ 0.9 ns	~ 1 to ~ 5 ns	~ 3.1 ps
SPR	~ 0.293	~ 0.412	~ 1
MDOC	0.0204 to 0.125	0.1 to 0.562	> 0.869

2.3 Discussion

In this section, I further discuss the shot-to-shot coherence properties of QML pulses, paying more attention to their correlation with the formation of a wave packet within the cavity. In the experiment, I kept the cavity length constant and precisely varied the saturation power via tweaking the PCs. Subsequently, I were able to monitor in real-time the subtle changes in the optical pulses built up in the cavity across the transitional moment between two different QML regimes, fully taking advantage of the spatio-temporal measurement technique. Phenomenologically, it was very important to resolve out such transitional behaviors in conjunction with measuring the corresponding MDOC and autocorrelation trace at the same time, because this allowed us to identify the cause and effect of soliton interactions in relation with the formation of a specific type of QML pulses.

While taking spatio-temporal measurement on QML pulses triggered under various cavity conditions, I observed two types of soliton interactions take place dominantly, which included a "local" type of soliton interaction via radiative dispersive waves and the "direct" soliton interaction [41-44]. It is worth noting that a "global" type of soliton interaction induced by unstable continuous-wave (CW) components [44] was not apparent, because the transitional QML pulses were primarily initiated from the MS regime, so that there were initially no noticeable CW components built up in the cavity. In addition, I could control the overall strengths

of solitons generated in the cavity as well as their separation intervals by means of varying the saturation power of the cavity via tweaking the PCs. In fact, the higher saturation power led to the higher loss being imposed onto the optical pulses in the cavity, thereby resulting in the lower intra-cavity soliton intensity, and vice versa.

I initially set the cavity conditions such that the operation regime was in an intermediate state in between the MS and symbiotic regimes, in order to take precise snapshots on the transitional behaviors of QML pulses across them. For example, two typical intermediate states are depicted in Fig. 2.3.1. The graphics on the upper half represent a state that was set closer to the MS regime [see Figs. 2.3.1(a)-2.3.1(c)], whereas those on the lower half represent a state that was set closer to the symbiotic regime [see Figs. 2.3.1(d)-2.3.1(f)]. Both intermediate states were accessible from the stabilized MS regime, in which the separation intervals among solitons were normally maintained more than 1 ns [see Fig. 2.2.2(c)]. By lowering the saturation power of the cavity, the overall intra-cavity soliton intensities tended to grow, and subsequently, the separation intervals among solitons became reduced.

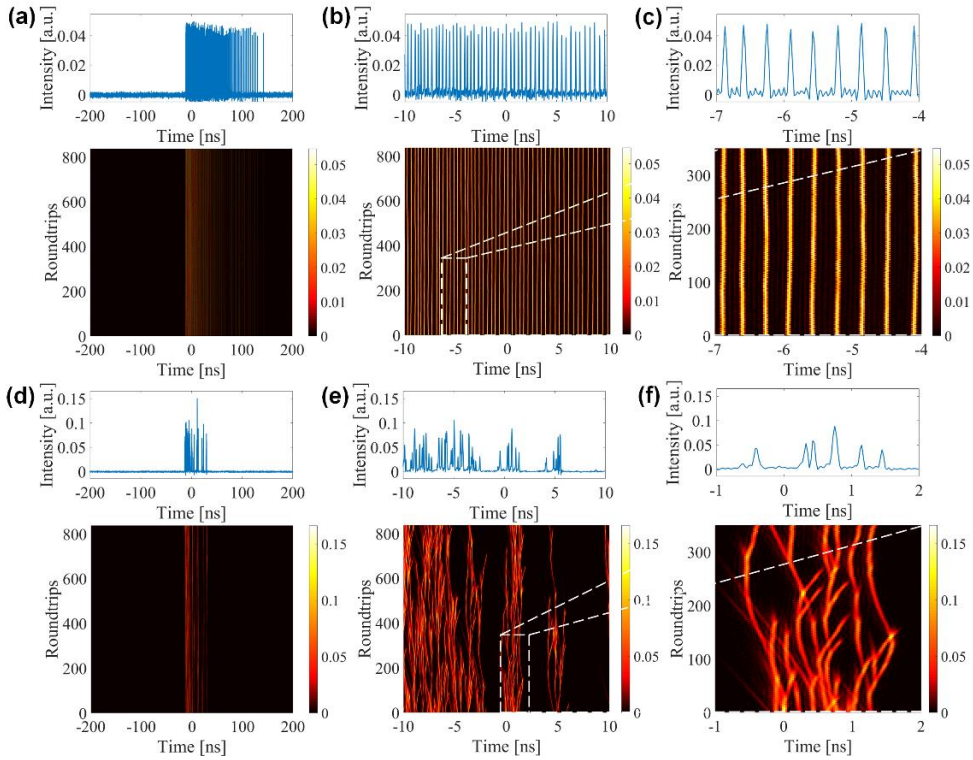

Fig. 2.3.1. Solitons in intermediate states: An intermediate state closer to the MS regime (a) in a 400−ns span, (b) 20−ns span, and (c) 3−ns span; an intermediate state closer to the symbiotic regime (d) in a 400−ns span, (e) 20−ns span, and (f) 3−ns span. Note that the color bars represent the matched normalized intensities.

In the former case shown in Figs. 2.3.1(a)−2.3.1(c), the intra−cavity solitons started to line up closely to one another with the increase of their overall intensities, and their separation intervals were significantly reduced to less than ~ 250 ps, so that the individual solitons seemed to have non−negligible influences on the adjacent solitons. It is worth noting that in this case the corresponding soliton interactions incorporated mainly a local type of soliton interaction [44], in which the increase in the soliton intensities resulted in

elongating the effective range of the radiative dispersive waves generated from the individual solitons, thereby giving rise to long-range resonant soliton interactions. However, the characteristic features of the MS regime was still more or less maintained, such that its optical spectrum remained within ~ 3-nm bandwidth, including Kelly sidebands, and the MDOC remained above at least 0.8. Figures 2.3.1 (b) and 2.3.1 (c) show the intermediate state in smaller spans of 20 and 3 ns, respectively. Owing to the effect of the local type of soliton interaction, the trail of solitons evolved with roundtrip times, lining up in a rather wiggly manner in the spatio-temporal domain as compared with that of the exact MS regime [compare Fig. 2.3.1(c) with Fig. 2.2.2(c)]. In general, solitons in the MS regime did not exhibit such behaviors, mainly because they had even wider soliton separation than 1 ns and even lower soliton peak intensity than 0.026, so that individual solitons and the corresponding dispersive waves could hardly interact within the cavity length, even between the nearest neighboring solitons.

By tweaking the PC even further, I could make the cavity operate with relatively higher peak intensity and with more soliton interactions [see Figs. 2.3.1(d)-2.3.1(f)]. This resulted in even higher degree of local-type soliton interactions and eventually making adjacent solitons interact directly. Figures 2.3.1(e) and 2.3.1(f) show that both local-type and direct soliton interactions were taking place simultaneously in smaller spans of 20 and 3 ns, respectively. In result, the solitons tended to evolve with roundtrip times in a tree-branch or lightning-strike manner in the spatio-

temporal domain, maintaining an average group velocity but with inter-solitonic collisions, attractions, and cross-overs, depending on their inter-solitonic phase differences [41,44]. Their intensities were noticeably higher than those of the solitons in the MS regime as well as in the former intermediate state. It is important to note that in this intermediate state, the optical spectrum looked more like that of the symbiotic regime, having bandwidth of ~ 5 nm, and the MDOC was reduced down to ~ 0.55, which was significantly lower than that of the former intermediate state. Actually, the further intensified soliton interactions increased soliton complexity, which in turn led to the optical spectrum losing the Kelly sidebands as shown in Fig. 2.2.1 (b). I also observed that even stronger soliton interactions could occasionally trigger rogue-wave-like behaviors during some inter-solitonic collisions [45], which are, however, outside the scope of my current discussion.

On the whole, both intermediate states exhibited significantly different features in their optical spectra and MDOC values, depending on the degree of soliton interactions in the cavity. In fact, the stronger soliton interactions led to the higher shot-to-shot fluctuations, thereby causing the lower MDOC values. The cavity condition in which such intermediate states could hold was relatively very tight that they tended to be short-lived, readily settling down into the symbiotic or MS regime if they were not exactly fit to survive. This was due to the fact that the degrees of soliton interactions grow "exponentially" with respect to increase in the intra-cavity soliton intensity as well as to decrease in the soliton separation interval

[41-44]. For example, when I further increased the intra-cavity soliton intensity from the intermediate states discussed above, the cavity regime abruptly made transition into the symbiotic regime close to the states shown in Figs. 2.2.3(e) and 2.2.3(f) where the formations of the solitons were already exhibiting a wave-packet-like feature, such that they were closely spaced, vividly interacting within a ~ 10-ns time window and having high relative intra-cavity intensities of well above 0.1. The whole wave-packet formation process can also explain the collapse of the wave packet that tended to happen when the intra-cavity soliton intensity was reduced beyond a certain critical value, with which the cavity could manage to bind individual solitons within a packet. Just like the wave-packet formation process, the transition from a wave packet to free running solitons was also an abrupt process.

I emphasize that both intermediate states, which I managed to spot and analyze by means of the real-time shot-to-shot measurement as discussed above, provide a way to finding the missing links between the formation of a wave packet of quasi-randomly-packed solitons and the intra-cavity soliton interactions. This aspect has been remaining unclear to date due to the fact that such regime transitions take place too abruptly and instantaneously to detect via conventional measurement methods. Whilst I were resolution-limited in analyzing the more detailed inter-soliton dynamics within the wave packet, my experimental observations somehow manifest that the growth of the intra-cavity soliton complexity, i.e., the degradation of the MDOC after the formation of

a wave packet out of multiple intra-cavity solitons was, in fact, triggered by strong soliton interactions, which were further parameterized by the intra-cavity soliton intensity and inter-soliton separation. Subsequently, it has become obvious that further increasing the intra-cavity soliton intensity from the symbiotic regime could readily lead to the regime transition into the NLP regime, which has the tightest soliton confinement in the wave packet and the highest intra-cavity soliton intensity among the three constitutional regimes. Therefore, one can expect that the corresponding MDOC would further degrade certainly via the strong NPS induced every roundtrip and the chaotic nature of the inter-soliton dynamics inside the wave packet. It is fair to say that the NLP or symbiotic regime in an anomalous-dispersion fiber ring cavity is an extreme operation state achievable when the soliton interaction is sufficiently intense.

In the previous numerical study [39], I showed that the MDOC is strongly correlated with the NPS induced to the intra-cavity solitons per roundtrip. In fact, an absolute experimental measurement of the NPS induced per cavity roundtrip would make a direct comparison with the numerical result previously obtained [39]; however, my spatio-temporal detection was resolution-limited to ~ 80 ps, so that it was not fast enough to measure and trace out the exact peak powers of the individual intra-cavity pulses that tended to be as short as sub- or a few ps (see the autocorrelation traces shown in Fig. 2.2.1). Thus, I would instead like to take the total intra-cavity intensity in order to make a relative comparison between the experimental and numerical results, because the total intra-cavity

intensity should obviously be proportional to the NPS accumulated per roundtrip. It is worth noting that the total intra-cavity intensity can readily be estimated by simply integrating the spatio-temporal detection data without justifying the exact peak powers of the individual intra-cavity pulses. Figure 2.3.2 shows the experimentally measured MDOC values for the 34 individual QML states classified into the three constitutional QML regimes, relying on the criteria given in Section 2.2, with respect to the relative total intra-cavity soliton intensity that is normalized to the maximum value obtained in the case of the incoherent NLP regime.

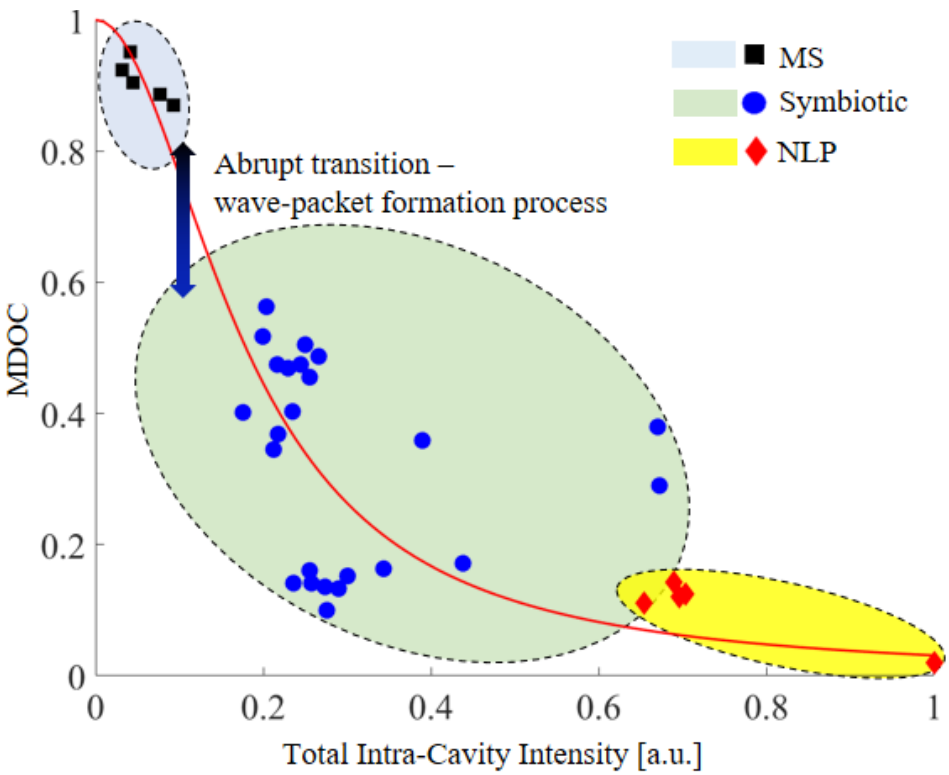

Fig. 2.3.2. Experimental data on the MDOC with respect to the relative total intra-cavity intensity; red solid line: Lorentzian fitting curve. All the data points are classified into the corresponding QML regimes, relying on the criteria given in Section 2.2.

In Qualitatively speaking, the general trend of the MDOC distribution is in good agreement with that obtained in the numerical study [39], which was also well fitted with a Lorentzian fitting curve, as shown in Fig. 2.3.3. (See Ref. [39]: Roughly, the normalized total-intra-cavity intensity parameter multiplied by a factor of ~ 10 would lead to a good match with the corresponding NPS per roundtrip.)

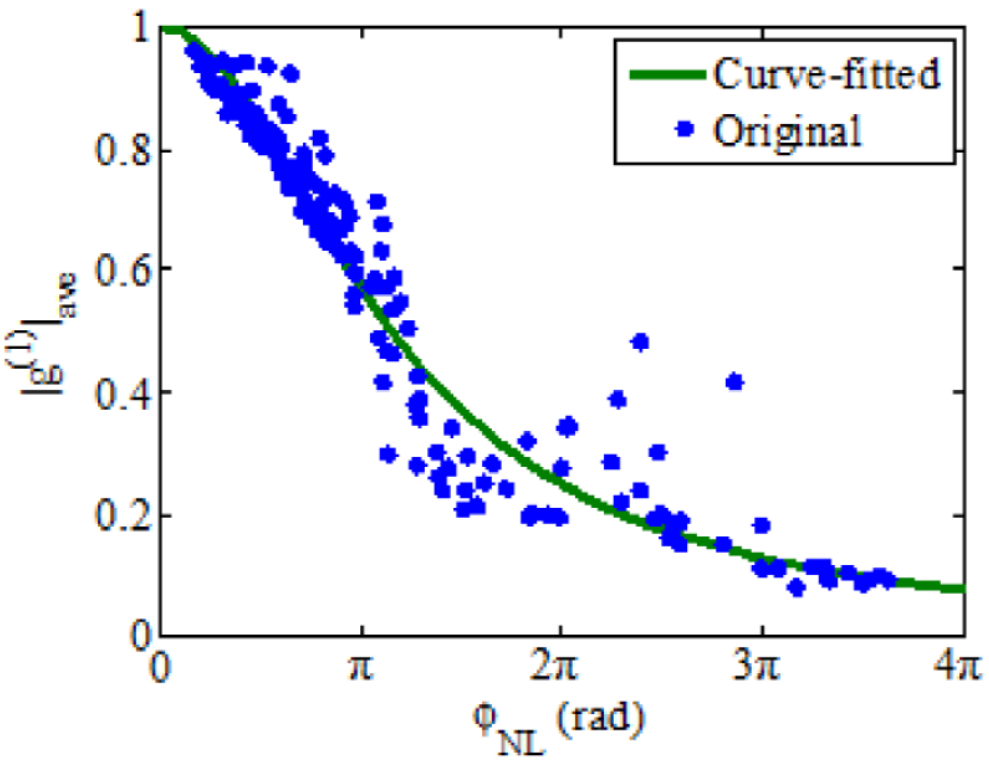

Fig. 2.3.3. Averaged MDOC as a function of the NPS per RT. The blue dots and the green curve represent the original data set and the fitted curve with a Lorentzian distribution function, respectively.

Thus, I stress that the strong correlation between the MDOC and the NPS per roundtrip, i.e., the total intra-cavity soliton intensity,

predicted by the numerical study has now been confirmed by the experimental observation.

Chapter 3

Extreme events and intermittent burst of super rogue wave in quasi-mode-locked regimes of fiber laser

History of monstrous waves, most commonly known as rogue waves, in the ocean that appear and disappear without a trace goes back to hundreds of years as only lore among sailors to prove their existence until a scientific observation verified that these waves are indeed product of nature and regularly observed in the deep sea environment [1]. Initial research focus on these rogue waves was in the field of oceanography to understand and overcome their disastrous and unpredictable characteristics to assist human activity in the ocean [1−8]. Because the rogue wave study in the ocean was stochastic and large−scaled, it was time consuming and required expensive equipment. Therefore, rogue waves in platforms other than the ocean started to draw considerable interest as a possibility for a smaller−scaled research platform, one of them being optical platform [9−12]. Optical platform, in which the light wave analogous to the ocean wave with incomparably faster and smaller scale, allows rogue wave research for greater science community. Ever since Solli et al. first reported optical rogue waves in the optical fiber based super continuum [13], research interest in the optical rogue waves

rocketed and spread to various optical platforms [14]. Number of rogue wave research has been conducted in different platforms of the excessively pumped passively mode-locked fiber lasers (PMLFLs). PMLFLs are a compact, flexible, and efficient platform known to generate stable ultrashort pulses[15-20]. However, PMLFLs are complex nonlinear dissipative system and if forced to operate in an extraordinary condition, normally known as quasi-mode-locked (QML) regimes, they exhibit a chaotic or stochastic nature of photon dynamics making them favorable platforms to observe rogue waves [21-45].

Among different regimes of QML regimes, multi-soliton (MS) regime is an ideal regime to observe rogue waves experimentally since it provides well-defined pulse dynamics compared to other QML regimes where pulses are likely to form a wave packet [30-36]. MS regime is a soliton complex in which multiple solitons are present in the cavity [33-36] and compared to single soliton operation, the behavior and physics of MS regime is highly nonlinear, and complex . The complexity arises from the fact that MS regime holds tens or even hundreds of solitons depending on the cavity configuration where these solitons are not always independent to one another, but interacting in many cases. In addition, dispersive waves shed from the solitons drive pulse dynamics in the cavity even more complex. Therefore, MS regime can operate in intriguing manner with just the slightest change in the inter pulse dynamics and serve as similar platform as the open ocean to study extreme events. Recently, soliton collision resulting in rogue wave generation in dissipative

system and rogue waves generated from soliton collision and soliton focusing mechanism have been reported [35,36]. However, due to the chaotic and random nature of rogue wave, analysis of the phenomenon has not been trivial and the rogue wave generation in MS platform still require thorough study.

In this paper, I report for the first time extraordinary RWs intermittently triggered with an interval in the order of no longer than ten seconds in the MS regime of a nonlinear-polarization-rotation (NPR)-mode-locked, anomalous-dispersion fiber ring cavity. I call them "super RWs" as their intensities exceed over ten times the average intensity of all events. With fine adjustment of the cavity saturation power, I make the laser cavity operate in an extremely narrow window of a heavily populated MS state, in which soliton interactions can grow rapidly in a cascade of interactions among solitons and dispersive waves once triggered. I investigate this specific MS regime by stochastically analyzing its shot-to-shot spatio-temporal behaviors in comparison with the dynamic changes observed in its optical spectrum, and eventually manage to capture the moment of intensifying dispersive-wave synchronization in the cavity, which culminates to a super RW burst. Based on the systematic, spectral and spatio-temporal measurements, I testify that the intensifying dispersive waves also signified in the gradual and abnormal increase of the Kelly sidebands, coincide with the elongation of the histogram distribution of the pulse events to the extreme events, and that their intermittent growth and collapse exactly match the cycle of the super RW burst. I stress that the origin

of the super RW burst in the MS regime is strongly correlated with the initial build-up and strong localization of constructively interfering dispersive waves and a cascade of interactions among the solitons and dispersive waves. I unveil and discuss further details in the following.

3.1 Experiment setup

Figure 3.1.1 shows the schematic of the experimental setup. I passively mode-locked fiber ring cavity based on nonlinear polarization rotation (NPR) with a fiberized polarizing beam splitter (PBS) and two in-line polarization controllers (PCs: λ/4-λ/2-λ/4) spliced before and after the PBS to achieve a fast-response saturable absorption. Erbium-doped fiber (EDF) with an absorption coefficient of 6 dB/m at 1530 nm was core-pumped at 980 nm with a single-mode diode laser through a wavelength division multiplexer (WDM). An additional WDM spliced after the EDF removed unabsorbed pump power. The polarization insensitive isolator on the left side maintains unidirectional operation of the cavity and the two 1/99 tap couplers were placed before and after the fast saturable absorber to monitor pulse evolution inside the cavity.

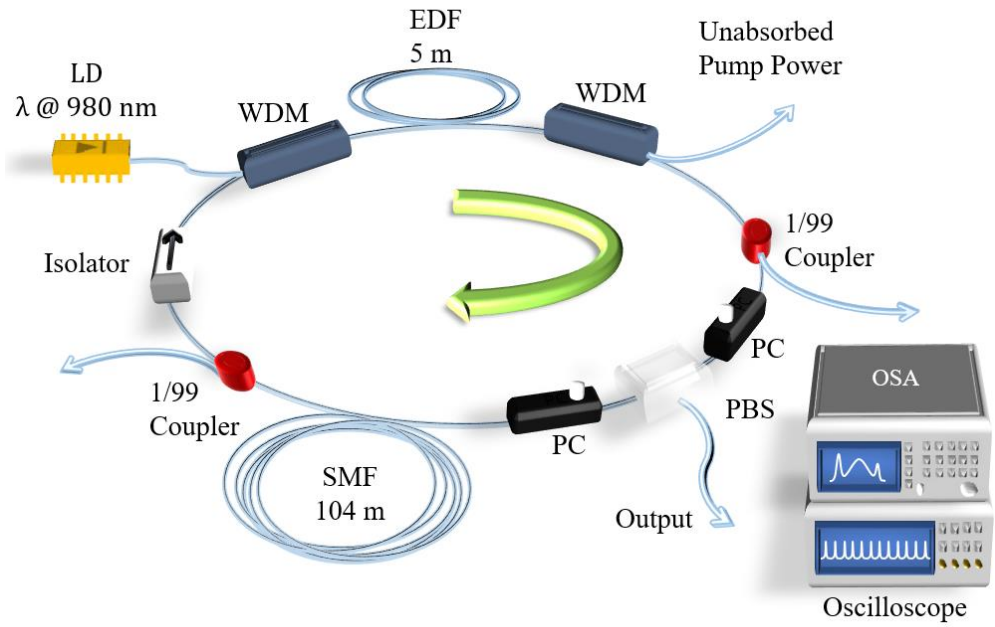

Fig. 3.1.1. Experimental setup for a passively mode-locked EDF ring laser cavity based on NPR.

I spliced additional SMF to lengthen the cavity length to better observe stochastic process. The cavity length was ~ 120 m and had a net anomalous dispersion of $\beta_2 \sim -2.95$ ps^2. At low pump power (< ~ 65 mW), the cavity operated in a single-pulse-soliton laser and entered MS regime, at higher pump power. I measured optical spectrum of the laser while obtaining spatio-temporal measurements at the same time using a 45-GHz bandwidth and a high-speed oscilloscope having an ~ 80-ps-time-scale resolution (DSO91204A, Agilent: 12-GHz bandwidth and 40-GS/s sampling rate) up to 837 consecutive roundtrip times.

3.2 Experiment result

I first locked the laser into a stable MS regime where more ~470 solitons were randomly spaced in a single roundtrip without noticeable interactions by pumping the EDF at ~ 410 mW and fine tunning the PCs. The operation characteristics of the stable MS soliton resembled the typical MS regime with an optical spectrum with Kelly sidebands, a single spike autocorrelation trace, and histogram representing an intensity probability density function (IPDF) of every soliton events taking place in the 837 roundtrips normalized with the average soliton intensity. The bandwidth of the stable MS regime was ~ 4 nm and the pulse width was ~3.1 ps. From the histogram, it was clear that there were no outliers of high intensity events, normally represented as long tail to the right, and rogue wave did not exist in this specific regime, as shown in Fig. 3.2.1(c).

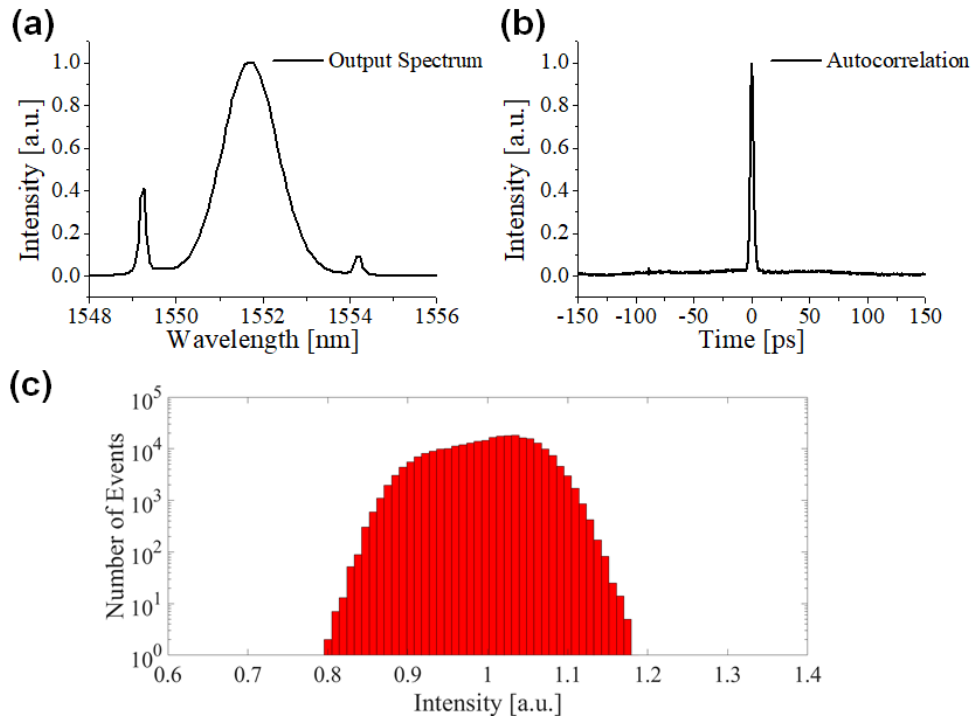

Fig. 3.2.1. Operation characteristics of the stable MS regime: (a) optical spectrum, (b) autocorrelation trace, and (c) histogram.

In order to have clear look at the pulse evolution over the roundtrips, I also conducted the real-time spatio-temporal measurement. Figure 3.2.2. Shows the shot-to-shot pulse evolution up to 837-roundtrip times. From the spatio-temporal measurement, it was clear that the solitons were indeed propagating with no interactions among them. The spacing between the solitons were normally more than ~ 1 ns.

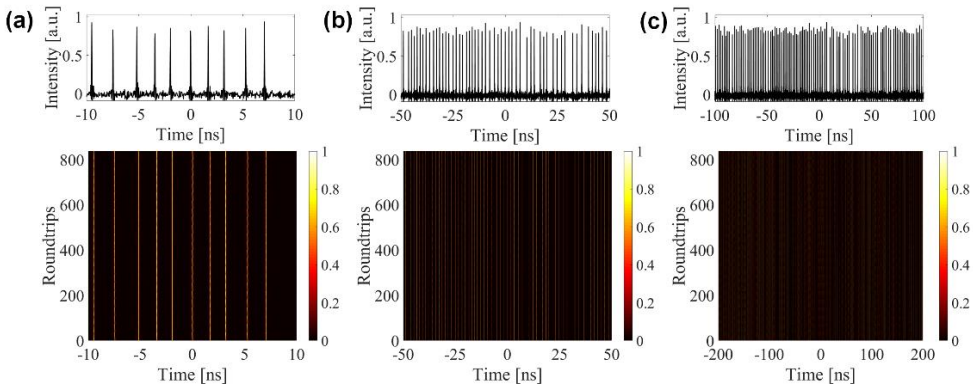

Fig. 3.2.2. Spatio-temporal shot-to-shot measurement results of the stable MS regime: (a) 20 ns span, (b) 100 ns span and (c) 400 ns span.

I managed to lock the laser cavity in numerous operation regimes with distinct characteristics just by tweaking the PCs with fixed pump power. In the cavities based on NPR, the slightest change in the saturation power of the cavity could change the pulse dynamics inside of the cavity in drastic ways. I tuned the cavity to operate in the MS regime heavily populated with ~790 solitons in a roundtrip, which is almost the double compared to the stable MS regime by fine tuning PCs with the pump power fixed at ~ 410 mW, the same level as the stable MS regime. At a glance, this specific MS regime, where I entitled it as 'the breathing MS regime' from now on to differentiate with the stable MS regime, did not seem that much different from the stable MS regime. Optical spectrum still exhibited the characteristic spectrum of the MS regime. However, I noticed that in this specific regime, the Kelly sideband was gradually increasing until it reached the maximum point and collapsed to the initial state to repeated the process. Figure 3.2.3(a) and (b) shows

the optical spectrum of 5 states within the cycle of roughly 10 seconds in the breathing MS regime, initial state being State 1. In the process, the Kelly sideband increased nearly 5 times from State 1 to State 5 before collapsing and restarting the cycle. The breathing Kelly sideband implied to us that the dispersive waves were constructively interfering in the cavity and the pulse dynamics was completely different from the stable MS regime. I took the IPDFs of each state to verify the pulse dynamics discrepancy between the stable MS regime and each incrementing states of the breathing MS regime. Surprisingly the histograms of the incrementing states of the breathing MS regime started to display longer and longer tails to the higher intensity events well exceeding value of 2 in the State 5, as show in Fig 3.2.3(c). The higher the level of the Kelly sideband, the more intense extreme events were taking place, suggesting that the pulse interaction enhances with the increasing sideband.

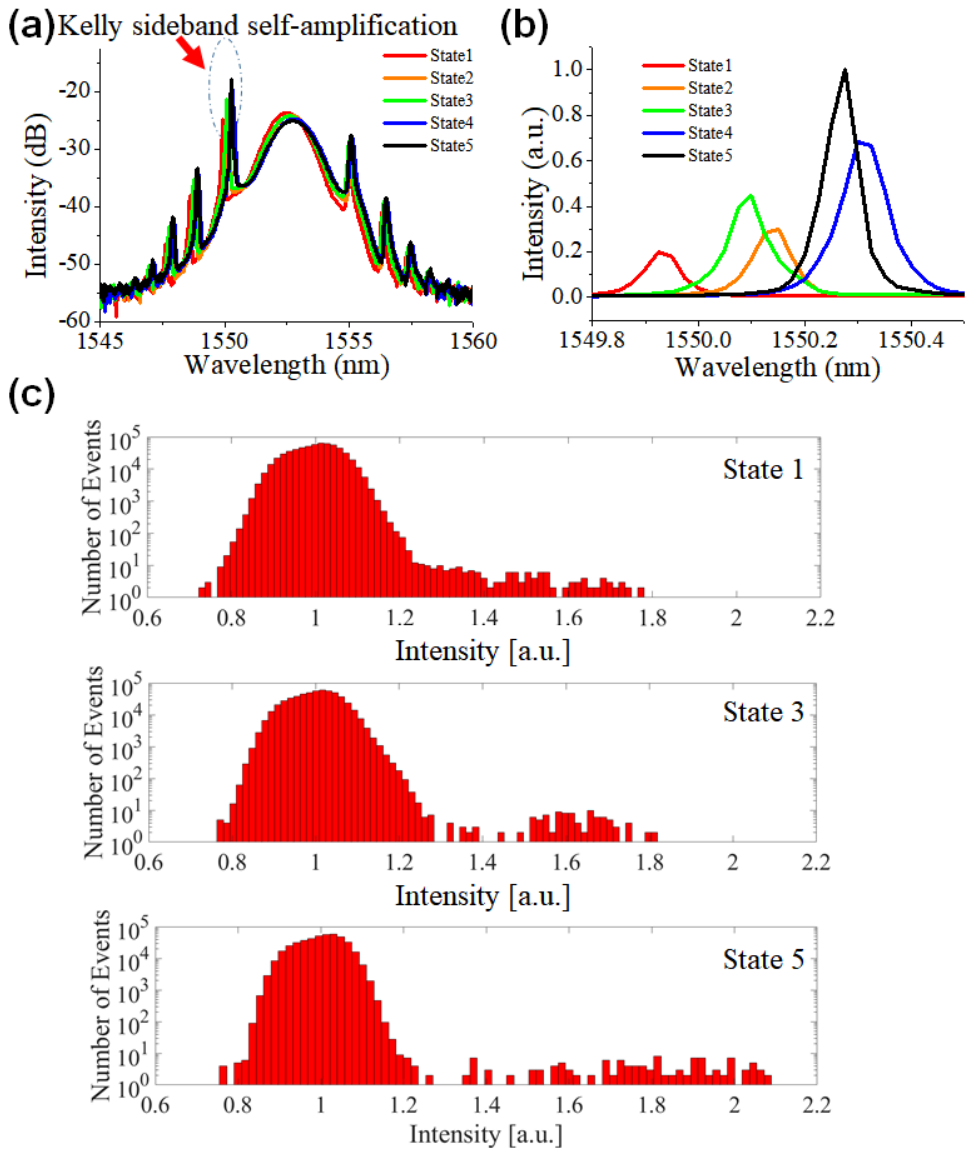

Fig. 3.2.3. Incrementing states of a single cycle in the breathing MS regime (a) optical spectrum, (b) Kelly sideband in a smaller span, and (c) histogram of the States 1, 3, and 5.

In addition to the above analysis, I took spatio-temporal measurement of each states observe the shot-to-shot pulse dynamics in the cavity. Pulse interaction was becoming more

frequent as the state progressed from State 1 to State 5. However, the most intriguing feature was that with every cycle of the sideband build-up, a burst of super rogue waves was observed when the sideband reaches State 5 and returns to State 1 with the super wave disappearing quickly. Figure 3.2.4 shows the spatio-temporal measurement of super wave emergence in different spans.

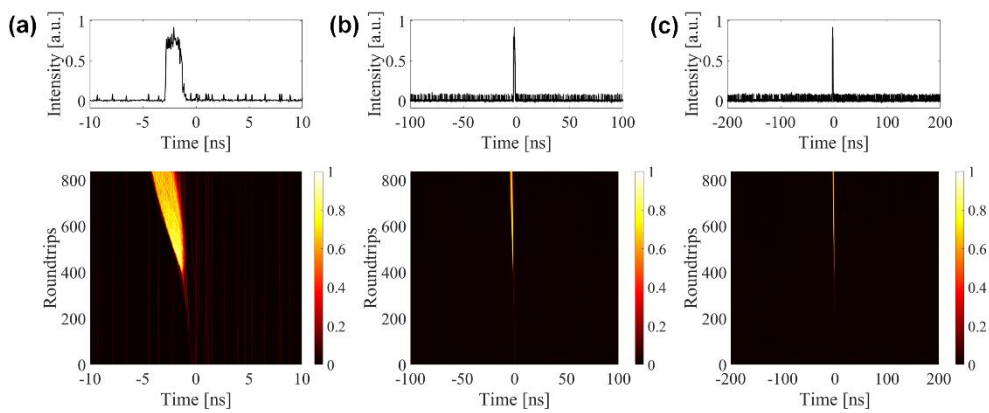

Fig. 3.2.4. Super rogue wave generation: Spatio-temporal measurement in (a) 20 ns span, (b) 200 ns span, and (c) 400 ns span.

The sudden burst appeared out of nowhere and started to break swiftly, though measured data points are limited with the oscilloscope scale to observe the entire decaying process. Figure 3.2.5 shows the spatio-temporal measurement in 3D view and the histogram of the moment of the super rogue wave burst. Intensity of the extreme events exceeded above 10 times the average wave height displaying highly localized pulse interaction. I have to note that the shot-to-shot spatio-temporal measurements were resolution-limited to ~ 80 ps. This means that highly localized extreme events might have been

measured as if they had been in a bunch within the resolution limit, so that I have to bear in my mind a possibility that the real peak intensity level of the utmost extreme event comprising the super RW might have been over- or underestimated to some degree.

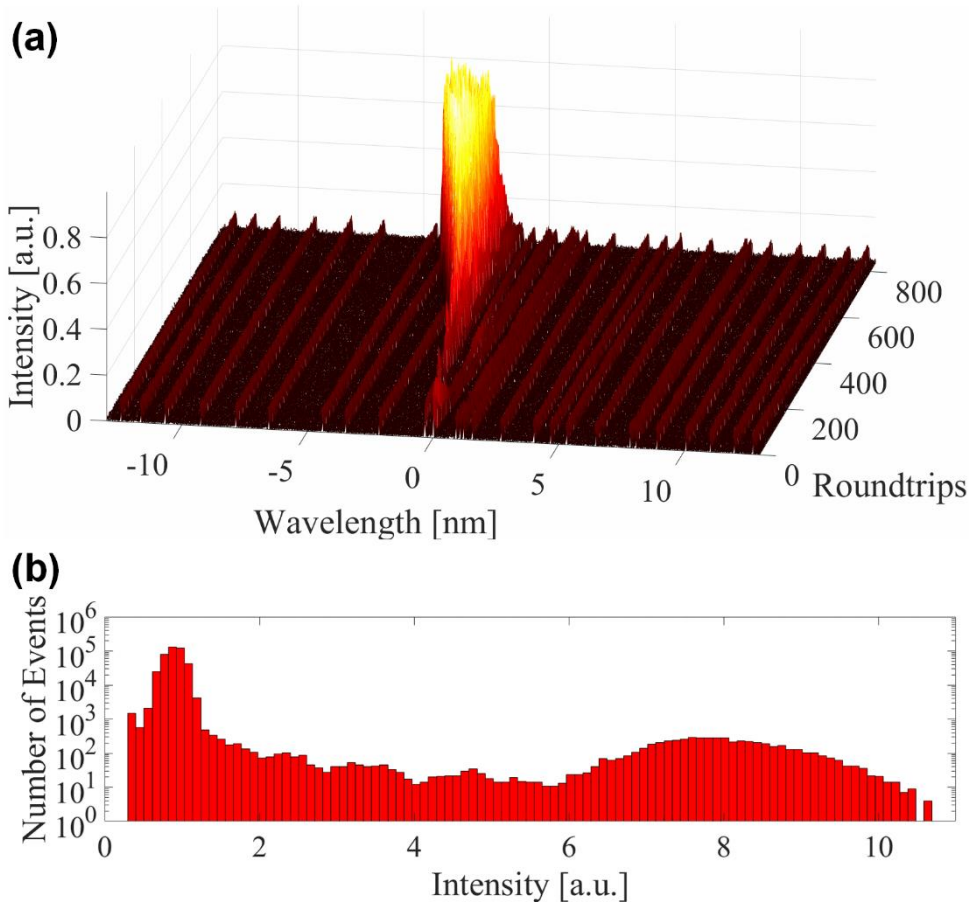

Fig. 3.2.5. Super rogue wave generation: Spatio-temporal measurement in (a) 3D plot, (b) 2D plot, and (c) histogram during the super rogue wave appearance.

3.3 Discussion

From the experiments conducted and discussed in the preceding section, I have figured out that the extreme events could be triggered and intensified inside the cavity via going through a cascade of vivid pulse interactions without having any external triggering or adjustment of the cavity parameters. In contrast with the case of the stable MS regime, where the intra-cavity solitons hardly interacted with one another, in the breathing MS regime the substantial growth of the soliton population inside the cavity, which subsequently reduced physical spacing among the intra-cavity solitons, exponentially escalated the probability of interactions among them directly or indirectly via dispersive waves. Thus, one can think of a possible scenario for the intermittent burst of a super RW as the following: Initially, some of the solitons generated in a place where their population density was most immensely high might start to interact with the nearest neighboring ones, resulting in the higher interactions among them and also producing the more intense dispersive waves that had been left over during the interactions [34,46-49]. The combination of these probabilistically initiated soliton interactions and constructively intensifying dispersive waves in their vicinity as a catalyst, in turn, triggered another extreme event, eventually leading to an avalanche of interactions resulting in extreme events with even higher intensities. In fact, the increasing trend in the extreme events observed in the histograms shown in Fig. 3.2.3(c) was completely in accord with the growing trend in the

utmost Kelly sideband shown in Fig. 3.2.3(a), which supports my aforementioned conjectures. In other words, once the build-up process driven by the initial soliton interactions at a place of the cavity where their population density had been most immensely high, had passed a certain threshold point, it became unstoppable, thereby going off a burst of a super RW and eventually being settled down into its initial state. It is worth noting that once there was a burst of a super RW in the cavity, it could sweep as much stored energy in the cavity as possible and subsequently dispersed into the calmed down state, i.e., the initial state of the breathing MS regime, because it must be by no means a form of wave that the cavity could stably support in the given condition and configuration. The settlement into the initial state of the breathing MS regime means that the cavity again returned to a state of excessively populated and irregularly distributed solitons within the fixed length of the cavity. Thus, this circumstance still must bear a very high chance of probabilistic initiation of casual soliton interactions. Therefore, the whole process of the burst of a super RW again could be initiated probabilistically, thereby being intermittent fully depending on the initial formation of the excessive number of solitons as well as the ambient conditions. In addition, I note that the burst of a super RW was a completely independent, stochastic event turning up out of nowhere, since one can see in Fig. 3.2.5(a) that even when it was happening in the middle of the cavity, it seemed as though all the intra-cavity solitons placed distant to it except for the very nearby ones had not known what was going on out there before it reached them.

In Fig. 3.3.1 I illustrate the spatio-temporal measurement result at the very specific moment of the burst of a super RW, taking an even closer look at it. The area enclosed by the dashed-circle indicates the strong localization of the extreme events right before the super RW burst, for which I deliberately set a dark color to the background events having their relative intensities below 0.02 for visual aids. One can clearly see that dispersive waves were heavily created and constructively synchronized from that specific area. With these intensifying dispersive waves as a catalyst, an avalanche of extreme events started to occur, eventually leading to strongly localized extreme events, i.e., a burst of a super RW, sweeping as much stored energy in the cavity as possible. It is worth noting that the saturation power of the cavity was unchanged throughout the entire cycle of the super RW burst, so that this extraordinary wave could not survive in the cavity and quickly dispersed. Since all the energy from the super RW was dispersed in the cavity upon its collapse, eventually being given away to the intra-cavity solitons, the cavity state became to return to its initial state to start the cycle again.

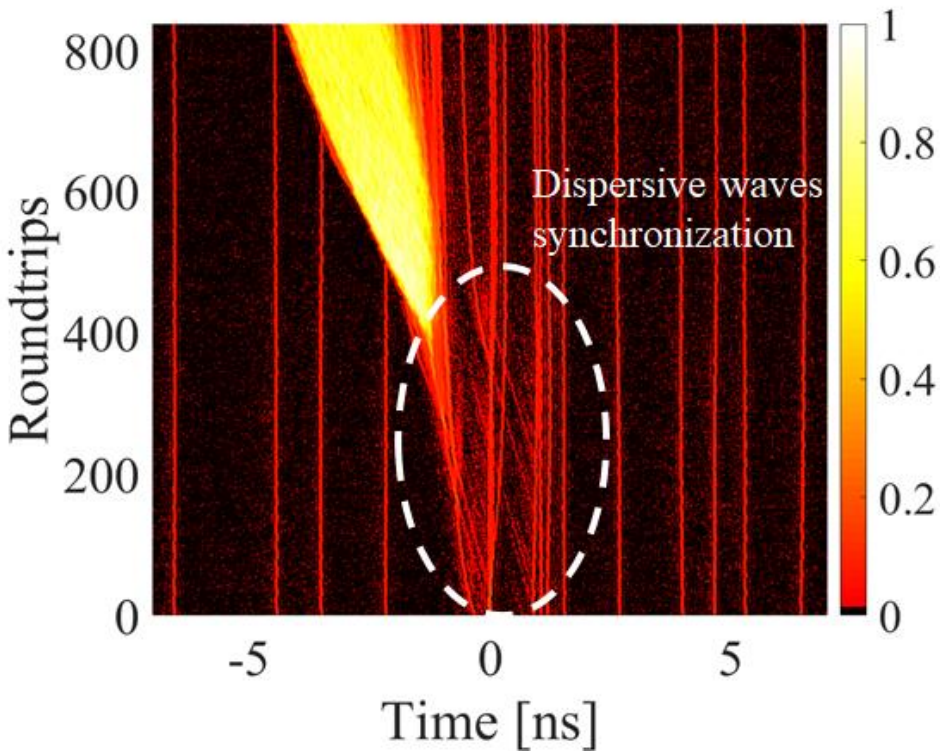

Fig. 3.3.1. Super rogue wave generation: closer view of concentrated dispersive waves.

These entire processes intriguingly resemble the precipitation of rain from a cloud. In fact, the rainfall process is briefly as the following: Small water droplets within a cloud initially grow in size, forming larger water droplets via collision with other water droplets or ice crystals in their vicinity, which is a random process called coalescence [50]. Ice crystals can play as a catalyst to accelerate the coalescence, and the enlarged water droplets become as a seed to draw more and more water droplets. Once the water droplets have grown heavy enough to overcome air resistance, they immediately start to fall to the ground, which are raindrops. The cycle will take

place again once another group of water droplets has been built up.

Bearing the precipitation of rain in my mind, solitons and dispersive waves in the cavity are the analogies to the water droplets and ice crystals in a cloud. With the stochastic events of soliton interactions together with dispersive wave synchronization as a catalyst, extreme events started to occur. Like the water droplets and ice crystals in a cloud, these initial coalescence events continue to lead to even more extreme events with even higher intensities, eventually forming and releasing a strong localized wave, i.e., a burst of a super RW, like the precipitation of rain, i.e., a real raindrop falling down. Once all the events reach the maximum degree that the cavity can hold, it retrieves to the initial state to start the cycle again, waiting for another series of significant interactions among the intra-cavity solitons and subsequent dispersive waves as water droplets and ice crystals do again in a cloud.

We have to note another compelling point from my experimental observation, which was the fact that a unit cycle of a super RW's emergence was in the order of no longer than ten seconds although it was not exactly periodic but intermittent. While I do not completely rule out that this type of time scale might be related with thermal relaxation of the cavity or the ambient environment [51,52], I think this possibility is quite unlikely, because I clearly observed from the shot-to-shot spatio-temporal measurements that the burst of a super RW was initiated from fully stochastic events that were probabilistically determined depending on the population density of solitons, and, moreover, the experiment were conducted in fully

temperature-controlled environment. From this perspective, I note that the super RW observed in my experiment is emphatically analogous to "the hundred-year wave" sporadically observed in the ocean. It is defined as "a statistically projected water wave, the height of which, on average, is met met or exceeded once in a hundred years for a given location" [53,54]. Ten seconds in an optical platform is roughly matched to sub-hundred years in the ocean, considering that the speed of light is million times faster than that of the wind wave in the open ocean [55]. This implies that the super RW I observed may be an analogy to the hundred-year wave in the ocean. Although a more thorough theoretical and numerical study of dispersive-wave-mediated super RW generation should follow, the experimental results and evidences presented here may provide significant physical insight into the extreme event formation in both optical and oceanographic platforms.

Chapter 4

Conclusion

Fiber lasers are exhibits different nonlinear phenomena owing to strong nonlinearity inherited from physical structure of optical fibers. Nonlinear affects may be detrimental in conventional means of power scaling of fiber lasers. However, high nonlinearity posed inside of an optical fiber can function as promising platform to observe and research intriguing nonlinear behaviors such as pulse-to-pulse interaction and extreme wave generation where the knowledge of nonlinear behavior study can spread to other disciplines.

QML fiber lasers is a compact and cost efficient platform to study various nonlinear wave dynamics owing to their multi-pulse and stochastic nature. In the dissertation, I carried out experimental analysis of QML regimes of fiber laser using the classical characterization techniques and real-time measurement spatio-temporal analysis. The studies presented in the dissertation provide novel approach in explaining the coherence degradation among QML regimes and wave-packet formation mechanism. Also for the first time, I have demonstrated cascaded pulse interaction without external control, which eventually leads to a repeated super rogue wave triggering.

In the first part of my dissertation, I have experimentally characterized the three constitutional QML regimes of a PMLFL of an anomalous-dispersion cavity, including the NLP, symbiotic, and MS regimes, analyzing and detailing out their shot-to-shot coherence properties, wave-packet-forming/bunching processes, and correlations with soliton interactions. I verified that solitons with higher intra-cavity intensities not only experienced greater NPSs but also exhibited stronger soliton interactions. By adjusting the saturation power of the cavity, controlling the intra-cavity intensities and simultaneously affecting the degree of soliton interactions, I analyzed the inter-soliton dynamics within narrow windows of transitional states across different QML regimes in real-time and showed that increase in the degree of soliton interactions could result in drastic degradation of the shot-to-shot coherence of the corresponding QML pulses generated in the cavity. The experiment results suggest that in an anomalous-dispersion cavity mainly governed by soliton dynamics, the NLP and symbiotic regimes could be regarded as mutant forms of the MS regime that are fit to survive in the cavity even when individual solitons are heavily interacting one another, thereby settling in a quasi-stable, soliton-clustered wave packet and incorporating chaotic or stochastic consequences in their spectral, temporal, and coherence properties. To the best of my knowledge, there have been no systematic and dedicated experimental investigations on the wave-packet formation mechanisms in the QML regimes and the corresponding consequences in their coherence properties, which have now been

clarified by the discussion presented in the dissertation. The experimental investigations also verified and confirmed to be in good agreement with the numerical analysis [ ].

In the second part of the dissertation, I have experimentally observed and analyzed periodic triggering of super rogue wave in MS regime of an anomalous-dispersion fiber ring cavity mode-locked by NPR. With the fixed cavity conditions, the cavity self-stimulated to trigger super rogue wave every 7 seconds. I demonstrated that forcing greater population of solitons to exist in the cavity drastically increased the natural probability for interactions among solitons and dispersive waves to occur, which resulted in cascaded soliton collisions eventually triggering super rogue wave. I verified that the synchronization of the dispersive waves was the main driving factor for the cascaded pulse interaction in the cavity by confirming the cycle of build-up and collapse of Kelly sideband matches the super rogue wave emerging cycle. In addition, IPDF histograms of incrementing states in the super rogue wave triggering cycle showed clear increase in number of extreme events toward higher intensity. Repeating cycle manifested that even if large soliton population naturally pushes the cavity to trigger more and more soliton interactions and extreme events, the cavity attempts to go back to the stable state with the lowest order of pulse interactions as long as the cavity condition remained fixed to support the initial state the best. There have been no experimental investigations of periodic triggering of super rogue wave in multi-soliton regime in PMLFLs.

To conclude, I presented a systematic experimental analysis on

the shot-to-shot coherence, wave-packet formation, cascaded pulse interaction and super rogue wave triggering in the realm of QML regimes of fiber laser using the real-time spatio-temporal measurement technique. I believe the studies demonstrated in the dissertation on experimental observations on the intra-cavity soliton interactions and their detailed dynamics and consequences, would fill the gaps in the existing knowledge on the QML regimes of PMLFLs, as well as putting a stepping stone to the further expansion of them. And also, the first demonstration of periodic super rogue wave in the QML fiber laser should provide richer perspective on the study of rogue waves not only in the field of optics but also in other disciplines.

Bibliography

Chapter 1.

1. K. C. Kao and G. A. Hockham, "Dielectric-fiber surface waveguides for optical frequencies", Proc. Inst. Elect. Eng. 113, 1151 (1966).
2. K. C. Kao and T. W. Davies, "Spectrophotometric studies of ultra low loss optical glasses – I: Single beam method", J. Phys. E 2 (1), 1063 (1968).
3. D. Gloge, "Weakly guiding fibers", Appl. Opt. 10 (10), 2252 (1971).
4. S. B. Poole, D. N. Payne, and M. E. Fermann, "Fabrication of low loss optical fibers containing rare earth ions", Electron. Lett. 21, 737 (1985).
5. S. B. Poole et al., "Fabrication and characterization of low-loss optical fibers containing rare earth ions", J. Lightwave Technol. 4 (7), 870 (1986).
6. J. E. Townsend et al., "Solution-doping technique for fabrication of rare earth doped optical fibres", Electron. Lett. 23, 329 (1987).
7. M. E. Fermann et al., "Efficient operation of an Yb-sensitised Er fiber laser at 1.56 μm", Electron. Lett. 24, 1135 (1988).
8. W. J. Miniscalco, "Erbium-doped glasses for fiber amplifiers at 1500 nm", J. Lightwave Technol. 9 (2), 234 (1991).
9. L. Wetenkamp et al., "Optical properties of rare earth-doped ZBLAN glasses", J. Non-Cryst. Solids 140, 35 (1992).
10. R. Paschotta et al., "Characterization and modeling of thulium:ZBLAN blue upconversion fiber lasers", J. Opt. Soc. Am. B 14 (5), 1213 (1997).
11. G. G. Vienne et al., "Fabrication and characterization of Yb3+:Er3+ phosphosilicate fibers for lasers", J. Lightwave Technol. 16 (11), 1990 (1998).
12. S. Tanabe, "Rare-earth-doped glasses for fiber amplifiers in broadband telecommunication", C. R. Chimie 5, 815 (2002).
13. E. Snitzer, "Proposed fiber cavities for optical masers", J. Appl. Phys. 32 (1), 36 (1961).
14. E. Snitzer, "Optical maser action in Nd3+ in a Barium crown glass", Phys. Rev. Lett. 7 (12), 444 (1961).
15. C. J. Koester and E. Snitzer, "Amplification in a fiber laser", Appl. Opt. 3 (10), 1182 (1964).
16. C. A. Burrus and J. Stone, "Nd3+ doped SiO2 lasers in an end-pumped fiber geometry", Appl. Phys. Lett. 23 (7), 388 (1973).
17. J. Stone and C. A. Burrus, "Neodymium-doped fiber lasers: room temperature CW operation with an injection laser pump", Appl. Opt. 13 (6), 1256 (1974).
18. R. J.Mears, L. Reekie, S. B. Poole, and D. N. Payne, "Neodymium-doped silica single-mode fibre lasers", Electron. Lett. 21 (17), 738 (1985).

19. L. Reekie et al., “Diode-laser-pumped Nd3+-doped fibre laser operating at 938 nm”, Electron. Lett. 23, 884 (1987).
20. W. L. Barnes et al., “Er3+-Yb3+ and Er3+ doped fiber lasers”, J. Lightwave Technol. 7 (10), 1461 (1989).
21. D. C. Hanna et al., “A 1-watt thulium-doped cw fibre laser operating at 2 μm”, Opt. Commun. 80, 52 (1990).
22. A. C. Tropper et al., “Thulium-doped silica fiber lasers”, Proc. SPIE 1373, 152 (1991).
23. R. B. Smart et al., “CW room temperature upconversion lasing at blue, green and red wavelengths in infrared-pumped Pr3+-doped fluoride fibre”, Electron. Lett. 27 (14), 1307 (1991).
24. H. M. Pask et al., “Ytterbium-doped silica fiber lasers: versatile sources for the 1–1.2 μm region”, IEEE J. Sel. Top. Quantum Electron. 1 (1), 2 (1995).
25. P. Xie and T. R. Gosnell, “Room-temperature upconversion fiber laser tunable in the red, orange, green, and blue spectral regions”, Opt. Lett. 20 (9), 1014 (1995).
26. R. Paschotta et al., “230 mW of blue light from a Tm-doped upconversion fibre laser”, IEEE J. Sel. Top. Quantum Electron. 3 (4), 1100 (1997).
27. Y. Takushima et al., “Polarization-stable and single-frequency fiber lasers”, J. Lightwave Technol. 16 (4), 661 (1998).
28. V. Dominic et al., “110 W fibre laser”, Electron. Lett. 35, 1158 (1999).
29. S. D. Jackson et al., “Diode-pumped 1.7 W erbium 3-μm fiber laser”, Opt. Lett. 24 (16), 1133 (1999).
30. M. Pollnau and S. D. Jackson, “Erbium 3-μm fiber lasers”, IEEE J. Sel. Top. Quantum Electron. 7 (1), 30 (2001).
31. Y. Jeong et al., “Ytterbium-doped large-core fiber laser with 1.36 kW continuous-wave output power”, Opt. Express 12 (25), 6088 (2004).
32. A. Polynkin et al., “Single-frequency fiber ring laser with 1 W output power at 1.5 μm”, Opt. Express 13 (8), 3179 (2005).
33. A. Tünnermann et al., “Fiber lasers and amplifiers: an ultrafast performance evolution”, Appl. Opt. 49 (25), F71 (2010).
34. M. J. F. Digonnet, Rare-Earth-Doped Fiber Lasers and Amplifiers, 2nd edn., CRC Press, Boca Raton, FL (2001).
35. L. Brillouin, “Diffusion de la Lumière et des Rayonnes X par un Corps Transparent Homogéne; Influence del'Agitation Thermique”, Annales des Physique 17, 88 (1922).
36. R. Y. Chiao et al., “Stimulated Brillouin scattering and coherent generation of intense hypersonic waves”, Phys. Rev. Lett. 12 (21), 592 (1964).
37. E. P. Ippen and R. H. Stolen, “Stimulated Brillouin scattering in optical fibers”, Appl. Phys. Lett. 21, 539 (1972).
38. R. G. Smith, “Optical power handling capacity of low loss optical fibers as determined by stimulated Raman and Brillouin scattering”, Appl. Opt. 11 (11), 2489 (1972).

39. K. O. Hill et al., “cw Brillouin laser”, Appl. Phys. Lett. 28 (10), 608 (1976).
40. D. Cotter, “Observation of stimulated Brillouin scattering in low-loss silica fibre at 1.3 μm”, Electron. Lett. 18, 495 (1982).
41. R. M. Shelby et al., “Guided acoustic-wave Brillouin scattering”, Phys. Rev. B 31 (8), 5244 (1985).
42. G. C. Valley, “A review of stimulated Brillouin scattering excited with a broad-band pump laser”, IEEE J. Quantum Electron. 22 (5), 704 (1986).
43. R. W. Boyd et al., “Noise initiation of stimulated Brillouin scattering”, Phys. Rev. A 42 (9), 5514 (1990).
44. S. P. Smith et al., “Narrow-linewidth stimulated Brillouin fiber laser and applications”, Opt. Lett. 16 (6), 393 (1991).
45. Y. Imai and N. Shimada, “Dependence of stimulated Brillouin scattering on temperature distribution in polarization-maintaining fibers”, IEEE Photon. Technol. Lett. 5, 1335 (1993).
46. R. G. Harrison et al., “SBS self-phase conjugation of CW Nd:YAG laser radiation in an optical fibre”, Opt. Commun. 163, 208 (1999).
47. J. Hansryd et al., “Increase of the SBS threshold in a short highly nonlinear fiber by applying a temperature distribution”, J. Lightwave Technol. 19 (11), 1691 (2001).
48. Y. Koyamada et al., “Simulating and designing Brillouin gain spectrum in single mode fibers”, J. Lightwave Technol. 22 (2), 631 (2004).
49. Y. Jeong et al., “Single-frequency, single-mode, plane-polarized ytterbium-doped fiber master oscillator power amplifier source with 264 W of output power”, Opt. Lett. 30 (5), 459 (2005).
50. A. H. McCurdy, “Modeling of stimulated Brillouin scattering in optical fibers with arbitrary radial index profile”, J. Lightwave Technol. 23 (11), 3509 (2005).
51. Y. Okawachi, “Tunable all-optical delays via Brillouin slow light in an optical fiber”, Phys. Rev. Lett. 94 (15), 153902 (2005).
52. J. Geng et al., “Highly stable low-noise Brillouin fiber laser with ultranarrow spectral linewidth”, IEEE Photon. Technol. Lett. 18 (17), 1813 (2006).
53. M. D. Mermelstein et al., “11.2 dB SBS gain suppression in a large mode area Yb-doped optical fiber”, Proc. SPIE 6873, U63 (2008).
54. B. Ward and J. Spring, “Finite element analysis of Brillouin gain in SBS-suppressing optical fibers with non-uniform acoustic velocity profiles”, Opt. Express 17 (18), 15685 (2009).
55. V. I. Kovalev and R. G. Harrison, “Suppression of stimulated Brillouin scattering in high-power single-frequency fiber amplifiers”, Opt. Lett. 31 (2), 161 (2006).
56. V. I. Kovalev and R. G. Harrison, “Abnormally low threshold gain of stimulated Brillouin scattering in long optical fiber with feedback”, Opt. Express 16 (16), 12272 (2008).
57. B. G. Ward and J. B. Spring, “Brillouin gain in optical fibers with inhomogeneous acoustic velocity”, Proc. SPIE 7195, 71951J (2009).

58. A. Kobyakov et al., “Stimulated Brillouin scattering in optical fibers”, Advances in Optics and Photonics 2 (1), 1 (2010).
59. V. V. Raman and K. S. Krishnan, “A new type of secondary radiation”, Nature 121, 501 (1928).
60. G. Eckhardt et al., “Stimulated emission of Stokes and anti-Stokes Raman lines from diamond, calcite and alpha-sulfur single crystals”, Appl. Phys. Lett. 3, 137 (1963).
61. N. Bloembergen, “The stimulated Raman effect”, Am. J. Phys. 35 (11), 989 (1967).
62. R. G. Smith, “Optical power handling capacity of low loss optical fibers as determined by stimulated Raman and Brillouin scattering”, Appl. Opt. 11 (11), 2489 (1972).
63. K. J. Blow and D. Wood, “Theoretical description of transient stimulated Raman scattering in optical fibers”, IEEE J. Quantum Electron. 25 (12), 2665 (1989).
64. R. H. Stolen et al., “Raman response function of silica-core fibers”, J. Opt. Soc. Am. B 6 (6), 1159 (1989).
65. D. Hollenbeck and C. D. Cantrell, “Multiple-vibrational-mode model for fiber-optic Raman gain spectrum and response function”, J. Opt. Soc. Am. B 19 (12), 2886 (2002).
66. J. Santhanam and G. P. Agrawal, “Raman-induced spectral shifts in optical fibers: general theory based on the moment method”, Opt. Commun. 222, 413 (2003).
67. J. M. Fini et al., “Distributed suppression of stimulated Raman scattering in an Yb-doped filter-fiber amplifier”, Opt. Lett. 31 (17), 2550 (2006).
68. Q. Lin and G. P. Agrawal, “Raman response function for silica fibers”, Opt. Lett. 31 (21), 3086 (2006).
69. D. J. Spence and R. P. Mildren, “Mode locking using stimulated Raman scattering”, Opt. Express 15 (13), 8170 (2007).
70. X. Ma et al., “Propagation-length independent SRS threshold in chirally-coupled-core fibers”, Opt. Express 19 (23), 22575 (2011).
71. F. Shimizu, “Frequency broadening in liquids by a short light pulse”, Phys. Rev. Lett. 19 (19), 1097 (1967).
72. R. R. Alfano and S. L. Shapiro, “Observation of self-phase modulation and small-scale filaments in crystals and glasses”, Phys. Rev. Lett. 24 (11), 592 (1970).
73. R. H. Stolen and C. Lin, “Self-phase-modulation in silica optical fibers”, Phys. Rev. A 17 (4), 1448 (1978).
74. F. X. Kärtner et al., “Stabilization of solitonlike pulses with a slow saturable absorber”, Opt. Lett. 20 (1), 16 (1995).
75. S. V. Marchese et al., “Pulse energy scaling to 5 μJ from a femtosecond thin-disk laser”, Opt. Lett. 31 (18), 2728 (2006).
76. K. R. Hansen et al., “Thermo-optical effects in high-power ytterbium-doped fiber amplifiers”, Opt. Express 19 (24), 23965 (2011).

77. E. Snitzer et al., “Double−clad, offset−core Nd fiber laser” (first report of cladding pumping), Proc. Conf. Optical Fiber Sensors, Postdeadline paper PD5 (1988)..
78. [D. J. Ripin et al., “High efficiency side−coupling of light into optical fibres using embedded v−grooves”, Electron. Lett. 31, 2204 (1995).
79. V. Dominic et al., “110 W fibre laser”, Electron. Lett. 35, 1158 (1999).
80. G. C. Valley, “Modeling cladding−pumped Er/Yb fiber amplifiers”, Opt. Fiber Technol. 7, 21 (2001).
81. D. Kouznetsov and J. V. Moloney, “Efficiency of pump absorption in double−clad fiber amplifiers. II. Broken circular symmetry”, J. Opt. Soc. Am. B 19 (6), 1259 (2002).
82. D. Kouznetsov and J. V. Moloney, “Efficiency of pump absorption in double−clad fiber amplifiers. III: Calculation of modes”, J. Opt. Soc. Am. B 19 (6), 1304 (2003).
83. Y. Jeong et al., “Ytterbium−doped large−core fiber laser with 1.36 kW continuous−wave output power”, Opt. Express 12 (25), 6088 (2004).
84. L. J. Cooper et al., “High−power Yb−doped multicore ribbon fiber laser”, Opt. Lett. 30 (21), 2906 (2005).
85. V. Filippov et al., “Double clad tapered fiber for high power applications”, Opt. Express 16 (3), 1929 (2008).
86. C. J. Koester and E. Snitzer, “Amplification in a fiber laser”, Appl. Opt. 3 (10), 1182 (1964).
87. R. J. Mears, L. Reekie, I. M. Jauncey, and D. N.Payne, “Low−noise erbium−doped fibre amplifier operating at 1.54 μm”, Electron. Lett. 23, 1026 (1987).
88. E. Desurvire, “Design optimization for efficient erbium−doped fiber amplifiers”, J. Lightwave Technol. 8 (11), 1730 (1990).
89. M. L. Dakss and W. J. Miniscalco, “Fundamental limits on Nd3+−doped fiber amplifier performance at 1.3 μm”, IEEE Photon. Technol. Lett. 2, 650 (1990).
90. C. R. Giles and E. Desurvire, “Modeling erbium−doped fiber amplifiers”, J. Lightwave Technol. 9 (2), 271 (1991).
91. M. Øbro et al., “Highly improved fibre amplifier for operation around 1300 nm”, Electron. Lett. 27, 470 (1991).
92. Y. Ohishi et al., “A high gain, high output saturation power Pr3+−doped fluoride fiber amplifier operating at 1.3 μm”, IEEE Photon. Technol. Lett. 3, 715 (1991).
93. T. Rasmussen et al., “Optimum design of Nd−doped fiber optical amplifiers”, IEEE Photon. Technol. Lett. 4, 49 (1992).
94. T. Whitely, “A review of recent system demonstrations incorporating 1.3−μm praseodymium−doped fluoride fiber amplifiers”, IEEE J. Lightwave Technol. 13 (5), 744 (1995).
95. T. Sakamoto et al., “35−dB gain Tm−doped ZBLYAN fiber amplifier operating at 1.65μm”, IEEE Photon. Technol. Lett. 8, 349 (1996).
96. R. Paschotta et al., “Ytterbium−doped fiber amplifiers”, IEEE J. Quantum Electron. 33 (7), 1049 (1997).

97. G. C. Valley, “Modeling cladding-pumped Er/Yb fiber amplifiers”, Opt. Fiber Technol. 7, 21 (2001).
98. J. Limpert et al., “High-power femtosecond Yb-doped fiber amplifier”, Opt. Express 10 (14), 628 (2002).
99. J. Limpert et al., “High-power ultrafast fiber laser systems”, IEEE J. Sel. Top. Quantum Electron. 12 (2), 233 (2006).
100. G. S. Mecherle, “Laser diode combining for free space optical communication”, Proc. SPIE 616, 281 (1986).
101. T. Y. Fan, “Laser beam combining for high-power, high-radiance sources”, IEEE J. Sel. Top. Quantum Electron. 11 (3), 567 (2005).
102. Special issue on beam combining: IEEE Sel. Top. Quantum Electron. 15 (2) (2009).
103. C. Jauregui et al., “High-power fibre lasers” (a review paper), Nature Photon. 7, 861 (2013).
104. R. Paschotta et al., “Passively Q-switched 0.1 mJ fiber laser system at 1.53 μm”, Opt. Lett. 24 (6), 388 (1999).
105. J. A. Alvarez-Chavez et al., “High-energy, high-power ytterbium-doped Q-switched fiber laser”, Opt. Lett. 25 (1), 37 (2000).
106. A. A. Fotiadi et al., “Dynamics of a self-Q-switched fiber laser with a Rayleigh-stimulated Brillouin scattering ring mirror”, Opt. Lett. 29 (10), 1078 (2004).
107. Y. Wang and C. Xu, “Modeling and optimization of Q-switched double-clad fiber lasers”, Appl. Opt. 45 (9), 2058 (2006).
108. L. McDonagh et al., “47 W, 6 ns constant pulse duration, high-repetition-rate cavity-dumped Q-switched TEM00 Nd:YVO4 oscillator”, Opt. Lett. 31 (22), 3303 (2006).
109. T. Hakulinen and O. G. Okhotnikov, “8 ns fiber laser Q switched by the resonant saturable absorber mirror”, Opt. Lett. 32 (18), 2677 (2007).
110. P. Dupriez et al., “High average power, high repetition rate, picosecond pulsed fiber master oscillator power amplifier source seeded by a gain-switched laser diode at 1060 nm”, IEEE Photon. Technol. Lett. 18 (9), 1013 (2006).
111. J. D. Kafka et al., “Mode-locked erbium-doped fiber laser with soliton pulse shaping”, Opt. Lett. 14 (22), 1269 (1989).
112. I. N. Duling III, “All-fiber ring soliton laser mode locked with a nonlinear mirror”, Opt. Lett. 16 (8), 539 (1991).
113. M. Hofer et al., “Characterization of ultrashort pulse formation in passively mode-locked fiber lasers”, IEEE J. Quantum Electron. 28 (3), 720 (1992).
114. W. H. Loh et al., “All-solid-state subpicosecond passively mode locked erbium-doped fiber laser”, Appl. Phys. Lett. 63 (1), 4 (1993).
115. K. Tamura et al., “77-fs pulse generation from a stretched-pulse mode-locked all-fiber ring laser”, Opt. Lett. 18 (13), 1080 (1993).
116. M. E. Fermann, “Passive mode locking by using nonlinear polarization evolution in a polarization-maintaining erbium-doped fiber”, Opt. Lett. 18 (11), 894 (1993).

117. K. Tamura et al., “Soliton versus nonsoliton operation of fiber ring lasers”, Appl. Phys. Lett. 64, 149 (1994).
118. K. Tamura, E. P. Ippen, and H. A. Haus, “Pulse dynamics in stretched-pulse fiber lasers”, Appl. Phys. Lett. 67, 158 (1995).
119. H. A. Haus et al., “Stretched-pulse additive pulse mode-locking in fiber ring lasers: theory and experiment”, IEEE J. Quantum Electron. 31 (3), 591 (1995).
120. M. E. Fermann et al., “High-power soliton fiber laser based on pulse width control with chirped fiber Bragg gratings”, Opt. Lett. 20 (2), 172 (1995).
121. M. E. Fermann et al., “Cladding-pumped passively mode-locked fiber laser generating femtosecond and picosecond pulses”, Opt. Lett. 21 (13), 967 (1996).
122. A. B. Grudinin and S. Gray, “Passive harmonic mode locking in soliton fiber lasers”, J. Opt. Soc. Am. B 14 (1), 144 (1997).
123. D. J. Jones et al., “Diode-pumped environmentally stable stretched-pulse fiber laser”, IEEE J. Sel. Top. Quantum Electron. 3 (4), 1076 (1997).
124. V. Cautaerts et al., “Stretched pulse Yb3+silica fiber laser”, Opt. Lett. 22 (5), 316 (1997).
125. B. C. Collings et al., “Short cavity erbium/ytterbium fiber lasers mode-locked with a saturable Bragg reflector”, IEEE J. Sel. Top. Quantum Electron. 3 (4), 1065 (1997).
126. M. E. Fermann et al., “Fiber-lasers for ultrafast optics”, Appl. Phys. B 65, 259 (1997).
127. L. E. Nelson et al., “Ultrashort-pulse fiber ring lasers”, Appl. Phys. B 65, 277 (1997).
128. K. S. Abedin et al., “154 GHz polarization-maintaining dispersion-managed actively modelocked fibre ring laser”, Electron. Lett. 36 (14), 1185 (2000).
129. F. Ö. Ilday and F. W. Wise, “Nonlinearity management: a route to high-energy soliton fiber lasers”, J. Opt. Soc. Am. B 19 (3), 470 (2002).
130. K. S. Abedin et al., “Self-stabilized passive, harmonically mode-locked stretched-pulse erbium fiber ring laser”, Opt. Lett. 27 (20), 1758 (2002).
131. M. Guina et al., “Stretched-pulse fiber lasers based on semiconductor saturable absorber mirrors”, Appl. Phys. B 74, S193 (2002).
132. F. Ö. Ilday et al., “Generation of 50-fs, 5-nJ pulses at 1.03 μm from a wave-breaking-free fiber laser”, Opt. Lett. 28 (15), 1365 (2003).
133. O. G. Okhotnikov et al., “Mode-locked ytterbium fiber laser tunable in the 980–1070-nm spectral range”, Opt. Lett. 28 (17), 1522 (2003).
134. F. Ö. Ilday et al., “Self-similar evolution of parabolic pulses in a laser”, Phys. Rev. Lett. 92 (21), 213902 (2004).

135. L. Schares et al., “40-GHz mode-locked fiber ring laser using a Mach–Zehnder interferometer with integrated SOAs”, IEEE J. Lightwave Technol. 22 (3), 859 (2004).
136. J. R. Buckley et al., “Femtosecond fiber lasers with pulse energies above 10 nJ”, Opt. Lett. 30 (14), 1888 (2005).
137. M. Nakazawa, “Ultrafast mode-locked fiber lasers for high-speed OTDM transmission and related topics”, J. Opt. Fiber Commun. Rep. 2, 462 (2005).
138. P. Polynkin et al., “All-fiber passively mode-locked laser oscillator at 1.5 μm with watts-level average output power and high repetition rate”, Opt. Lett. 31 (5), 592 (2006).
139. D. Y. Tang and L. M. Zhao, “Generation of 47-fs pulses directly from an erbium-doped fiber laser”, Opt. Lett. 32 (1), 41 (2007).
140. A. M. Heidt et al., “High power and high energy ultrashort pulse generation with a frequency shifted feedback fiber laser”, Opt. Express 15 (24), 15892 (2007).
141. [A. Chong et al., “Properties of normal-dispersion femtosecond fiber lasers”, J. Opt. Soc. Am. B 25 (2), 140 (2008).
142. K. Kieu and M. Mansuripur, “All-fiber bidirectional passively mode-locked ring laser”, Opt. Lett. 33 (1), 64 (2008).
143. A. Ruehl et al., “Normal dispersion erbium-doped fiber laser with pulse energies above 10 nJ”, Opt. Express 16 (5), 3130 (2008).
144. K. Kieu and F. W. Wise, “All-fiber normal-dispersion femtosecond laser”, Opt. Express 16 (15), 11453 (2008).
145. D. Turchinovich et al., “Monolithic all-PM femtosecond Yb-fiber laser stabilized with a narrow-band fiber Bragg grating and pulse-compressed in a hollow-core photonic crystal fiber”, Opt. Express 16 (18), 14004 (2008).
146. M. E. Fermann and I. Hartl, “Ultrafast Fiber Laser Technology”, IEEE J. Sel. Top. Quantum Electron. 15 (1), 191 (2009).
147. O. Prochnow et al., “Quantum-limited noise performance of a femtosecond all-fiber ytterbium laser”, Opt. Express 17 (18), 15525 (2009).
148. R. Paschotta, “Timing jitter and phase noise of mode-locked fiber lasers”, Opt. Express 18 (5), 5041 (2010).
149. M. Baumgartl et al., “Sub-80 fs dissipative soliton large-mode-area fiber laser”, Opt. Lett. 35 (13), 2311 (2010).
150. D. Ma et al., “37.4 fs pulse generation in an Er:fiber laser at a 225 MHz repetition rate”, Opt. Lett. 35 (17), 2858 (2010).
151. W. H. Renninger et al., “Pulse shaping and evolution in normal-dispersion mode-locked fiber lasers”, IEEE J. Sel. Top. Quantum Electron. 18 (1), 389 (2012).
152. P. Grelu and N. Akhmediev, “Dissipative solitons for mode-locked lasers”, Nature Photon. 6, 84 (2012).
153. M. Baumgartl et al., “66 W average power from a microjoule-class sub-100 fs fiber oscillator”, Opt. Lett. 37 (10), 1640 (2012).
154. M. E. Fermann and I. Hartl, “Ultrafast fibre lasers” (a review paper), Nature Photon. 7, 868 (2013).

155. D. Brida et al, “Ultrabroadband Er:fiber lasers” (review paper), Laser & Photon. Rev. 8 (3), 409 (2014).
156. J. Kim and Y. Song, “Ultralow-noise mode-locked fiber lasers and frequency combs: principles, status, and applications”, Advances in Optics and Photonics 8 (3), 465 (2016).
157. T. Yu et al., “Dispersion-managed soliton interactions in optical fibers”, Opt. Lett. 22 (11), 793 (1997).
158. P. Kaiser and H. W. Astle, “Low-loss single-material fibers made from pure fused silica”, Bell Syst. Tech. J. 53, 1021 (1974).
159. J. C. Knight et al., “All-silica single-mode optical fiber with photonic crystal cladding”, Opt. Lett. 21 (19), 1547 (1996).
160. T. A. Birks et al., “Endlessly single-mode photonic crystal fibre”, Opt. Lett. 22 (13), 961 (1997).
161. J. C. Knight et al., “Large mode area photonic crystal fibre”, Electron. Lett. 34, 1347 (1998).
162. D. Mogilevtsev et al., “Group-velocity dispersion in photonic crystal fibres”, Opt. Lett. 23 (21), 1662 (1998).
163. R. F. Cregan et al., “Single-mode photonic band gap guidance of light in air”, Science 285, 1537 (1999).
164. J. C. Knight et al., “Anomalous dispersion in photonic crystal fiber”, IEEE Photon. Technol. Lett. 12, 807 (2000).
165. A. Ortigosa-Blanch et al., “Highly birefringent photonic crystal fibres”, Opt. Lett. 25 (18), 1325 (2000).
166. J. K. Ranka et al., “Visible continuum generation in air–silica microstructure optical fibers with anomalous dispersion at 800 nm”, Opt. Lett. 25 (1), 25 (2000).
167. T. A. Birks et al., “Supercontinuum generation in tapered fibers”, Opt. Lett. 25 (19), 1415 (2000).
168. F. Benabid et al., “Stimulated Raman scattering in hydrogen-filled hollow-core photonic crystal fiber”, Science 298, 399 (2002).
169. H. Han et al., “Terahertz pulse propagation in a plastic photonic crystal fiber”, Appl. Phys. Lett. 80 (15), 2634 (2002).
170. V. V. Ravi Kanth Kumar et al., “Extruded soft glass photonic crystal fiber for ultrabroad supercontinuum generation”, Opt. Express 10 (25), 1520 (2002).
171. W. H. Reeves et al., “Transformation and control of ultrashort pulses in dispersion-engineered photonic crystal fibres”, Nature 424, 511 (2003).
172. [J. C. Knight, “Photonic crystal fibres”, Nature 424, 847 (2003).
173. P. St. J. Russell, “Photonic crystal fibers” (review paper), Science 299, 358 (2003).
174. D. G. Ouzounov et al., “Generation of megawatt optical solitons in hollow-core photonic band-gap fibers”, Science 301, 1702 (2003).
175. D. A. Nolan et al., “Single-polarization fiber with a high extinction ratio”, Opt. Lett. 29 (16), 1855 (2004).
176. K. Hougaard and F. D. Nielsen, “Amplifiers and lasers in PCF configurations”, J. Opt. Fiber Commun. Rep. 1, 63–83 (2004).

177. W. J. Wadsworth et al., “Very high numerical aperture fibers”, IEEE Photon. Technol. Lett. 16, 843 (2004).
178. P. J. Roberts et al., “Ultimate low loss of hollow-core photonic crystal fibres”, Opt. Express 13 (1), 236 (2005).
179. K. Saitoh and M. Koshiba, “Empirical relations for simple design of photonic crystal fibers”, Opt. Express 13 (1), 267 (2005).
180. J. G. Rarity et al., “Photonic crystal fiber source of correlated photon pairs”, Opt. Express 13 (2), 534 (2005).
181. T. Schreiber et al., “Stress-induced single-polarization single-transverse mode photonic crystal fiber with low nonlinearity”, Opt. Express 13 (19), 7621 (2005).
182. L. A. Zenteno et al., “Suppression of Raman gain in single-transverse-mode dual-hole-assisted fiber”, Opt. Express 13 (22), 8921 (2005).
183. W. S. Wong et al., “Breaking the limit of maximum effective area for robust single-mode propagation in optical fibers”, Opt. Lett. 30 (21), 2855 (2005).
184. J. M. Fini, “Aircore microstructure fibers with suppressed higher-order modes”, Opt. Express 14 (23), 11354 (2006).
185. J. M. Dudley et al., “Supercontinuum generation in photonic crystal fiber”, Rev. Mod. Phys. 78, 1135 (2006).
186. P. St. J. Russell, “Photonic-crystal fibers”, J. Lightwave Technol. 24 (12), 4729 (2006).
187. G. Ren et al., “Low-loss all-solid photonic bandgap fiber”, Opt. Lett. 32 (9), 1023 (2007).
188. Y. Tsuchida et al., “Design of single-moded holey fibers with large-mode-area and low bending losses: the significance of the ring-core region”, Opt. Express 15 (4), 1794 (2007).
189. H. Ebendorff-Heidepriem et al., “Fluoride glass microstructured optical fiber with large mode area and mid-infrared transmission”, Opt. Lett. 33 (23), 2861 (2008).
190. H. Ebendorff-Heidepriem et al., “Suspended nanowires: fabrication, design and characterization of fibers with nanoscale cores”, Opt. Express 17 (4), 2646 (2009).
191. Z. Chen et al., “More than threefold expansion of highly nonlinear photonic crystal fiber cores for low-loss fusion splicing”, Opt. Lett. 34 (14), 2240 (2009).
192. K. Sano and Y. Fuji, “Polarization transmission characteristics of optical fibers with elliptical cross section”, Electron. Commun. Jpn. 63, 87 (1980).
193. A. Kumar et al., “Birefringence calculations in elliptical-core optical fibers”, Electron. Lett. 20, 112 (1984).
194. J. Noda et al., “Polarization-maintaining fibers and their applications”, J. Lightwave Technol. 4 (8), 1071 (1986).
195. D. Mogilevtsev et al., “Design of polarization-preserving photonic crystal fibres with elliptical pores”, J. Opt. A: Pure Appl. Opt. 3, S141 (2001).

196. J. R. Folkenberg et al., “Polarization maintaining large mode area photonic crystal fiber”, Opt. Express 12 (5), 956 (2004).
197. T. Schreiber et al., “Stress-induced single-polarization single-transverse mode photonic crystal fiber with low nonlinearity”, Opt. Express 13 (19), 7621 (2005).
198. A. Einstein, “Zur Quantentheorie der Strahlung”, Physikalische Zeitschrift XVIII, 121 (1917).
199. C. L. Tang et al., “Spectral output and spiking behavior of solid-state lasers”, J. Appl. Phys. 34 (8), 2289 (1963)
200. R. Paschotta et al., “Single-frequency ytterbium-doped fiber laser stabilized by spatial hole burning”, Opt. Lett. 22 (1), 40 (1997).
201. H. Sabert and E. Brinkmeyer, "Pulse generation in fiber lasers with frequency shifted feedback," Journal of Lightwave Technology, vol. 12, no. 8, pp. 1360-1368, (1994).
202. B. K. Garside and T. K. Lim, “Laser mode locking using saturable absorbers”, J. Appl. Phys. 44 (5), 2335 (1973).
203. K. A. Stankov, “A mirror with an intensity-dependent reflection coefficient”, Appl. Phys. B 45, 191 (1988).
204. M. E. Fermann et al., “Nonlinear amplifying loop mirror”, Opt. Lett. 15 (13), 752 (1990).
205. T. Brabec et al., “Kerr lens mode locking”, Opt. Lett. 17 (18), 1292 (1992).
206. U. Keller et al., “Semiconductor saturable absorber mirrors (SESAMs) for femtosecond to nanosecond pulse generation in solid-state lasers”, IEEE J. Sel. Top. Quantum Electron. 2, 435 (1996).
207. A. Sennaroglu, “Continuous wave thermal loading in saturable absorbers: theory and experiment”, Appl. Opt. 36 (36), 9528 (1997).
208. J. Mark et al., “Femtosecond pulse generation in a laser with a nonlinear external resonator”, Opt. Lett. 14 (1), 48 (1989).
209. M. E. Fermann, “Passive mode locking by using nonlinear polarization evolution in a polarization-maintaining erbium-doped fiber”, Opt. Lett. 18 (11), 894 (1993).
210. P. T. Guerreiro and S. Ten, “PbS quantum-dot doped glasses as saturable absorbers for mode locking of a Cr:forsterite laser”, Appl. Phys. Lett. 71 (12), 1595 (1997).
211. A. M. Malyarevich et al., “V:YAG – a new passive Q-switch for diode-pumped solid-state lasers”, Appl. Phys. B 67, 555 (1998)
212. Z. Burshtein et al., “Excited-state absorption studies of Cr4+ ions in several garnet host crystals”, IEEE J. Quantum Electron. 34 (2), 292 (1998).
213. R. Paschotta and U. Keller, “Passive mode locking with slow saturable absorbers”, Appl. Phys. B 73 (7), 653 (2001).
214. S. Y. Set et al., “Laser mode locking using a saturable absorber incorporating carbon nanotubes”, J. Lightwave Technol. 22 (1), 51 (2004).

215. H. Ridderbusch and T. Graf, “Saturation of 1047- and 1064-nm absorption in Cr4+:YAG crystals”, IEEE J. Quantum Electron. 43 (2), 168 (2007).
216. Y. Y. Dvoyrin et al., “Yb-Bi pulsed fiber lasers”, Opt. Lett. 32 (5), 451 (2007).
217. A. Schmidt et al., “Passive mode locking of Yb:KLuW using a single-walled carbon nanotube saturable absorber”, Opt. Lett. 33 (7), 729 (2008).
218. F. Shohda et al., “147 fs, 51 MHz soliton fiber laser at 1.56 μm with a fiber-connector-type SWNT/P3HT saturable absorber”, Opt. Express 16 (25), 20943 (2008).
219. D. D. Hudson et al., “Nonlinear femtosecond pulse reshaping in waveguide arrays”, Opt. Lett. 33 (13), 1440 (2008).
220. T. Tsai et al., “Passively Q-switched erbium all-fiber lasers by use of thulium-doped saturable-absorber fibers”, Opt. Express 18 (10), 10049 (2010).
221. A. Martinez and S. Yamashita, “Multi-gigahertz repetition rate passively modelocked fiber lasers using carbon nanotubes”, Opt. Express 19 (7), 6155 (2011).
222. M. N. Cizmeciyan et al., “Graphene mode-locked femtosecond Cr:ZnSe laser at 2500 nm”, Opt. Lett. 38 (3), 341 (2013).
223. N. J. Doran and D. Wood, “Nonlinear-optical loop mirror”, Opt. Lett. 13 (1), 56 (1988).
224. K. J. Blow et al., “Demonstration of the nonlinear fibre loop mirror as an ultrafast all-optical demultiplexer”, Electron. Lett. 26, 962, (1990)
225. M. E. Fermann et al., “Nonlinear amplifying loop mirror”, Opt. Lett. 15 (13), 752 (1990).
226. K. Smith et al., “Pulse shaping, compression, and pedestal suppression employing a nonlinear-optical loop mirror”, Opt. Lett. 15 (22), 1294 (1990).
227. D. J. Richardson et al., “Selfstarting passively mode-locked fibre laser based on the amplifying Sagnac switch”, Electron. Lett. 27, 542 (1991).
228. I. N. Duling, III, “Operation of a nonlinear loop mirror in a laser cavity”, IEEE J. Quantum Electron. 30 (1), 194 (1994).
229. S. Feng et al, “Reflectivity characteristics of the fiber loop mirror with a polarization controller”, Opt. Commun. 277 (2), 322 (2007).
230. J. W. Nicholson and M. Andrejco, “A polarization maintaining, dispersion managed, femtosecond figure-eight laser”, Opt. Express 14 (18), 8160 (2006).
231. O. Frazão et al., “Recent advances in high-birefringence fiber loop mirror sensors”, Sensors 7, 2970 (2007).
232. M. Hofer et al., “Characterization of ultrashort pulse formation in passively mode-locked fiber lasers”, IEEE J. Quantum Electron. 28 (3), 720 (1992).
233. M. E. Fermann, “Passive mode locking by using nonlinear polarization evolution in a polarization-maintaining erbium-doped fiber”, Opt. Lett. 18 (11), 894 (1993).

234. V. J. Matsas et al., “Self-starting passively mode-locked fibre ring soliton laser exploiting nonlinear polarisation rotation”, Electron. Lett. 28, 1391 (1992).
235. K. Tamura et al., “Self-starting additive pulse mode-locked erbium fibre ring laser”, Electron. Lett. 28, 2226 (1992).
236. F. Doutre et al., “Large temporal narrowing of subnanosecond pulses in a low-birefringence optical fiber”, Opt. Lett. 33 (16), 1789 (2008).
237. L. Shah, M. E. Fermann, “High power femtosecond fiber chirped pulse amplification system for high speed micromachining,” J. Laser Micro/Nanoeng. 1 176–180 (2006).
238. T. Schibli, K. Minoshima, F.L. Hong, H. Inaba, A. Onae, H. Matsumoto, I. Hartl, M.E. Fermann, “Frequency metrology with a turnkey all-fiber system,” Opt. Lett. 29 2467–2469 (2004).
239. J. Unruh, E.S. Price, R.G. Molla, L. Stehno-Bittel, C.K. Johnson, R. Hui, “Two-photon microscopy with wavelength switchable fiber laser excitation,” Opt. Express 14 9825–9831 (2006).
240. H. Lim, Y. Jiang, Y. Wang, Y.C. Huang, Z. Chen, “Ultrahigh-resolution optical coherence tomography with a fiber laser source at 1 um,” Opt. Lett. 30 1171–1173 (2005).
241. J. Clowes, “Next generation light sources for biomedical applications,” Opt. Photon. 3 36-38 (2008).
242. U. Keller, “Ultrafast all-solid-state laser technology,” Appl. Phys. B– Lasers O. 58 347–363 (1994).
243. A. Tünnermann, T. Schreiber, J. Limpert, “Fiber lasers and amplifiers: an ultrafast performance evolution,” Appl. Opt. 49 F71–F78 (2010).
244. D. Richardson, J. Nilsson, W.A. Clarkson, “High power fiber lasers: current status and future perspectives,” J. Opt. Soc. Am. B 27 B63–B92 (2010).
245. L. Nelson, D. Jones, K. Tamura, H. Haus, E. Ippen, “Ultrashort-pulse fiber ring lasers,” Appl. Phys. B 65 277–294 (1997).
246. K. Tamura, E.P. Ippen, H.A. Haus, and L.E. Nelson, “77-fs pulse generation from a stretched-pulse mode-locked all-fiber ring laser,” Opt. Lett. 18 1080–1082 (1993).
247. F.Ö. Ilday, J.R. Buckley, W.G. Clark, F.W. Wise, “Self-similar evolution of parabolic pulses in a laser,” Phys. Rev. Lett. 92 213902 (2004).
248. A. Chong, J. Buckley, W. Renninger, F. Wise, All-normal-dispersion femtosecond fiber laser, Opt. Express 14 (2006), pp. 10095–10100.
249. N. Akhmediev, J. M. Soto-Crespo, Ph. Grelu, Roadmap to ultra-short record high-energy pulses out of laser oscillators, Phys. Lett. A 372 3124–3128 (2008).
250. W. Chang, A. Ankiewicz, J.M. Soto-Crespo, N. Akhmediev, “Dissipative soliton resonances in laser models with parameter management,” J. Opt. Soc. Am. B 25 1972–1977 (2008).
251. D. Y. Tang, L. M. Zhao, B. Zhao, “Soliton collapse and bunched noise-like pulse generation in a passively mode-locked fiber ring laser,” Opt. Express 13 2289–2294 (2005).

252. M. Horowitz, Y. Barad, Y. Silberberg, “Noiselike pulses with a broadband spectrum generated from an erbium−doped fiber laser,” Opt. Lett. 22 799–801 (1997).
253. J.U. Kang, “Broadband quasi−stationary pulses in mode−locked fiber ring laser,” Opt. Commun. 182433–436 (2000).
254. L.M. Zhao, D.Y. Tang, J. Wu, X.Q. Fu, S.C. Wen, “Noise−like pulse in a gain−guided soliton fiber laser,” Opt. Express 15 2145–2150 (2007).
255. O. Pottiez, R. Grajales−Coutiño, B. Ibarra−Escamilla, E.A. Kuzin, J.C. Hernández−García, “Adjustable noiselike pulses from a figure−eight fiber laser,” Appl. Opt. 50, E24–E31 (2011).
256. L.A. Vazquez−Zuniga, Y. Jeong, “Super−broadband noise−like pulse erbium−doped fiber ring laser with a highly nonlinear fiber for Raman gain enhancement,” IEEE Photon. Technol. Lett. 24 1549–1551 (2012).
257. L.M. Zhao, D.Y. Tang, T.H. Cheng , H.Y. Tam, C. Lu, :120 nm bandwidth noise−like pulse generation in an erbium−doped fiber laser,: Opt. Commun. 281 157–161 (2008).
258. L.M. Zhao, D.Y. Tang, “Generation of 15−nJ bunched noise−like pulses with 93−nm bandwidth in an erbium−doped fiber ring laser,” Appl. Phys. B – Lasers O. 83 553–557 (2006).
259. A.F.J. Runge, C. Aguergaray, N.G.R. Broderick, M. Erkintalo, “Raman rogue waves in a partially mode−locked fiber laser,” Opt. Lett. 39 319– 322. (2014).
260. P. Grelu, N. Akhmediev, “Dissipative solitons for mode−locked lasers,” Nature Photon. 6 84–92 (2012).
261. S. Keren, E. Brand, Y. Levi, B. Levit, M. Horowitz, “Data storage in optical fibers and reconstruction by use of low−coherence spectral interferometry,” Opt. Lett. 27 125–127 (2002).
262. S. Keren, M. Horowitz, “Interrogation of fiber gratings by use of low−coherence spectral interferometry of noiselike pulses,” Opt. Lett. 26 328–330 (2001).
263. M.A. Putnam, M.L. Dennis, I.N. Duling III, C.G. Askins, E.J. Friebele, “Broadband square−pulse operation of a passively mode−locked fiber laser for fiber Bragg grating interrogation,” Opt. Lett. 23 138–140 (1998).
264. K. Özgören, B. Öktem, S. Yılmaz, F.Ö. Ilday, K. Eken, “83W, 3.1 MHz, square−shaped,” 1 ns−pulsed all−fiber−integrated laser for micromachining, Opt. Express 19 17647–17652 (2011).
265. A. Zaytsev, C.−H. Lin, Y.J. You, C.−C Chung, C.L. Wang, C.L. Pan, “Supercontinuum generation by noise−like pulses transmitted through normally dispersive standard single−mode fibers,” Opt. Express 21 6056–16062. (2013).
266. J.C. Hernandez−Garcia, O. Pottiez, and J.M. Estudillo−Ayala, “Supercontinuum generation in a standard fiber pumped by noise−like pulses from a figure−eight fiber laser,” Laser Phys. 22 221–226 (2012).

267. A. Runge, C. Aguergaray, N.G.R. Broderick, M. Erkintalo, “Coherence and shot−to−shot spectral fluctuations in noise−like ultrafast fiber lasers,” Opt. Lett. 38 4327–4330 (2013).
268. V.J. Matsas, T.P. Newson, M.N. Zervas, “Self−starting passively mode−locked fibre ring laser exploiting nonlinear polarisation switching,” Opt. Comm. 92 61–66. (1992).
269. M. Horowitz, Y. Silberberg, “Control of noiselike pulse generation in erbium−doped fiber lasers,” IEEE Photonics Technol. Lett. 10 1389–1391. (1998).
270. D. Lei, H. Yang, H. Dong, S. Wen, H. Xu, J. Zhang, J. Mod, “Effect of birefringence on the bandwidth of noise−like pulse in an erbium doped fiber laser,” J. Mod. Optic 56 572–576. (2009).
271. A.I. Chernykh, S.K. Turitsyn, “Soliton and collapse regimes of pulse generation in passively mode−locking laser systems,” Opt. Lett. 20 398– 400 (1995).
272. T. North, M. Rochette, “Raman−induced noiselike pulses in a highly nonlinear and dispersive all−fiber ring laser”, Opt. Lett. 38 890–892 (2013).
273. S. Smirnov, S. Kobtsev, S. Kukarin, A. Ivanenko, “Three key regimes of single pulse generation per round trip of all−normal−dispersion fiber lasers mode−locked with nonlinear polarization rotation,” Opt. Express 20 27447–27453 (2012).
274. S. Kobtsev, S. Kukarin, S. Smirnov, S. Turitsyn, A. Latkin, “Generation of double−scale femto/pico−second optical lumps in mode−locked fiber lasers,” Opt. Express 17 20707–20713 (2009).
275. B. Xu, A. Martinez, S.Y. Set, C.S. Goh, S. Yamashita, “Generation of dissipative solitons and noise−like pulse from figure of eight fiber laser,” Proc. of ACP, ATh2A.2 (2013).
276. H.A. Haus, J.G. Fujimoto, E.P. Ippen, “Structures for additive pulse mode locking,” JOSA B, 8 2068–2076 (1991).
277. S. Yamashita, “A tutorial on nonlinear photonic applications of carbon nanotube and graphene,” J. Lightw. Technol., 30 427 – 447 (2012).
278. F.X. Kärtner, J.A. der Au, U. Keller, “Mode−locking with slow and fast saturable absorbers–what’s the difference?” IEEE J. Sel. Top. Quant. 4 159–168 (1998).
279. S. Chouli and P. Grelu, “Soliton rains in a fiber laser: an experimental study,” Phys. Rev. A 81, 063829 (2010).
280. A. Runge, Neil G. R. Broderick, and Miro Erkintalo, "Observation of soliton explosions in a passively mode−locked fiber laser," Optica 2, 36−39 (2015).
281. D. Y. Tang, L. M. Zhao, B. Zhao, and A. Q. Liu, “Mechanism of multisoliton formation and soliton energy quantization in passively mode locked fiber lasers,” Phys. Rev. A 72(4), 043816 (2005).
282. D. V. Churkin, S. Sugavanam, N. Tarasov, S. Khorev, S. V. Smirnov, S. M. Kobtsev, and S. K. Turitsyn, “Stochasticity, periodicity and localized light structures in partially mode−locked fibre lasers,” Nat. Commun. 6, 7004 (2015).

283. Y. You, C. Wang, P. Xue, A. Zaytsev, and C. Pan, "Supercontinuum Generated by Noise-like Pulses for Spectral-domain Optical Coherence Tomography," in CLEO: 2015, OSA Technical Digest, JW2A.94 (2015).
284. Y. Jeong, L. A. V.-Zuniga, S. Lee, and Y. Kwon, "On the formation of noise-like pulses in fiber ring cavity configurations," Opt. Fiber Technol. 20(6), 575-592 (2014).
285. K. Özgören, B. Öktem, S. Yilmaz, F. Ilday, and K. Eken, "83 W, 3.1 MHz, square-shaped, 1 ns-pulsed all-fiber-integrated laser for micromachining," Opt. Express 19, 17647-17652 (2011).
286. K. Goda & B. Jalali, "Dispersive Fourier transformation for fast continuous single-shot measurements," Nature Photonics 7, 102–112 (2013).

Chapter 2.

1. L. Nelson, D. Jones, K. Tamura, H. Haus, and E. Ippen, "Ultrashort-pulse fiber ring lasers," Appl. Phys. B 65, 277–294 (1997).
2. K. Tamura, E.P. Ippen, H.A. Haus, and L.E. Nelson, "77-fs pulse generation from a stretched-pulse mode-locked all-fiber ring laser," Opt. Lett. 18(13), 1080–1082 (1993).
3. F. Ö. Ilday, J. R. Buckley, W. G. Clark, and F. W. Wise, "Self-similar evolution of parabolic pulses in a laser," Phys. Rev. Lett. 92, 213902 (2004).
4. A. Chong, J. Buckley, W. Renninger, and F. Wise, "All-normal-dispersion femtosecond fiber laser," Opt. Express 14(21), 10095–10100 (2006).
5. N. Akhmediev, J. M. Soto-Crespo, and Ph. Grelu, "Roadmap to ultra-short record high-energy pulses out of laser oscillators," Phys. Lett. A 372, 3124–3128 (2008).
6. W. Chang, A. Ankiewicz, J. M. Soto-Crespo, and N. Akhmediev, "Dissipative soliton resonances in laser models with parameter management," J. Opt. Soc. Am. B 25, 1972–1977 (2008).
7. L. Shah and M. E. Fermann, "High power femtosecond fiber chirped pulse amplification system for high speed micromachining," J. Laser Micro/Nanoeng. 1(3), 176-180 (2006).
8. H. Lim, Y. Jiang, Y. Wang, Y.-C. Huang, Z. Chen, and F. W. Wise, "Ultrahigh-resolution optical coherence tomography with a fiber laser source at 1 μm," Opt. Lett. 30(10), 1171-1173 (2005).
9. T. R. Schibli, K. Minoshima, F.-L. Hong, H. Inaba, A. Onae, H. Matsumoto, I. Hartl, and M. E. Fermann, "Frequency metrology with a turnkey all-fiber system," Opt. Lett. 29(21), 2467-2469 (2004).
10. J. R. Unruh, E. S. Price, R. G. Molla, L. S.-Bittel, C. K. Johnson, and R. Hui, "Two-photon microscopy with wavelength switchable fiber laser excitation," Opt. Express 14(21), 9825-9831 (2006).
11. J. Clowes, "Next generation light sources for biomedical applications," Optik & Photonic. 3(1), 36-38 (2008).

12. N. Nishizawa and J. Takayanagi, “Octave spanning high-quality supercontinuum generation in all-fiber system,” J. Opt. Soc. Am. B 24(8), 1786-1792 (2007).
13. Y. Kwon, L. A. V.-Zuniga, K. Park, S. Lee, H. Chang, and Y. Jeong, “Combinatorial study of supercontinuum generation dynamics in photonic crystal fibers pumped by ultrafast fiber lasers,” IEEE J. Quant. Electron. 52(6), 6400311 (2016).
14. P. Grelu and N. Akhmediev, “Dissipative solitons for mode-locked lasers,” Nat. Photon. 6, 84-92 (2012).
15. M. E. Fermann and I. Hartl, “Ultrafast fiber lasers,” Nat. Photon. 7, 868-874 (2013).
16. M. Horowitz, Y. Barad, and Y. Silberberg, “Noiselike pulses with a broadband spectrum generated from an erbium-doped fiber laser,” Opt. Lett. 22(1), 799-801 (1997).
17. A. I. Chernykh and S. K. Turitsyn, “Soliton and collapse regimes of pulse generation in passively mode-locking laser systems,” Opt. Lett. 20(4), 398-400 (1995).
18. D. E. Pelinovsky, V. V. Afanasjev, and Y. S. Kivshar, “Nonlinear theory of oscillating, decaying, and collapsing solitons in the generalized nonlinear Schrödinger equation,” Phys. Rev. E 53(2), 1940-1953 (1996).
19. J. U. Kang, “Broadband quasi-stationary pulses in mode-locked fiber ring laser,” Opt. Commun. 182(4-6), 433-436 (2000).
20. D. Y. Tang, L. M. Zhao, and B. Zhao, “Soliton collapse and bunched noise-like pulse generation in a passively mode-locked fiber ring laser,” Opt. Express 13(7), 2289-2294 (2005).
21. D. Y. Tang, L. M. Zhao, B. Zhao, and A. Q. Liu, “Mechanism of multisoliton formation and soliton energy quantization in passively mode-locked fiber lasers,” Phys. Rev. A 72(4), 043816 (2005).
22. A. Komarov, H. Leblond, and F. Sanchez, “Multistability and hysteresis phenomena in passively mode-locked fiber lasers,” Phys. Rev. A 71(5), 053809 (2005).
23. L. M. Zhao, D. Y. Tang, J. Wu, X. Q. Fu, and S. C. Wen, “Noise-like pulse in a gain-guided soliton fiber laser,” Opt. Express 15(5), 2140-2150 (2007).
24. L. M. Zhao, D. Y. Tang, T. H. Cheng, H. Y. Tam, and C. Lu, “120 nm bandwidth noise-like pulse generation in an erbium-doped fiber laser,” Opt. Commun. 281(1), 157-161 (2008).
25. S. Chouli and P. Grelu, “Soliton rains in a fiber laser: An experimental study,” Phys. Rev. A 81(6), 063829 (2010).
26. O. Pottiez, R. G-Coutiño, B. I.-Escamilla, E. A. Kuzin, and J. C. H.-García, “Adjustable noiselike pulses from a figure-eight fiber laser,” Appl. Opt. 50(25) E24-E31 (2011).
27. J. M. S.-Crespo, P. Grelu, and N. Akhmediev, “Dissipative rogue waves: Extreme pulses generated by passively mode-locked lasers,” Phys. Rev. E 84(1), 016604 (2011).
28. L. A. V.-Zuniga and Y. Jeong, “Super-broadband noise-like pulse erbium-doped fiber ring laser with a highly nonlinear fiber for

Raman gain enhancement," IEEE Photon. Technol. Lett. 24(17), 1549-1551 (2012).
29. S. Smirnov, S. Kobtsev, S. Kukarin, and A. Ivanenko, "Three key regimes of single pulse generation per round trip of all-normal-dispersion fiber lasers mode-locked with nonlinear polarization rotation," Opt. Express 20(24), 27447-27453 (2012).
30. H. S.-Hernandez, O. Pottiez, M. D.-Sanchez, R. I. A.-Tamayo, J. P. L.-Cruz, J. C. H.-Garcia, B. I.-Escamilla, and E. A. Kuzin, "Dynamics of noise-like pulsing at sub-ns scale in a passively mode-locked fiber laser," Opt. Express 23(15), 18840-18849 (2015).
31. Z. Cheng, H. Li, and P. Wang, "Simulation of generation of dissipative soliton, dissipative soliton resonance and noise-like pulse in Yb-doped mode-locked fiber lasers," Opt. Express 23(5), 5972-5981 (2015).
32. Y.-Q. Huang, Z.-A. Hu, H. Cui, Z.-C. Luo, A.-P. Luo, and W.-C. Xu, "Coexistence of harmonic soliton molecules and rectangular noise-like pulses in a figure-eight fiber laser," Opt. Lett. 41(17), 4056-4059 (2016).
33. Y. E. B.-Rodriguez, O. Pottiez, E. G. Sánchez, J. L.-Cruz, H. I.-Villalón, J. C. H.-Garcia, M. B.-Jimenez, G. B. Pérez, B. I.-Escamilla, and E. Kuzin, "Dual noise-like pulse and soliton operation of a fiber ring cavity," J. Opt. 19 (2017) 035502.
34. E. G.-Sanchez, O. Pottiez, Y. B.-Rodriguez, J. P. L.-Cruz, H. E. I.-Villalon, J. C. H.-Garcia, M. B.-Jimenez, E. A. Kuzin, "Complex dynamics of a fiber laser in nonstationary pulsed operation," Opt. Express 24(17), 18917-18930 (2016).
35. D. V. Churkin, S. Sugavanam, N. Tarasov, S. Khorev, S. V. Smirnov, S. M. Kobtsev, and S. K. Turitsyn, "Stochasticity, periodicity and localized light structures in partially mode-locked fibre lasers," Nat. Commun. 6, 1 6 (2015).
36. A. F. J. Runge, C. Aguergaray, N. G. R. Broderick, and M. Erkintalo, "Coherence and shot-to-shot spectral fluctuations in noise-like ultrafast fiber lasers," Opt. Lett. 38(21), 4327-4330 (2013).
37. L. Gao, T. Zhu, S. Wabnitz, M. Liu, and W. Huang, "Coherence loss of partially mode-locked fibre laser," Sci. Rep. 6, 24995 (2016).
38. Y. Jeong, L. A. V.-Zuniga, S. Lee, and Y. Kwon, "On the formation of noise-like pulses in fiber ring cavity configurations," Opt. Fiber Technol. 20(6), 575-592 (2014).
39. Y. Kwon, L. A. V.-Zuniga, S. Lee, H. Kim, and Y. Jeong, "Numerical study on multi-pulse dynamics and shot-to-shot coherence property in quasi-mode-locked regimes of a highly-pumped anomalous dispersion fiber ring cavity," Opt. Express 25(4), 4456-4469, (2017).
40. S. Lee, L. A. V.-Zuniga, Y. Kwon, H. Kim, H. Kim, and Y. Jeong, "Experimental study on the coherence of non-stationary optical pulses generated from a ring laser cavity," CLEO 2016, San Jose, USA, 5 Jun.-10 Jun., 2016, paper STh4O.7.

41. G. P. Agrawal, Nonlinear Fiber Optics, 4th ed. (Academic, 2007).
42. J. P. Gordon, “Interaction forces among solitons in optical fibers,” Opt. Lett. 8(11), 596–598 (1983).
43. F. M. Mitschke and L. F. Mollenauer, “Experimental observation of interaction forces between solitons in optical fibers,” Opt. Lett. 12(5), 355–357 (1987).
44. D. Y. Tang, B. Zhao, L.M. Zhao, and H. Y. Tam, “Soliton interaction in a fiber ring laser,” Phys. Rev. E 72(1), 016616 (2005).
45. J. Peng, N. Tarasov, S. Sugavanam, and D. Churkin, “Rogue waves generation via nonlinear soliton collision in multiple−soliton state of a mode−locked fiber laser,” Opt. Express 24(19), 21256–21263 (2016).

Chapter 3.

1. S. Haver, “Freak wave event at Draupner jacket January 1 1995. Statoil,” Technical report. PTT−KU−MA (2003).
2. M. Onorato, A. Osborne, M. Serio, and S. Bertone, “Freak waves in random oceanic sea states.” Phys. Rev. Lett. 86, 5831–5834 (2001).
3. M. Hopkin, “Sea snapshots will map frequency of freak waves.” Nature 430, 492 (2004)
4. S. Perkins, “Dashing rogues: freak ocean waves pose threat to ships, deep−sea oil platforms.” Science News 170, 328–329 (2006)
5. P. Muller, C. Garrett, and A. Osborne, “Rogue waves.” Oceanography 18, 66–75 (2005)
6. M. Onorato, A. Osborne, and M. Serio, “Modulational instability in crossing sea states: A possible mechanism for the formation of freak waves” Phys. Rev. Lett. 96, 014503 (2006).
7. N. Akhmediev and E. Pelinovsky, “Editorial–Introductory remarks on “Discussion & Debate: Rogue waves− towards a unifying concept?”,” Eur. Phys. J. Spec. Top. 185(1), 1–4 (2010).
8. A. Chabchoub, N. P. Hoffmann, and N. Akhmediev, “Rogue wave observation in a water wave tank,” Phys. Rev. Lett. 106(20), 204502 (2011).
9. Y. Bludov , V. Konotop , and N. Akhmediev, “Matter rogue waves,” Phys. Rev. A 80, 033610 (2009).
10. M. Shats, H. Punzmann, and H. Xia, “Capillary rogue waves,” Phys. Rev. Lett. 104, 104503 (2010).
11. L. Stenflo, and M. Marklund, “Rogue waves in the atmosphere,” Journal of Plasma Physics, 76(3–4), 293−295 (2010).
12. T. Horikis and M. Ablowitz, “Rogue waves in nonlocal media,” Phys. Rev. E 95, 042211 (2017).
13. D. R. Solli, C. Ropers, P. Koonath, and B. Jalali, “Optical rogue waves,” Nature 450(7172), 1054–1057 (2007).
14. N. Akhmediev, J. Dudley, D. Solli, and S. Turitsyn, “Recent progress in investigating optical rogue waves,” J. Opt. 15(6), 060201 (2013).

15. L. Nelson, D. Jones, K. Tamura, H. Haus, and E. Ippen, “Ultrashort-pulse fiber ring lasers,” Appl. Phys. B 65, 277–294 (1997).
16. A. Chong, J. Buckley, W. Renninger, and F. Wise, “All-normal-dispersion femtosecond fiber laser,” Opt. Express 14(21), 10095–10100 (2006).
17. N. Akhmediev, J. M. Soto-Crespo, and Ph. Grelu, “Roadmap to ultra-short record high-energy pulses out of laser oscillators,” Phys. Lett. A 372, 3124–3128 (2008).
18. P. Grelu and N. Akhmediev, “Dissipative solitons for mode-locked lasers,” Nat. Photon. 6, 84-92 (2012).
19. M. E. Fermann and I. Hartl, “Ultrafast fiber lasers,” Nat. Photon. 7, 868-874 (2013).
20. Y. Kwon, L. A. V.-Zuniga, K. Park, S. Lee, H. Chang, and Y. Jeong, “Combinatorial study of supercontinuum generation dynamics in photonic crystal fibers pumped by ultrafast fiber lasers,” IEEE J. Quant. Electron. 52(6), 6400311 (2016).
21. M. Horowitz, Y. Barad, and Y. Silberberg, “Noiselike pulses with a broadband spectrum generated from an erbium-doped fiber laser,” Opt. Lett. 22(1), 799-801 (1997).
22. A. Komarov, H. Leblond, and F. Sanchez, “Multistability and hysteresis phenomena in passively mode-locked fiber lasers,” Phys. Rev. A 71(5), 053809 (2005).
23. S. Chouli and P. Grelu, “Soliton rains in a fiber laser: An experimental study,” Phys. Rev. A 81(6), 063829 (2010).
24. L. A. V.-Zuniga and Y. Jeong, “Super-broadband noise-like pulse erbium-doped fiber ring laser with a highly nonlinear fiber for Raman gain enhancement,” IEEE Photon. Technol. Lett. 24(17), 1549-1551 (2012).
25. A. F. J. Runge, C. Aguergaray, N. G. R. Broderick, and M. Erkintalo, “Coherence and shot-to-shot spectral fluctuations in noise-like ultrafast fiber lasers,” Opt. Lett. 38(21), 4327-4330 (2013).
26. Y. Jeong, L. A. V.-Zuniga, S. Lee, and Y. Kwon, “On the formation of noise-like pulses in fiber ring cavity configurations,” Opt. Fiber Technol. 20(6), 575-592 (2014).
27. D. V. Churkin, S. Sugavanam, N. Tarasov, S. Khorev, S. V. Smirnov, S. M. Kobtsev, and S. K. Turitsyn, “Stochasticity, periodicity and localized light structures in partially mode-locked fibre lasers,” Nat. Commun. 6, 1-6 (2015).
28. E. G.-Sanchez, O. Pottiez, Y. B.-Rodriguez, J. P. L.-Cruz, H. E. I.-Villalon, J. C. H.-Garcia, M. B.-Jimenez, E. A. Kuzin, “Complex dynamics of a fiber laser in nonstationary pulsed operation,” Opt. Express 24(17), 18917-18930 (2016).
29. L. Gao, T. Zhu, S. Wabnitz, M. Liu, and W. Huang, “Coherence loss of partially mode-locked fibre laser,” Sci. Rep. 6, 24995 (2016).
30. D. Y. Tang, L. M. Zhao, and B. Zhao, “Soliton collapse and bunched noise-like pulse generation in a passively mode-locked fiber ring laser,” Opt. Express 13(7), 2289-2294 (2005).

31. D. Y. Tang, L. M. Zhao, B. Zhao, and A. Q. Liu, “Mechanism of multisoliton formation and soliton energy quantization in passively mode-locked fiber lasers,” Phys. Rev. A 72(4), 043816 (2005).
32. S. Lee, L. A. V.-Zuniga, Y. Kwon, H. Kim, H. Kim, and Y. Jeong, “Experimental study on the coherence of non-stationary optical pulses generated from a ring laser cavity,” CLEO 2016, San Jose, USA, 5 Jun.-10 Jun., 2016, paper STh4O.7.
33. Y. Kwon, L. A. V.-Zuniga, S. Lee, H. Kim, and Y. Jeong, “Numerical study on multi-pulse dynamics and shot-to-shot coherence property in quasi-mode-locked regimes of a highly-pumped anomalous dispersion fiber ring cavity,” Opt. Express 25(4), 4456 4469 (2017).
34. S. Lee, L. A. Vazquez-zuniga, H. Kim, Y. Kwon, K. Park, H. S. Kim, and Y. Jeong, "Experimental spatio-temporal analysis on the shot-to-shot coherence and wave-packet formation in quasi-mode-locked regimes in an anomalous dispersion fiber ring cavity." Optics Express, 25(23), 28385-28397 (2017).
35. J. Peng, N. Tarasov, S. Sugavanam, and D. Churkin, “Rogue waves generation via nonlinear soliton collision in multiple-soliton state of a mode-locked fiber laser,” Opt. Express 24(19), 21256–21263 (2016).
36. A. Slunyaev and E. Pelinovsky, “Role of multiple soliton interactions in the generation of rogue waves: The modified Korteweg–de Vries framework,” Phys. Rev. Lett. 117, 214501 (2016).
37. C. Lecaplain, P. Grelu, J. M. Soto-Crespo, and N. Akhmediev, “Dissipative rogue waves generated by chaotic pulse bunching in a mode-locked laser,” Phys. Rev. Lett. 108(23), 233901 (2012).
38. J. M. S.-Crespo, P. Grelu, and N. Akhmediev, “Dissipative rogue waves: Extreme pulses generated by passively mode-locked lasers,” Phys. Rev. E 84(1), 016604 (2011).
39. A. F. Runge, C. Aguergaray, N. G. Broderick, and M. Erkintalo, “Raman rogue waves in a partially mode-locked fiber laser,” Opt. Lett. 39(2), 319–322 (2014).
40. M. Liu, Z. R. Cai, S. Hu, A. P. Luo, C. J. Zhao, H. Zhang, W. C. Xu, and Z. C. Luo, “Dissipative rogue waves induced by long-range chaotic multi-pulse interactions in a fiber laser with a topological insulator-deposited microfiber photonic device,” Opt. Lett. 40(20), 4767–4770 (2015).
41. C. Lecaplain and P. Grelu, “Rogue waves among noiselike-pulse laser emission: an experimental investigation,”Phys. Rev. A 90(1), 013805 (2014).
42. M. I. Afzal, K. Alameh, and Y. T. Lee, “Blue-Shifted rogue waves generation in normal dispersion fiber laser,”IEEE Photonics Technol. Lett. 27(22), 2323–2326 (2015).
43. J. M. Soto-Crespo, P. Grelu, and N. Akhmediev, “Dissipative rogue waves: extreme pulses generated by passively mode-locked lasers,” Phys. Rev. E Stat. Nonlin. Soft Matter Phys. 84(1), 016604 (2011).

44. A. Zaviyalov, O. Egorov, R. Iliew, and F. Lederer, “Rogue waves in mode-locked fiber lasers,” Phys. Rev. A 85(1), 013828 (2012).
45. N. Akhmediev et al, “Roadmap on optical rogue waves and extreme events,” J. Optics 18, 063001 (2016).
46. G. P. Agrawal, Nonlinear Fiber Optics, 4th ed. (Academic press, 2007).
47. J. P. Gordon, “Interaction forces among solitons in optical fibers,” Opt. Lett. 8(11), 596–598 (1983).
48. F. M. Mitschke and L. F. Mollenauer, “Experimental observation of interaction forces between solitons in optical fibers,” Opt. Lett. 12(5), 355–357 (1987).
49. D. Y. Tang, B. Zhao, L.M. Zhao, and H. Y. Tam, “Soliton interaction in a fiber ring laser,” Phys. Rev. E 72(1), 016616 (2005).
50. E. Agurado and J. Burt, Understanding Weather and Climate, 7th ed. (Pearson, 2015).
51. S. Shiue and Y. Tu, “Relaxation of thermal stresses in double-coated optical fibers,” Journal of Applied Physics 86, 4085 (1999).
52. M. K. Davis, M. J. F. Digonnet, and Richard H. Pantell, "Thermal Effects in Doped Fibers," J. Lightwave Technol. 16, 1013 1023 (1998).
53. J. Brooke, Engineering Committee on Oceanic Resources Working Group on Wave Energy Conversion (Elsevier, 2003).
54. P. Le Tirant and J. Meunier, Anchoring of floating structures, (Scientific and Technical Information, 1990).
55. C. Zheng, J. Pan, and C. Li, “Global oceanic wind speed trends,” Ocean & Coastal Management 129, 15-24 (2016).

한글 초록

본 논문은 광섬유 레이저의 준 모드 잠금 영역에 대한 실험연구를 다룬다. 논문은 크게 다음의 4개의 주제로 나눌 수 있다: (1) 코히런스 (coherence) 특성, (2) 웨이브 패킷 (wave paket) 형성, (3) 연속되는 펄스 상호작용, (4) 분산 파들의 동기화에 의한 슈퍼 로그 웨이브 유도. 주제 (1)과 (2)는 비선형 위상 변환과 솔리톤 상호 작용에 대해 서술하고, 주제 (3)은 광섬유 내에서 진행하는 펄스들의 상호작용에 대해 기술한다. 그리고 주제 (4)는 이러한 펄스들의 상호작용이 연속적으로 발생하여 축적되었을 때의 현상을 기술한다. 서론에서는 본 논문의 연구 결과를 설명하기 위해 광섬유 광학, 광섬유 레이저, 모드 잠금, 수동 모드잠금 비선형 레이저 그리고 준 모드잠금 레이저들에 대한 기초적인 지식과 배경에 대한 설명과 연구의 목적과 범위에 대하여 기술한다.

논문의 첫 부분에서는 비정상분산(anomalous dispersion) 광섬유 공진기에서의 코히런스 특성과 웨이브 패킷 형성에 대한 심도있는 실험적 분석을 수행한다. 준 모드잠금 영역의 경우 noise-like pulse (NLP), symbiotic, multi-soliton (MS)를 중점적으로 다룬다. 준 모드잠금 영역은 다중펄스와 확률적인 변화를 갖는 특성때문에 정확한 분석을 위해서 실시간 측정이 필요하며 스펙트럼 측정, 자기상관측정(autocorrelation)과 같은 전통적 방식의 광 측정으로는 이러한 실시간 측정이 불가능하므로 spatio-temporal 분석을 이용하여 준 모드 잠금 영역에서의 펄스변화를 확인하였다. 각 준 모드 잠금 영역들은 명확하게 구분가능한 코히런스 특성을 보였으며 이를 통해 펄스의 비선형 위상 변환의 축적과 솔리톤 상호작용의 정도에 관련이

있음이 나타났다. 또한 이는 준 모드 잠금 영역에서의 웨이브 패킷 형성과 소멸에도 영향을 끼쳤다. 높은 강도를 갖는 솔리톤들은 더 많은 비선형 위상 변환과 더 강한 솔리톤 상호작용을 겪게 되고 그에 따라 MS 영역에서 솔리톤들이 모이게 되어 NLP, symbiotic 영역에서 웨이브 패킷으로 형성이 된다. 그리고 그 반대로 솔리톤 상호작용이 작아짐에 따라 NLP symbiotic 영역의 웨이브 패킷이 MS 영역으로 가며 소멸된다. 이런 복잡한 비선형 과정은 또한 코히런스의 강한 저하를 동반하며 각 준 모드 잠금영역은 명확한 코히런스 특성을 가지고 있는 것을 확인하였다. 이러한 경향은 수치해석적 연구와 일치하였으며 이는 준 모드 잠금 영역의 코히런스 특성이 비선형 roundtrip 당 위상변환의 축적과 높은 연관성이 있음을 증명한다. 이러한 경향과 웨이브 패킷 형성 과정은 비정상 분산 영역에서 공진기의 NLP, symbiotic, MS등의 준 모드 잠금 영역이 솔리톤 상호작용의 정도로 결정된다고 볼 수 있다.

논문의 두 번째 부분에서는 MS 영역에서 동작하는 비정상 분산 광섬유 공진기에서의 슈퍼 로그웨이브의 주기적 유도에 대한 분석이다. 공진기 내에서 일어나는 extreme wave의 형성을 측정하기 위하여 spatio-temporal 측정방법을 이용하였고, 이를 분석하기 위해 공진기 내의 펄스들의 생성에 대한 확률분포함수를 히스토그램을 이용하여 나타내었다. 수 백 개의 솔리톤 펄스들과 분산 펄스들이 복잡한 상호작용을 하며 비선형역학을 나타내는 MS 영역에서 분산펄스들이 보강간섭을 일으키며 동기화되어 일반적인 솔리톤의 강도의 10배에 달하는 extreme wave가 나타나는 현상은 공진기 내의 포화 흡수 출력을 조절하여 솔리톤 개수를 늘림으로써 솔리톤 밀도를 조절하여 솔리톤 상호작용이 일어날 확률을 증가시킴으로써 유도할 수 있다. 확률적으로 일어난 솔리톤 상호작용은 주변 솔리톤들을 불안정하게 만들며 이는 계속되는 솔리톤 상호작용으로 이어져 분산 파들의 보강

간섭 또한 강해지게 된다. 이러한 보상 간섭이 최고점에 달하게 되면 슈퍼 로그웨이브를 유도하게 되며 빠르게 솔리톤 상호작용이 최소화된 상태로 돌아간다. 이 현상은 공진기의 변화나 추가적인 외부 조절 없이 10초 내에서 반복되며 이는 일반적인 파도의 속력을 고려했을 때 백 년에 한번 정도로 예측할 수 있다. 따라서 대양의 조건이 일정하다고 가정 했을 때 이러한 슈퍼 로그웨이브가 주기적으로 나타날 수 있음을 의미한다.

이 논문에서 실행한 비선형 광섬유 레이저의 준 모드 잠금 영역에 대한 실험적 분석은 준 모드 잠금 영역에서의 펄스 역학 연구와 extreme wave 생성에 관한 중요한 기초가 될 것으로 기대되며 광학 분야뿐만이 아니라 비선형성을 기반으로 하는 다른 영역에서도 중요한 역할을 할 것으로 기대된다.

주요어: 비선형 광학, 광섬유 레이저, 초단광파, 모드잠금 레이저, 로그웨이브.
학 번: 2012-30943